공학박사 학위논문

# Microwave absorption properties of Zn-substituted W-type hexaferrites and carbonyl iron for 5G communication

## 5 세대 통신을 위한 Zn 치환된 W-타입 헥사페라이트와 카보닐 철의 마이크로파 흡수 특성

**2021 년 8 월**

서울대학교 대학원

재료공학부

최 성 준

# Microwave absorption properties of Zn-substituted W-type hexaferrites and carbonyl iron for 5G communication

## 5세대 통신을 위한 Zn 치환된 W-타입 헥사페라이트와 카보닐 철의 마이크로파 흡수 특성

지도교수 유 상 임

이 논문을 공학박사학위논문으로 제출함
2021년 8월

서울대학교 대학원
재료공학부
최 성 준

최성준의 박사학위논문을 인준함
2021년 08월

위 원 장 박 찬

부 위 원 장 유 상 임

위 원 정 인 호

위 원 최 광 보

위 원 박 승 영

# Abstract

## Microwave absorption properties of Zn-substituted W-type hexaferrites and carbonyl iron for 5G communication

Sungjoon Choi

Department of Materials Science and Engineering

The Graduate School

Seoul National University

With the development of the fifth-generation (5G) technology, microwave electronic devices for wireless telecommunication have been used. Simultaneously, electromagnetic interference (EMI) has been a challenging problem as it can human or animal health and also cause a serious malfunction in electronic devices. To solve the EMI problem, many research groups have tried to develop highly efficient thin broadband microwave absorbing materials (MAM) with lightweight of low filler loading. Meanwhile, since the microwave absorption properties of MAMs are mainly determined by the relative complex permittivity ($\varepsilon_r=\varepsilon'-j\varepsilon''$) and permeability ($\mu_r=\mu'-j\mu''$), and their thickness values are inversely proportional to their refractive

indices ($n = \mathrm{Re}\sqrt{\mu_r \varepsilon_r}$), researchers have focused on the improvement of their real and imaginary parts of $\varepsilon_r$ and $\mu_r$ for real applications.

Among various MAMs, while both spinel ferrites and M-type hexaferrites have been most widely used for real applications, W-type hexaferrites and carbonyl iron have been rarely reported. In particular, 3.5 and 28 GHz are regarded as the frequencies for 5G communication. Thus, in this study, the microwave absorption properties of the partially Zn-substituted W-type hexaferrites ($SrFe_{2-x}Zn_xFe_{16}O_{27}$; $SrFe_{2-x}Zn_xW$, $0.0 \leq x \leq 2.0$) were carefully investigated to develop thin broadband microwave absorbers at two different frequencies of 3.5 and 28 GHz. In addition, the $Al_2O_3$-coated carbonyl irons prepared by the sol-gel method were investigated to develop high performance microwave absorbers at 3.5 GHz. The reason for the selection of partial Zn substitution is as follows. First, according to our previous study on Zn-substituted SrW-type hexaferrites, with increasing $x$ up to 1.0 in $SrFe_{2-x}Zn_xW$, the saturation magnetization ($M_s$) is almost linearly increased while the magnetic anisotropy field ($H_a$) is abruptly decreased. With further increase of $x$ up to 2.0, the $M_s$ value is largely decreased while the $H_a$ value is slightly decreased. Therefore, the real parts of $\mu_r$ are expected to continuously increase up to $x$ =1.0 since they are proportional to the ratio of $M_s/H_a$. Second, higher real and imaginary parts of the $\varepsilon_r$ value is expected due to an increased electric conductivity through electron hopping between $Fe^{2+}$ and $Fe^{3+}$ ions. Therefore, the partial substitution of $Zn^{2+}$ for the $Fe^{2+}$ site of SrW-type hexaferrite is expected to increase the real and imaginary parts of both $\varepsilon_r$ and $\mu_r$ values, leading to an improvement in the microwave absorption properties.

On the other hand, since the carbonyl iron has very high $M_s$ with very low $H_a$, it is possible to obtain high real parts of $\mu_r$. However, an excessive eddy current loss

hindered to achieve high performance microwave absorber. To overcome this problem, we synthesized a core-shell of carbonyl iron-amorphous alumina by the sol-gel method since the inter-particular current path can be effectively reduced. As the alumina insulation coating layer acts as a non-magnetic material which deteriorates their magnetic properties, especially the real part of $\mu_r$, its thickness was carefully controlled. Also, the dielectric materials such as amorphous alumina and α-alumina were mixed additionally to control the complex permittivity.

In order to evaluate the microwave absorption properties of composite samples, our specimens were prepared by the following procedures; At first, each hexaferrite filler or carbonyl iron was mixed with the epoxy-resin matrix, and then each powder mixture was pressed into a thin rectangular plate or a toroidal shape, respectively, and subsequently hardened at 175 ˚C for 1 h in air. The measurements of complex permittivity and permeability were carried out for our specimens using the VNA (Agilent PNA N5525A). Their complex permittivity and permeability values were calculated from S-parameters by using a transmission and reflection method based on the algorithm developed by Nicolson and Ross.

The microwave absorption properties of $SrFe_{2-x}Zn_xW$ ($0.0 \leq x \leq 2.0$) hexaferrite-epoxy resin composites were investigated in both Ku (0.5–18 GHz) and Ka (26.5-40 GHz) bands. For $Al_2O_3$-coated carbonyl iron-epoxy resin composites, their microwave absorption properties were studied only in the Ku-band. As expected, owing to the increased real and imaginary parts $\varepsilon_r$ and $\mu_r$, the partially Zn-substituted SrW-type hexaferrite composites exhibited lower *RL* values with wider bandwidth. Especially, a 2.8 mm-thick $SrFe_{1.5}Zn_{0.5}W$ ($x$ = 0.5) composite with $V_f$ of 90% exhibited the most appropriate for 5G application at 3.5 GHz in the Ku-band, having the *RL* value of −46 dB at 3.6 GHz with the bandwidth of 0.43 GHz (3.38-3.81 GHz)

below −10 dB. In the Ka-band, a 0.64 mm-thick $SrFe_{1.75}Zn_{0.25}W$ ($x$ = 0.25) composite with the $V_f$ of 30% exhibited the most appropriate for 5G application at 28 GHz, having the *RL* value of −68.4 dB at 28 GHz with the bandwidths of 5.16 GHz (26.50-31.66 GHz) and 2.48 GHz (26.50-28.98 GHz) below −10 and −20 dB, respectively. Meanwhile, $Al_2O_3$-coated carbonyl iron composite with amorphous alumina of 5wt.% exhibited the highest performance having the *RL* value of −28.9 dB at 3.5 GHz with a thickness of 4.36 mm and the bandwidth of 0.51 GHz (3.25-3.76 GHz) below −20 dB.

In conclusion, partially Zn-substituted SrW-type hexaferrites are appropriate as the filler of MAM for 5G application near 3.5 and 28 GHz since thin broadband microwave absorbers can be fabricated with epoxy resin. Nano-coating of amorphous alumina on the surface of carbonyl iron is essential for the improvement of microwave absorption properties of carbonyl iron by greatly reducing the eddy current loss, leading to higher performance broadband microwave absorbers at 3.5 GHz. Further improvement of microwave absorption properties is expected by the following approaches. One is to fully optimize the processing parameters of partially Zn-substituted SrW-type hexaferrite composites, including the amount of Zn substituent $x$, its $V_f$, the kind and amount of polymer matrix, and the fabrication processing of specimen. Another may be to make other SrW-type hexaferrite fillers by the partial substitution of other stable divalent ions such as $Co^{2+}$, $Ni^{2+}$, $Mn^{2+}$, $Mg^{2+}$, and etc. for the $Fe^{2+}$ sites.

---

**Keywords:** W-type hexaferrite, Zn-substitution, Carbonyl iron, Alumina coating, Microwave absorption property, 5G application

**Student number:** 2014-21446

# Table of contents

# List of tables

# List of figures

# Chapter 1

## General introduction

With the development of fifth-generation (5G) wireless devices operating in the microwave region, electromagnetic interference (EMI) has become a serious pollution problem since it can harm human or animal health and surrounding electronic systems [1, 2]. In order to solve the electromagnetic problem, a tremendous effort has been made for the development of high-performance microwave absorbers possessing high absorption efficiency with wide bandwidth, lightweight, and thin thickness simultaneously [3]. Since the microwave absorption properties of microwave absorption materials (MAMs) are mainly determined by the relative complex permittivity ($\varepsilon_r=\varepsilon'-j\varepsilon''$) and permeability ($\mu_r=\mu'-j\mu''$), and their thickness values are inversely proportional to their refractive indices ($n = \mathrm{Re}\sqrt{\mu_r\varepsilon_r}$), researchers have focused on the improvement of their real and imaginary parts of $\varepsilon_r$ and $\mu_r$ for real applications. In particular, since 3.5 and 28 GHz are regarded as frequencies for 5G communications as shown in Fig. 1.1, a high-performance microwave absorber is investigated at 3.5 and 28 GHz.

In general, MAMs are classified into two different types: (1) magnetic materials, such as ferromagnetic metals of carbonyl iron [4, 5], and ferrite materials of spinel ferrites [6] and hexagonal ferrites [7-10]; and (2) dielectric materials, such as $Al_2O_3$ [11], $BaTiO_3$ [12], polymers [13], and carbon-based materials [14-16]. Carbon-based materials have been considered as a promising MAM since it has superior electrical

conductivity and extreme lightweight [17]. Nevertheless, their real and imaginary parts of $\mu_r$ are considered to be close to those of the matrix material, so that it is difficult to obtain a strong absorption composite absorber composed of single carbon-based materials. Therefore, carbon-based materials with other materials are currently being researched in order to enhance microwave absorption properties [18]. Among magnetic MAMs, both hexagonal ferrites and ferromagnetic metals have been most widely used for real applications. While spinel ferrites are normally used at the frequency region below 1 GHz due to their relatively lower ferromagnetic resonance (FMR) frequencies [19]. Especially, M and W-type hexaferrites can be regarded as promising materials for microwave absorber applications since FMR frequencies of M and W-type hexaferrites are in the region of 30-60 GHz due to their strong uniaxial anisotropies [20]. The hexaferrites can be categorized into six different types: M, X, U, Y, Z, and W [21]. Among these, most researchers have focused on M-type hexaferrites owing to their high FMR frequencies and excellent chemical stability [22, 23]. However, W-type hexaferrites must also be promising candidates for MAMs since they also possess high $M_s$ values, high $H_a$, and high FMR frequency comparable to M-type hexaferrites [20], implying that W-type hexaferrites can be more suitable for applications.

However, the thickness, volume fraction ($V_f$) of the composite absorber with broad bandwidth should be considered for a real application. Since the thickness of the absorber is normally thicker to satisfy higher than 99% incident microwave, which makes it challenging to use as absorbers [24]. Also, high loading of $V_f$ is generally required to be higher value of real and imaginary parts $\varepsilon_r$ and $\mu_r$ for better absorption property [25]. Next, the wide bandwidth of the composite absorber is another important factor, which is covering at an aimed frequency for the application.

In order to solve the above problems for a real application, many researchers have focused on the enhancement of $\varepsilon_r$ and $\mu_r$ of W-type hexaferrites. For this purpose, various divalent cations have been fully substituted for the $Fe^{2+}$ sites of W-type hexaferrites such as $Fe^{2+}$, $Co^{2+}$, $Ni^{2+}$ $Zn^{2+}$, and etc [26, 27]. However, unlike a full cation substitution for the $Fe^{2+}$ site, partially Zn-substituted W hexaferrites with the nominal compositions of the $SrFe_{2-x}Zn_xFe_{16}O_{27}$ were synthesized by sintering in the low oxygen pressure ($PO_2$) to fabricate efficiently high-performance MAMs in this thesis. The main reason for the selection of partial Zn-substituted SrW-type hexaferrites is as follows. First, according to our previous study on magnetic properties of Zn-substituted SrW-type hexaferrites [28], the $M_s$ values are continuously increased with increasing $x$ up to 1.0 but decreased with further increase of $x$ up to 2.0. Therefore, $\mu_r$ is expected to continuously increase up to $x$ =1.0 since $\mu_r$ is proportional to $M_s$ [29]. Second, higher real and imaginary parts of the relative complex permittivity are expected due to an increased electric conductivity through electron hopping between $Fe^{2+}$ and $Fe^{3+}$ ions [30]. As a result, the partial Zn-substituted SrW-type hexaferrites is expected to enhance the real and imaginary parts of $\varepsilon_r$ and $\mu_r$ at the same time. Thus, **in Chapter 3** and **4**, the microwave absorption properties of the partially Zn-substituted W-type hexaferrites ($SrFe_{2-x}Zn_xW$, $0.0 \leq x \leq 1.0$) are investigated in the range of Ku and Ka-band, respectively.

On the other hand, carbonyl iron is also considered as a promising candidate for high-performance MAM because it exhibits high saturation magnetization ($M_s$) and $\mu_r$ in the microwave region [31]. However, the reason metal materials have excellent magnetic properties but were not used in high-frequency applications such as MAMs is that the magnetic properties of metal magnetic materials are decreased rapidly with

increasing frequency due to eddy current loss. Thus, high imaginary part of $\mu_r$ causes severe impedance mismatch. In order to reduce the eddy current loss, researchers have focused on the insulation coating on the surface of carbonyl iron particles [32]. Among oxide insulator materials, $SiO_2$ is the most commonly reported insulation coating material due to its high electrical resistivity, chemical stability, and non-toxicity [33-35]. In the case of alumina, although it must be a promising candidate for insulator material because it also possesses high electrical resistivity and good thermal stability, reports on its use as the insulation coating are very limited so far. Thus, **in Chapter 5**, the microwave absorption properties of the $Al_2O_3$-coated carbonyl iron are systematically studied. Furthermore, in order to improve the microwave absorption property, the effect of carbonyl iron mixed with dielectric powders has also been studied as a function of frequency and thickness in the range of Ku-band for 5G communication.

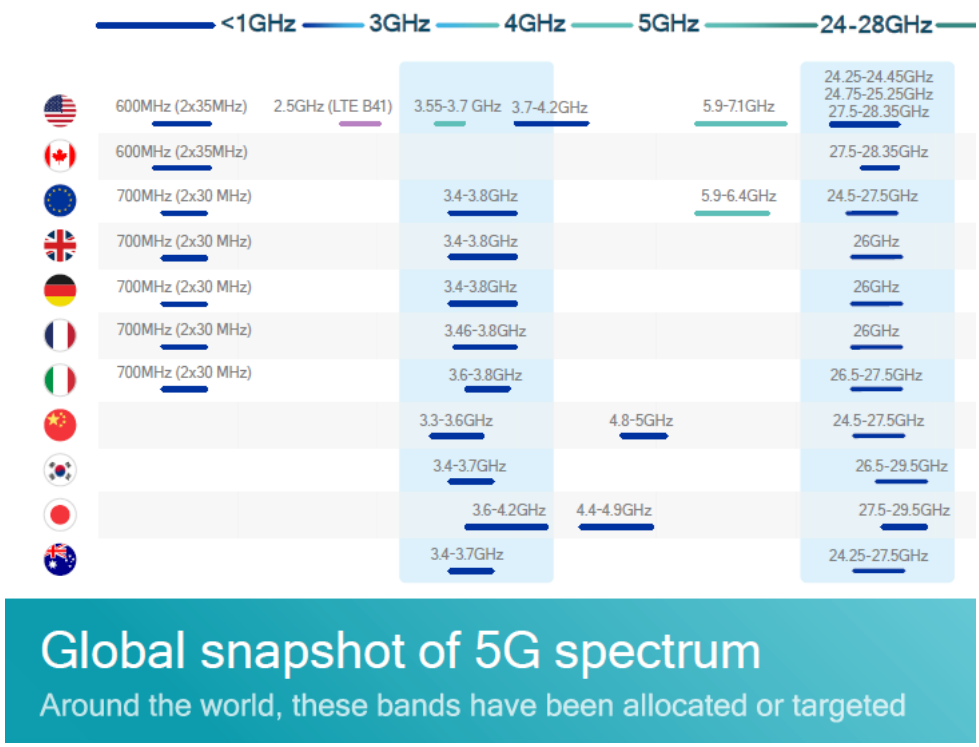


**Fig. 1.1.** Global frequencies for 5G communication.

# References

[1] G. Shao, J.F. Liang, W.Y. Zhao, B. Zhao, W. Liu, H.L. Wang, B.B. Fan, H.L. Xu, H.X. Lu, Y.G. Wang, R. Zhang, Co decorated polymer-derived SiCN ceramic aerogel composites with ultrabroad microwave absorption performance, Journal of Alloys and Compounds, 813 (2020) 152007.

[2] V. Pratap, A.K. Soni, S. Dayal, S.M. Abbas, A.M. Siddiqui, N.E. Prasad, Electromagnetic and absorption properties of U-type barium hexaferrite-epoxy composites, Journal of Magnetism and Magnetic Materials, 465 (2018) 540-545.

[3] Y.P. Sun, X.G. Liu, C. Feng, J.C. Fan, Y.H. Lv, Y.R. Wang, C.T. Li, A facile synthesis of $FeNi_3$@C nanowires for electromagnetic wave absorber, Journal of Alloys and Compounds, 586 (2014) 688-692.

[4] X.L. Guo, Z.J. Yao, H.Y. Lin, J.T. Zhou, Y.X. Zuo, X.Y. Xu, B. Wei, W.J. Chen, K. Qian, Epoxy resin addition on the microstructure, thermal stability and microwave absorption properties of core-shell carbonyl iron@epoxy composites, Journal of Magnetism and Magnetic Materials, 485 (2019) 244-250.

[5] B.C. Wang, J.Q. Wei, Y. Yang, T. Wang, F.S. Li, Investigation on peak frequency of the microwave absorption for carbonyl iron/epoxy resin composite, Journal of Magnetism and Magnetic Materials, 323 (2011) 1101-1103.

[6] C. Stergiou, Magnetic, dielectric and microwave absorption properties of rare earth doped Ni-Co and Ni-Co-Zn spinel ferrites, Journal of Magnetism and Magnetic Materials, 426 (2017) 629-635.

[7] A. Ghasemi, G.R. Gordani, E. Ghasemi, $Co_2W$ hexaferrite nanoparticles-carbon nanotube microwave absorbing nanocomposite, Journal of Magnetism and Magnetic Materials, 469 (2019) 391-397.

[8] H. Nikmanesh, M. Moradi, G.H. Bordbar, R.S. Alam, Effect of multi dopant barium hexaferrite nanoparticles on the structural, magnetic, and X-Ku bands microwave absorption properties, Journal of Alloys and Compounds, 708 (2017) 99-107.

[9] A. Baniasadi, A. Ghasemi, A. Nemati, M.A. Ghadikolaei, E. Paimozd, Effect of Ti-Zn substitution on structural, magnetic and microwave absorption characteristics of strontium hexaferrite, Journal of Alloys and Compounds, 583 (2014) 325-328.

[10] J. Chen, P. Meng, M. Wang, G. Zhou, X. Wang, G. Xu, Electromagnetic and microwave absorption properties of $BaMg_xCo_{1-x}TiFe_{10}O_{19}$, Journal of Alloys and Compounds, 679 (2016) 335-340.

[11] Z.D. Zhang, Z.C. Shi, R.H. Fan, M. Gao, J.Y. Guo, X.G. Qi, K.N. Sun, Microwave absorption properties of $Fe@Al_2O_3$ nanoembedments prepared by mechanosynthesis, Materials Chemistry and Physics, 130 (2011) 615-618.

[12] X.D. Chen, G.Q. Wang, Y.P. Duan, S.H. Liu, Microwave absorption properties of barium titanate/epoxide resin composites, Journal of Physics D-Applied Physics, 40 (2007) 1827-1830.

[13] I.S. Unver, Z. Durmus, Magnetic and Microwave Absorption Properties of Magnetite ($Fe_3O_4$)@ Conducting Polymer (PANI, PPY, PT) Composites, Ieee Transactions on Magnetics, 53 (2017) 2001708.

[14] Y.H. Chen, Z.H. Huang, M.M. Lu, W.Q. Cao, J. Yuan, D.Q. Zhang, M.S. Cao, 3D $Fe_3O_4$ nanocrystals decorating carbon nanotubes to tune electromagnetic properties and enhance microwave absorption capacity, Journal of Materials Chemistry A, 3 (2015) 12621-12625.

[15] H. Wang, F. Meng, J. Li, T. Li, Z. Chen, H. Luo, Z. Zhou, Carbonized Design of Hierarchical Porous Carbon/$Fe_3O_4$@Fe Derived from Loofah Sponge to Achieve Tunable High-Performance Microwave Absorption, Acs Sustainable Chemistry & Engineering, 6 (2018) 11801-11810.

[16] K.Q. He, L.M. Yu, L.M. Sheng, K. An, Y. Ando, X.L. Zhao, Doping Effect of Single-Wall Carbon Nanotubes on the Microwave Absorption Properties of Nanocrystalline Barium Ferrite, Japanese Journal of Applied Physics, 49 (2010) 125101.

[17] H.L. Lv, Y.H. Guo, Z.H. Yang, Y. Cheng, L.Y.P. Wang, B.S. Zhang, Y. Zhao, Z.C.J. Xu, G.B. Ji, A brief introduction to the fabrication and synthesis of graphene based composites for the realization of electromagnetic absorbing materials, Journal of Materials Chemistry C, 5 (2017) 491-512.

[18] S. Bi, X.J. Su, G.L. Hou, C.H. Liu, W.L. Song, M.S. Cao, Electrical conductivity and microwave absorption of shortened multi-walled carbon nanotube/alumina ceramic composites, Ceram. Int., 39 (2013) 5979-5983.

[19] S. Kumar, R. Chatterjee, Complex permittivity, permeability, magnetic and microwave absorbing properties of $Bi^{3+}$ substituted U-type hexaferrite, Journal of Magnetism and Magnetic Materials, 448 (2018) 88-93.

[20] P. Azizi, S.M. Masoudpanah, S. Alamolhoda, Magnetic and microwave absorption properties of $SrZnCoFe_{16}O_{27}$ powders synthesized by solution combustion method, Journal of Alloys and Compounds, 739 (2018) 211-217.

[21] G. Ramezanzaeh, A. Ghasemi, R. Mozaffarinia, A. Alizadeh, Electromagnetic wave reflection loss and magnetic properties of M-type $SrFe_{12-x}(Mn_{0.5}Sn_{0.5})_xO_{19}$ hexagonal ferrite nanoparticles in the Ku microwave band, Ceram. Int., 43 (2017) 10231-10238.

[22] A. Sharbati, J.M.V. Khani, Effect of $Ho^{3+}$ substitution on magnetic and microwave absorption properties of $Sr(ZnZr)_{0.5}Fe_{12}O_{19}$ hexagonal ferrite nanoparticles, Journal of Materials Science-Materials in Electronics, 24 (2013) 3629-3633.

[23] A. Arora, S.B. Narang, Investigation of electrical, dielectric and microwave properties of double substituted M-type $Ba_{(1-2x)}La_xNa_xFe_{10}Co_{0.5}TiMn_{0.5}O_{19}$ hexaferrite, Journal of Materials Science-Materials in Electronics, 29 (2018) 12718-12728.

[24] Z. Hou, J. Xiang, X. Zhang, L. Gong, J. Mi, X. Shen, K. Zhang, Microwave absorption properties of single- and double-layer absorbers based on electrospun nickel-zinc spinel ferrite and carbon nanofibers, Journal of Materials Science-Materials in Electronics, 29 (2018) 12258-12268.

[25] A.A. Mahani, S. Motahari, V. Nayyeri, Electromagnetic and microwave absorption characteristics of PMMA composites filled with a nanoporous resorcinol formaldehyde based carbon aerogel, Rsc Advances, 8 (2018) 10855-10864.

[26] M. Sun, J. Zheng, L. Liang, K. Sun, Y. Song, S. Zhao, Effect of Zn substitution on the electromagnetic and microwave absorbing properties of $BaCo_2$ hexaferrite, Journal of Materials Science-Materials in Electronics, 26 (2015) 9970-9976.

[27] M.J. Iqbal, R.A. Khan, S. Mizukami, T. Miyazaki, Mossbauer, magnetic and microwave absorption characteristics of substituted W-type hexaferrites nanoparticles, Ceram. Int., 38 (2012) 4097-4103.

[28] J.H. You, S.I. Yoo, Improved magnetic properties of Zn-substituted strontium W-type hexaferrites, Journal of Alloys and Compounds, 763 (2018) 459-465.

[29] R.S. Meena, S. Bhattachrya, R. Chatterjee, Complex permittivity, permeability and microwave absorbing properties of $(Mn_{2-x}Zn_x)$U-type hexaferrite, Journal of Magnetism and Magnetic Materials, 322 (2010) 2908-2914.

[30] J.H. You, S. Choi, S.Y. Park, S.I. Yoo, Enhanced microwave absorption properties of Zn-substituted Y-type hexaferrites, Journal of Magnetism and Magnetic Materials, 491 (2019) 165640.

[31] C.Q. Ge, L.Y. Wang, G. Liu, T. Wang, Enhanced electromagnetic properties of carbon nanotubes and $SiO_2$-coated carbonyl iron microwave absorber, Journal of Alloys and Compounds, 767 (2018) 173-180.

[32] W.C. Li, C. Le, J.J. Lv, W. Huang, L. Qiao, J.W. Zheng, Y. Ying, J. Yu, S.L. Che, Electromagnetic and oxidation resistance properties of core-shell structure flaked carbonyl iron powder@$SiO_2$ nanocomposite, Physica Status Solidi a-Applications and Materials Science, 214 (2017) 1600747.

[33] J. Topfer, A. Angermann, Complex additive systems for Mn-Zn ferrites with low power loss, Journal of Applied Physics, 117 (2015) 17A504.

[34] X. Fan, J. Wang, Z.Y. Wu, G.Q. Li, Core-shell structured FeSiAl/$SiO_2$ particles and $Fe_3Si/Al_2O_3$ soft magnetic composite cores with tunable

insulating layer thicknesses, Materials Science and Engineering B-Advanced Functional Solid-State Materials, 201 (2015) 79-86.

[35] D. Wang, G.P. Bierwagen, Sol–gel coatings on metals for corrosion protection, Progress in Organic Coatings, 64 (2009) 327-338.

# Chapter 2

# General background

## 2.1 Theory of microwave absorption

Fig. 2.1 illustrates a schematic geometry of a single-layer microwave absorber backed by a metal plate. When an EM wave goes through the air and encounters another medium, the incident wave is reflected, transmitted, and absorbed [1]. These phenomena are due to differences in the impedance matching conditions between air and the microwave absorber. However, when an EM wave transmits through the absorbing layer and encounters a metal substrate, the EM waves are completely reflected on the metal surface due to a large difference in impedance [2]. But when the reflected EM wave contacts the air/absorbing layer interface, some of the EM waves are reflected again within the absorbing layer [3]. This process can be repeated in a phenomenon known as internal multi-reflection as shown in Fig. 2.1. As a result, microwave absorption can be expressed as reflection loss (*RL*), the difference between the number of incident waves (wave (1) in Fig. 2.1) and the total number of waves reflected at the surface of the absorber and the conductor plate (wave (2) and (5) in Fig. 2.1) [4]. To be specific, *RL* is a value expressing how much the reflected waves compared to incident waves are suppressed by a microwave absorber. As a unit of *RL*, dB is used and the absorbed energy with respect to the *RL* values is summarized in Table 2.1.

In general, in order to evaluate the microwave absorption property of sample, the microwave absorber is fabricated in the form of composite with MAM as filler in the epoxy resin matrix [5]. The microwave absorption property of the absorber is mainly determined by the relative complex permittivity and permeability of the MAM. The real parts of $\varepsilon_r$ and $\mu_r$ stand for the storage ability of microwave energy, whereas the imaginary parts of $\varepsilon_r$ and $\mu_r$ symbolize the loss of electromagnetic energy [6]. Thus, the MAM can effectively attenuate the intensity of EM wave by minimizing the reflection of the incident wave and converting remaining microwave into heat energy [7].

Generally, the MAMs are divided into two types: (1) magnetic loss ($\tan\delta_m=\mu''/\mu'$) materials, such as ferromagnetic materials, spinel ferrites, and hexagonal ferrites [8-18]; and (2) dielectric loss ($\tan\delta_e=\varepsilon''/\varepsilon'$) materials, including $Al_2O_3$, $BaTiO_3$, polymers, carbon-based materials, etc [19-26]. It is well known that the $\mu''$ mainly comes from hysteresis loss, domain wall resonance, eddy current loss, and FMR [27]. However, the hysteresis loss can be ignored in a weak applied magnetic field and the domain wall resonance is reported to generally occur at a frequency around 1 GHz [28, 29]. If the main mechanism of magnetic loss is from the eddy current loss, the value of $\mu''(\mu')^{-2}(f)^{-1}$ should be almost constant as a function of frequency [30]. On the other hand, the $\varepsilon''$ mainly arises from conductivity loss and polarization loss [31], where polarization loss can be classified into dipole, interfacial, ionic, and electronic polarization [32]. According to free electron theory ($\varepsilon'' = 1/2\varepsilon_o\rho\pi f$) [33], higher conductivity results in larger $\varepsilon''$. However, ionic and electronic polarizations are negligible in microwave absorption since these polarizations are detectable only at a much higher frequency region ($10^3$–$10^6$ GHz) [34]. On the other hand, interfacial polarization loss occurs at the interfaces between filler and epoxy-resin matrix in the

MAM composites, and thus non-uniform distribution of space charges at the interfaces will enhance $\varepsilon''$ [35].

Back again, in terms of the *RL*, although the tan$\delta_e$ is an important factor to consider in microwave absorption ability and the tan$\delta_m$ is able to explain some of the features in microwave absorption ability, it does not always guarantee excellent *RL*. To fully understand the factors determining microwave absorption, it is important to consider quarter wavelength principle and impedance matching. Quarter wavelength principle is when the thickness of the absorber becomes 1/4 of the wavelength, the wave reflected at the surface of the absorber and the metal plate (wave (2) and (4) in Fig. 2.1) have a phase difference of 180° and cancel each other due to the destructive interference . The quarter wavelength principle can be expressed as follows [36, 37],

$$d = \frac{\lambda}{4} = \frac{c}{4f\sqrt{\mu_r \varepsilon_r}} \tag{2.1}$$

where $d$ is the thickness of the absorber, $\lambda$ is the wavelength of the microwave, $f$ is the frequency of the microwave, and $c$ is the speed of light. On the other hand, the impedance matching is also a factor to consider for excellent *RL* value. If the input impedance ($Z_{in}$) of microwave absorber becomes equal to the impedance of free space ($Z_0$), the EM wave is not reflected and is converted into heat energy all inside the microwave absorber. This condition is called perfect matching, and according to the transmission line theory [38, 39], is given by

$$Z_{\text{in}} = Z_0 \sqrt{\frac{\mu_r}{\varepsilon_r}} \tanh\left[ j(2\pi fd / c)\sqrt{\mu_r \varepsilon_r} \right] = 1 \tag{2.2}$$

where $Z_0 = \sqrt{\mu_0 / \varepsilon_0}$ is the characteristic impedance of free space. $c$ is the speed of light, $f$ is the frequency of the microwave, and $d$ is the thickness of the absorber. The microwave absorption property can be measurable by the *RL* of a single-layer absorber backed by a metal plate [40, 41], which is the absorption of the incident microwave in the absorber, is related to $Z_{in}$ as

$$\text{Reflection loss (dB)} = 20\log\left|\frac{Z_{in} - Z_0}{Z_{in} + Z_0}\right| \tag{2.3}$$

In general, higher the real and imaginary parts of $\varepsilon_r$ and $\mu_r$ are required in order to have strong microwave absorption, but exceedingly higher the real and imaginary parts of $\varepsilon_r$ and $\mu_r$ induce impedance mismatch due to incident microwave reflections on the surface of the microwave absorber. However, it is not simple to find the $f_m$ and $d_m$ by numerical calculation because of the many variables as can be seen in Eq. (2.2). Therefore, impedance matching solution map is a method for determining appropriate values of $\varepsilon_r$ and $\mu_r$ [42]. After the real and imaginary parts of $\varepsilon_r$ and $\mu_r$ of a material is measured, the $\tan\delta_e$ value can be calculated, the imaginary part of $\mu_r$ can be plotted as a function of the real part of $\mu_r$, and the real part of $\varepsilon_r$ can be plotted which is shown as a dotted line in Fig. 2.2. Perfect impedance matching is satisfied where the $\mu_r$, $\varepsilon'$, and $d/f$ values intersect. Therefore, one can see that the minimum *RL* value is obtainable at this condition. On the other hand, if there is no point of intersection, the impedance matching solution map can be used to determine how the real and imaginary parts of $\varepsilon_r$ and $\mu_r$ should be adjusted to satisfy optimal impedance matching conditions.

## 2.2 Hexaferrites

Hexagonal ferrite is generally composed of iron oxide ($\alpha$-$Fe_2O_3$), barium (or strontium), and divalent transition metals ions ($Fe^{2+}$, $Zn^{2+}$, $Co^{2+}$, $Ni^{2+}$, $Mn^{2+}$, etc.) and represents the crystal structure of hexagonal plate as an oxide generated by reacting at high temperatures. It is used as ferromagnetic or soft magnetic material due to its stable chemical stability and high $M_s$. It can be applied to electromagnetic products in the GHz regions because the hexagonal ferrite is beyond the Snoek's limit by the large uniaxial anisotropy of the *C*-axis. Since it was first discovered by Philips laboratory in the 1950s, a lot of studies have been done so far. The basic composition of hexaferrites can be expressed by the ternary phase diagram of BaO-MeO-$Fe_2O_3$ and is divided into 6 types as shown in Fig. 2.3 [43].

- M-type hexaferrites, (Ba or Sr)$Fe_{12}O_{19}$
- W-type hexaferrites, (Ba or Sr)$Me_2Fe_{16}O_{27}$
- Y-type hexaferrites (Ba or Sr)$_2Me_2Fe_{12}O_{22}$
- Z-type hexaferrites (Ba or Sr)$_3Me_2Fe_{24}O_{41}$
- X-type hexaferrites (Ba or Sr)$_2Me_2Fe_{28}O_{46}$
- U-type hexaferrites (Ba or Sr)$_4Me_2Fe_{36}O_{60}$

### W-type hexaferrite

W-type hexaferrite was first discovered in 1952 as a phase mixed with M-type and X-type hexaferrites. The crystal structure of W-type hexaferrite is very similar to that of M-type hexaferrite, but there is a slight difference in the stacking order. All hexaferrites can be represented by a combination of S, R, and T-block [44]. The S-

block consists of two spinel units with a molecular formula of $2MeFe_2O_4$ and contains two layers of oxygen atoms. The R-block consists of 3 layers of hexagonal structure having a molecular formula of (Ba or Sr)$Fe_6O_{11}$. Each layer contains 4 oxygen atoms, but in the middle layer, one oxygen atom is substituted for a Ba (or Sr) atom. The T-block is composed of 4 layers of oxygen atoms, in which oxygen atoms are substituted with Ba (or Sr) atoms in the middle two layers and has a molecular formula of ($Ba_2$ or $Sr_2$)$Fe_2O_{14}$. From Fig. 2.4, the block of W-type hexaferrite ($BaMe_2Fe_{16}0_{27}$) can be expressed by RSS block. Further simplification enables W-type hexaferrite structure to be represented as M + S where M is M-type hexaferrite and S is spinel block.

In the early stage, W-type hexaferrites have focused for their application as a permanent magnet [45-47]. However, compared to M-type hexaferrite, the application of the permanent magnet is limited due to its low coercivity ($H_c$) [48, 49]. On the other hand, W-type hexaferrites exhibit a high anisotropy field ($H_a$) and thus high FMR frequency in the range of several GHz. Therefore, W-type hexaferrites have been regarded as promising materials for high-frequency microwave absorber applications [50-53].

**Table 2.1.** Absorbed energy with respect to the *RL* values.

| **Reflection loss (dB)** | **Absorbed energy (%)** |
|---|---|
| 0 | 0 |
| −10 | 90 |
| −20 | 99 |
| −30 | 99.9 |
| ⋮ | ⋮ |
| $-\infty$ | 100 |

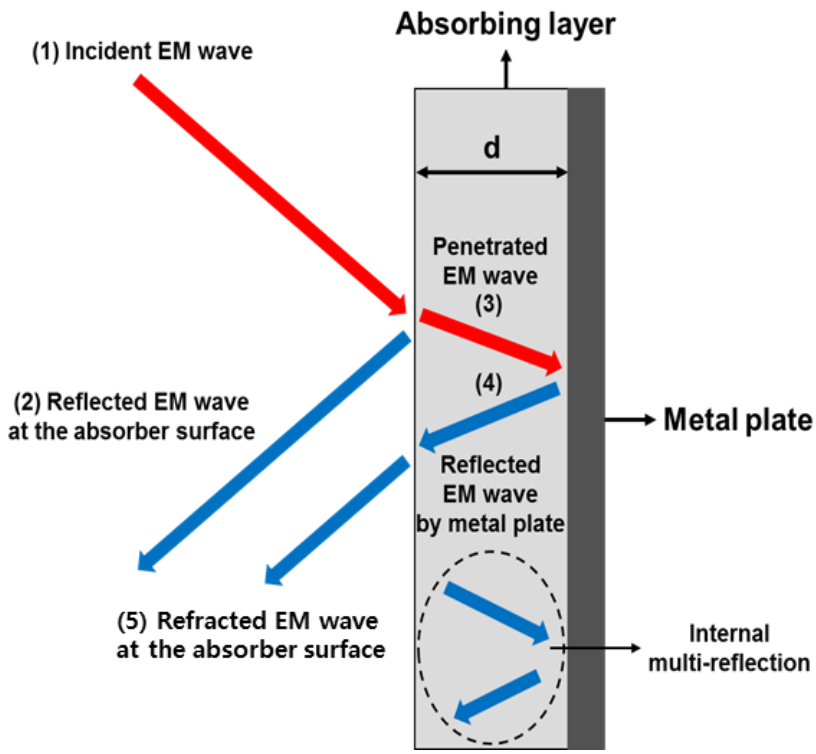


**Figure 2.1.** Schematic of single-layer microwave absorber backed by a metal plate.

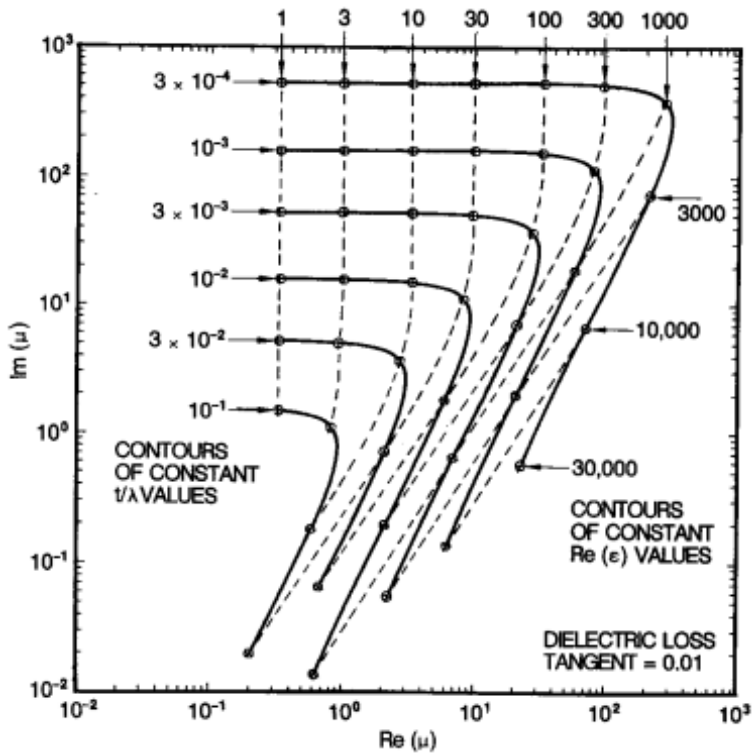


**Figure 2.2.** Impedance matching solution map of $\tan\delta_e = 0.01$ [42].

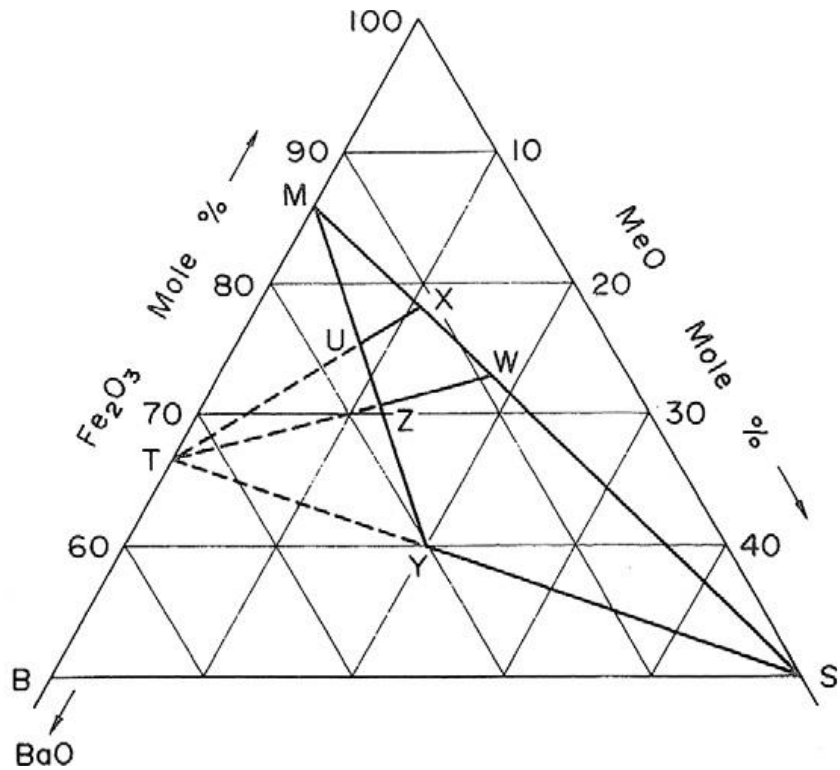


**Figure 2.3.** The BaO-MeO-$Fe_2O_3$ phase diagram [43].

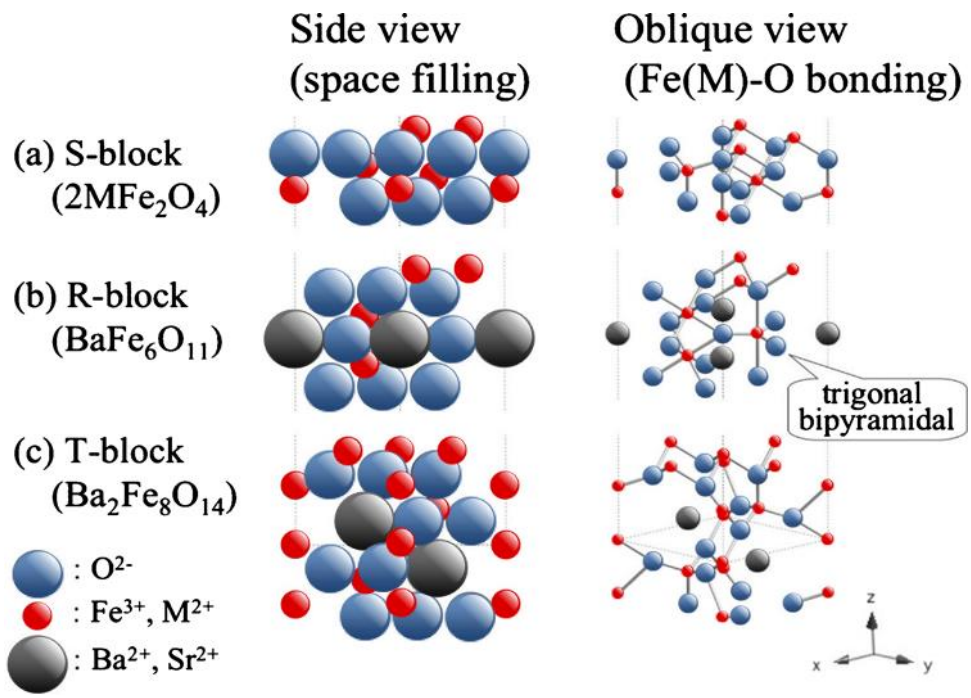


**Figure 2.4.** Basic constituent block in hexagonal ferrite [44].

# References

[1] S.B. Narang, P. Kaur, S. Bahel, K. Pubby, Absorption Characterization of Mn-Zr-Substituted La-Sr Hexaferrite Using Open-Circuit and Short-Circuit Approaches in 8.2-18 GHz Frequency Range, Journal of Electronic Materials, 47 (2018) 820-827.

[2] J. Singh, C. Singh, D. Kaur, S.B. Narang, R. Joshi, S.R. Mishra, R. Jotania, M. Ghimire, C.C. Chauhan, Tunable microwave absorption in Co-Al substituted M-type Ba-Sr hexagonal ferrite, Materials & Design, 110 (2016) 749-761.

[3] B.C. Wang, J.Q. Wei, Y. Yang, T. Wang, F.S. Li, Investigation on peak frequency of the microwave absorption for carbonyl iron/epoxy resin composite, Journal of Magnetism and Magnetic Materials, 323 (2011) 1101-1103.

[4] A. Arora, S.B. Narang, Effect of La-Na Doping in Co-Ti Substituted Barium Hexaferrite on Electrical and X-Band Microwave Absorption Properties, Journal of Electronic Materials, 47 (2018) 4919-4928.

[5] S. Chakraborty, N.S. Bhattacharyya, S. Bhattacharyya, Effect of Co substitution on absorption properties of $SrCo_xFe_{12-x}O_{19}$ hexagonal ferrites based nanocomposites in X-band, Journal of Magnetism and Magnetic Materials, 443 (2017) 244-251.

[6] S.B. Narang, P. Kaur, S. Bahel, C. Singh, Microwave characterization of Co-Ti substituted barium hexagonal ferrites in X- band, Journal of Magnetism and Magnetic Materials, 405 (2016) 17-21.

[7] J. Jin, Y. Liu, M.G.B. Drew, Y. Liu, Preparation and characterizations of $Ba_{1-x}Pb_xFe_{12}O_{19}$/polypyrrole composites, Journal of Materials Science-Materials in Electronics, 28 (2017) 11325-11331.

[8] X.L. Guo, Z.J. Yao, H.Y. Lin, J.T. Zhou, Y.X. Zuo, X.Y. Xu, B. Wei, W.J. Chen, K. Qian, Epoxy resin addition on the microstructure, thermal stability and microwave absorption properties of core-shell carbonyl iron@epoxy composites, Journal of Magnetism and Magnetic Materials, 485 (2019) 244-250.

[9] S.C. Dang, Y. Lin, X.Z. Wei, H. Ye, Design and preparation of an ultrawideband gradient triple-layered planar microwave absorber using flaky carbonyl iron as absorbent, Journal of Materials Science-Materials in Electronics, 29 (2018) 17651-17660.

[10] Q.C. Liu, Z.F. Zi, M. Zhang, A.B. Pang, J.M. Dai, Y.P. Sun, Enhanced microwave absorption properties of carbonyl iron/$Fe_3O_4$ composites synthesized by a simple hydrothermal method, Journal of Alloys and Compounds, 561 (2013) 65-70.

[11] Z. Ma, Y. Zhang, C.T. Cao, J. Yuan, Q.F. Liu, J.B. Wang, Attractive microwave absorption and the impedance match effect in zinc oxide and carbonyl iron composite, Physica B-Condensed Matter, 406 (2011) 4620-4624.

[12] C. Stergiou, Magnetic, dielectric and microwave absorption properties of rare earth doped Ni-Co and Ni-Co-Zn spinel ferrites, Journal of Magnetism and Magnetic Materials, 426 (2017) 629-635.

[13] Y. Liu, X. Liu, X. Wang, Synthesis and microwave absorption properties of Ni-Zn-Mn spinel ferrites, Advances in Applied Ceramics, 114 (2015) 82-86.

[14] A. Ghasemi, G.R. Gordani, E. Ghasemi, $Co_2W$ hexaferrite nanoparticles-carbon nanotube microwave absorbing nanocomposite, Journal of Magnetism and Magnetic Materials, 469 (2019) 391-397.

[15] H. Nikmanesh, M. Moradi, G.H. Bordbar, R.S. Alam, Effect of multi dopant barium hexaferrite nanoparticles on the structural, magnetic, and X-Ku bands microwave absorption properties, Journal of Alloys and Compounds, 708 (2017) 99-107.

[16] A. Baniasadi, A. Ghasemi, A. Nemati, M.A. Ghadikolaei, E. Paimozd, Effect of Ti-Zn substitution on structural, magnetic and microwave absorption characteristics of strontium hexaferrite, Journal of Alloys and Compounds, 583 (2014) 325-328.

[17] J. Chen, P. Meng, M. Wang, G. Zhou, X. Wang, G. Xu, Electromagnetic and microwave absorption properties of $BaMgxCo_{1-x}TiFe_{10}O_{19}$, Journal of Alloys and Compounds, 679 (2016) 335-340.

[18] H. Sozeri, Z. Mehmedi, H. Erdemi, A. Baykal, U. Topal, B. Aktas, Microwave properties of $BaFe_{11}Mg^{2+}_{0.25}X^{2+}_{0.25}Ti^{4+}_{0.25}O_{19}$ ($X^{2+}$ = Cu, Mn, Zn, Ni and Co) nanoparticles in 0-26.5 GHz range, Ceram. Int., 42 (2016) 2611-2625.

[19] Z.D. Zhang, Z.C. Shi, R.H. Fan, M. Gao, J.Y. Guo, X.G. Qi, K.N. Sun, Microwave absorption properties of $Fe@Al_2O_3$ nanoembedments prepared by mechanosynthesis, Materials Chemistry and Physics, 130 (2011) 615-618.

[20] X.D. Chen, G.Q. Wang, Y.P. Duan, S.H. Liu, Microwave absorption properties of barium titanate/epoxide resin composites, Journal of Physics D-Applied Physics, 40 (2007) 1827-1830.

[21] I.S. Unver, Z. Durmus, Magnetic and Microwave Absorption Properties of Magnetite ($Fe_3O_4$)@ Conducting Polymer (PANI, PPY, PT) Composites, Ieee Transactions on Magnetics, 53 (2017).

[22] D.C. Tiwari, P. Dipak, S.K. Dwivedi, T.C. Shami, P. Dwivedi, PPy/$TiO_2$(np)/CNT polymer nanocomposite material for microwave absorption, Journal of Materials Science-Materials in Electronics, 29 (2018) 1643-1650.

[23] Y.H. Chen, Z.H. Huang, M.M. Lu, W.Q. Cao, J. Yuan, D.Q. Zhang, M.S. Cao, 3D $Fe_3O_4$ nanocrystals decorating carbon nanotubes to tune electromagnetic properties and enhance microwave absorption capacity, Journal of Materials Chemistry A, 3 (2015) 12621-12625.

[24] K.Q. He, L.M. Yu, L.M. Sheng, K. An, Y. Ando, X.L. Zhao, Doping Effect of Single-Wall Carbon Nanotubes on the Microwave Absorption Properties of Nanocrystalline Barium Ferrite, Japanese Journal of Applied Physics, 49 (2010) 125101.

[25] S. Kumar, G. Datt, A.S. Kumar, A.C. Abhyankar, Enhanced absorption of microwave radiations through flexible polyvinyl alcohol-carbon black/barium hexaferrite composite films, Journal of Applied Physics, 120 (2016) 164901.

[26] J. Qiu, T.T. Qiu, Fabrication and microwave absorption properties of magnetite nanoparticle-carbon nanotube-hollow carbon fiber composites, Carbon, 81 (2015) 20-28.

[27] W. Xing, J. Chen, H. Wang, Q. Fan, Q. Lei, G. Xu, Introduction of $Zn^{2+}$ in $BaCoTiFe_{10}O_{19}$ to tune electromagnetic parameters and improve microwave absorption properties, Journal of Alloys and Compounds, 731 (2018) 279-287.

[28] G.T. Rado, MAGNETIC SPECTRA OF FERRITES, Reviews of Modern Physics, 25 (1953) 81-89.

[29] H.J. Kwon, J.Y. Shin, J.H. Oh, The microwave absorbing and resonance phenomena of Y-type hexagonal ferrite microwave absorbers, Journal of Applied Physics, 75 (1994) 6109-6111.

[30] F.S. Wen, F. Zhang, Z.Y. Liu, Investigation on Microwave Absorption Properties for Multiwalled Carbon Nanotubes/Fe/Co/Ni Nanopowders as Lightweight Absorbers, Journal of Physical Chemistry C, 115 (2011) 14025-14030.

[31] Y. Wei, H. Liu, S. Liu, M. Zhang, Y. Shi, J. Zhang, L. Zhang, C. Gong, Waste cotton-derived magnetic porous carbon for high-efficiency microwave absorption, Composites Communications, 9 (2018) 70-75.

[32] L.J. Yu, Y.F. Zhu, Y.Q. Fu, Waxberry-like carbon@polyaniline microspheres with high-performance microwave absorption, Applied Surface Science, 427 (2018) 451-457.

[33] X. Sun, J.P. He, G.X. Li, J. Tang, T. Wang, Y.X. Guo, H.R. Xue, Laminated magnetic graphene with enhanced electromagnetic wave absorption properties, Journal of Materials Chemistry C, 1 (2013) 765-777.

[34] F. Wan, F. Luo, H.Y. Wang, Z.B. Huang, W.C. Zhou, D.M. Zhu, Effects of carbon black (CB) and alumina oxide on the electromagnetic- and

microwave-absorption properties of SiC fiber/aluminum phosphate matrix composites, Ceram. Int., 40 (2014) 15849-15857.

[35] H. Wang, F. Meng, J. Li, T. Li, Z. Chen, H. Luo, Z. Zhou, Carbonized Design of Hierarchical Porous Carbon/$Fe_3O_4$@Fe Derived from Loofah Sponge to Achieve Tunable High-Performance Microwave Absorption, Acs Sustainable Chemistry & Engineering, 6 (2018) 11801-11810.

[36] P. Kaur, S. Bahel, S.B. Narang, Broad-band microwave absorption of $Sr_{0.85}La_{0.15}(MnZr)_xFe_{12-2x}O_{19}$ hexagonal ferrite in 18-40 GHz frequency range, Journal of Magnetism and Magnetic Materials, 460 (2018) 489-494.

[37] P. Kaur, S.B. Narang, S. Bahel, Modulation of microwave properties of La-Sr hexagonal ferrite with doping of Co-Zr and change in thickness, Journal of Materials Science-Materials in Electronics, 28 (2017) 16077-16085.

[38] G. Shao, J.F. Liang, W.Y. Zhao, B. Zhao, W. Liu, H.L. Wang, B.B. Fan, H.L. Xu, H.X. Lu, Y.G. Wang, R. Zhang, Co decorated polymer-derived SiCN ceramic aerogel composites with ultrabroad microwave absorption performance, Journal of Alloys and Compounds, 813 (2020) 152007.

[39] D.F. Zhang, Z.F. Hao, Y.N. Qian, B. Zeng, H.P. Zhu, Q.B. Wu, C.J. Yan, M.Y. Chen, The design and performance of the nano-carbon based double layers flexible coating for tunable and high-efficiency microwave absorption, Applied Physics a-Materials Science & Processing, 124 (2018) 374.

[40] M.M. Syazwan, M. Hashim, R.S. Azis, I. Ismail, S. Kanagesan, A.N. Hapishah, Enhancing absorption properties of Mg-Ti substituted barium hexaferrite nanocomposite through the addition of MWCNT, Journal of Materials Science-Materials in Electronics, 28 (2017) 8429-8436.

[41] C. Liu, Y. Chen, Y. Yue, Y. Tang, Z. Wang, N. Ma, P. Du, Formation of $BaFe_{12-x}Nb_xO_{19}$ and its high electromagnetic wave absorption properties in millimeter wave frequency range, Journal of the American Ceramic Society, 100 (2017) 3999-4010.

[42] H.M. Musal, H.T. Hahn, Thin-layer electromagnetic absorber design, Ieee Transactions on Magnetics, 25 (1989) 3851-3853.

[43] R.C. Pullar, Hexagonal ferrites: A review of the synthesis, properties and applications of hexaferrite ceramics, Progress in Materials Science, 57 (2012) 1191-1334.

[44] K. Kamishima, N. Hosaka, K. Kakizaki, N. Hiratsuka, Crystallographic and magnetic properties of $Cu_2X$, $Co_2X$, and $Ni_2X$ hexaferrites, Journal of Applied Physics, 109 (2011) 13904.

[45] T. Kagotani, N. Abe, M. Okada, M. Homma, Effects of Alkali-Earth and Rare-Earth-Metal Fluorides Additions on Magnetic-Properties of W-Type Sr Ferrite Powders, Materials Transactions Jim, 31 (1990) 879-883.

[46] S. Ram, J.C. Joubert, Synthesis and magnetic properties of $SrZn_2$-W type hexagonal ferrites using a partial $2Zn^{2+} \rightarrow Li^{+}Fe^{3+}$ substitution: a new series of permanent magnets materials, Journal of Magnetism and Magnetic Materials, 99 (1991) 133-144.

[47] S. Ram, J.C. Joubert, Development of high-quality ceramic powders for $Sr_{0.9}Ca_{0.1}Zn_2$-W type hexagonal ferrite for permanent magnet devices, Ieee Transactions on Magnetics, 28 (1992) 15-20.

[48] G.H. An, T.Y. Hwang, J. Kim, J. Kim, N. Kang, K.W. Jeon, M. Kang, Y.H. Choa, Novel method for low temperature sintering of barium hexaferrite

with magnetic easy-axis alignment, Journal of the European Ceramic Society, 34 (2014) 1227-1233.

[49] X.S. Liu, P. Hernandez-Gomez, K. Huang, S.Q. Zhou, Y. Wang, X. Cai, H.J. Sun, B. Ma, Research on $La^{3+}$-$Co^{2+}$-substituted strontium ferrite magnets for high intrinsic coercive force, Journal of Magnetism and Magnetic Materials, 305 (2006) 524-528.

[50] X.-f. Yang, Q. Jin, Z.-p. Chen, Q.-l. Li, B. Liu, Fabrication and microwave absorbent properties of Cobate zinc substituted W-type $BaCoZnFe_{16}O_{27}$, Journal of Magnetism and Magnetic Materials, 367 (2014) 64-68.

[51] Z.F. Zi, J.M. Dai, Q.C. Liu, H.Y. Liu, X.B. Zhu, Y.P. Sun, Magnetic and microwave absorption properties of W-type $Ba(Zn_xCo_{1-x})_2Fe_{16}O_{27}$ hexaferrite platelets, Journal of Applied Physics, 109 (2011) 7E536.

[52] J.H. You, S.I. Yoo, Improved magnetic properties of Zn-substituted strontium W-type hexaferrites, Journal of Alloys and Compounds, 763 (2018) 459-465.

[53] M.J. Iqbal, R.A. Khan, S. Takeda, S. Mizukami, T. Miyazaki, W-type hexaferrite nanoparticles: A consideration for microwave attenuation at wide frequency band of 0.5-10 GHz, Journal of Alloys and Compounds, 509 (2011) 7618-7624.

# Chapter 3

# Microwave absorption properties of Zn-substituted W-type hexaferrites in the Ku-band (0.5-18 GHz)

## 3.1 Introduction

Among MAMs, the hexaferrites have been most widely used for real applications. Especially W-type hexaferrite can be regarded as promising materials for microwave absorber applications. Since they possess high $M_s$ [1] and further their dielectric loss and magnetic loss parts are relatively high in the microwave region [2], implying that microwave absorbance can be enhanced through a complementation between $\varepsilon''$ and $\mu''$ parts.

Most of researchers on W-type hexaferrites for microwave absorbers have focused on the improvement of their relative complex permittivity and permeability since a W-type hexaferrite composite with higher real and imaginary parts in both $\mu_r$ and $\varepsilon_r$ is more desirable for the fabrication of highly efficient absorber with lower $V_f$ and wider bandwidth. It is also desirable for the fabrication of thinner absorber since the most efficient thickness is known to be inversely proportional to its refractive index. For this purpose, various divalent cations have been fully substituted for the $Fe^{2+}$ sites of W-type hexaferrites [3-8]. Other strategies for improving $\mu_r$ include coating of dielectric material such as $TiO_2$ [9] on the surface of W-type hexaferrites and forming the composite filler composed of W-type hexaferrites and dielectric materials such as $BaTiO_3$ and $TiO_2$ [10-12].

Unlike previous reports on W-type hexaferrites, utilizing a full substitution of divalent cations for the $Fe^{2+}$ site [3-8], we tried to develop highly efficient MAMs from partially Zn-substituted SrW-type hexaferrites. The reason for the selection of partially Zn-substituted SrW-type hexaferrites is as follows. First, according to our previous study on magnetic properties of Zn-substituted SrW-type hexaferrites [13], the $M_s$ values are continuously increased with increasing $x$ up to 1.0 but decreased with further increase of $x$ up to 2.0. Therefore, $\mu_r$ is expected to continuously increase up to $x$ =1.0 since $\mu_r$ is proportional to $M_s$ [14]. Second, higher real and imaginary parts of the relative complex permittivity are expected due to an increased electric conductivity through electron hopping between $Fe^{2+}$ and $Fe^{3+}$ ions [15]. As a result, the partial Zn-substituted SrW-type hexaferrites is expected to enhance the real and imaginary parts of $\varepsilon_r$ and $\mu_r$ at the same time.

Therefore, the microwave absorption properties of the partially Zn-substituted SrW-type hexaferrites were investigated in two distinct frequency regions of 3.4-3.8 and 5.9-7.1 GHz which have been suggested for 5G communications [16-18].

## 3.2 Experimental

Zn-substituted SrW-type ferrites of $SrFe_{2-x}Zn_xW$ with $x$ = 0.0, 0.5, 1.0, and 2.0 were synthesized by solid-state reaction. The $SrCO_3$, $Fe_2O_3$, and ZnO powders of 99.9% purity were used as precursors. The precursors were weighed, ball-milled for 24 h with zirconia balls in ethanol, and dried in an oven at 45 ˚C. As-dried powders were calcined at 1150 ˚C for 8 h in air, ball-milled again for 24 h, and then uniaxially pressed into the pellets of 15 mm in diameter and 2 mm in thickness at a pressure of 180 kg/cm$^2$. As-pressed pellets were sintered at 1315, 1280, and 1250 ˚C for 2 h,

respectively, in low oxygen partial pressure ($PO_2$) of $10^{-3}$ atm, and finally furnace-cooled to room temperature. The $PO_2$ was controlled by using $O_2$-$N_2$ mixed gas (1000 ppm $O_2$ in $N_2$), and the gas flow of rate of 0.5 *l*/min was controlled by a MFC controller. The fully Zn-substituted $SrZn_2W$ ($x$ = 2.0) sample was sintered at 1300 ˚C for 2 h and furnace-cooled in air.

In order to evaluate the microwave absorption properties of all composite samples, the specimens were prepared as follows. Sintered hexaferrite pellets were ground into powder with an alumina mortar and pestle. As-ground hexaferrite powder of each composition was mixed with epoxy resin powder to have the $V_f$ values of 30, 50, 70, and 90%. Each powder mixture was pressed into a toroidal shape with an outer diameter of 7 mm and an inner diameter of 3.04 mm, and subsequently hardened at 175 ˚C for 1 h in air. The measurement of microwave $\varepsilon_r$ and $\mu_r$ was conducted for our toroidal samples by using a vector network analyzer (VNA) (Agilent PNA N5525A) with a coaxial airline. To avoid a resonance effect due to the thickness of toroidal sample within the VNA, the thickness was varied from 0.8 to 4 mm. Both $\varepsilon_r$ and $\mu_r$ were simultaneously measured in the Ku-band frequency region of 0.5–18 GHz by using a transmission and reflection method based on the algorithm developed by Nicolson and Ross [19].

## 3.3 Results and discussion

It is well known that the $\varepsilon'$ and $\mu'$ represent the storage capability of electromagnetic energy while the $\varepsilon''$ and $\mu''$ indicate the loss of electric and magnetic energy, respectively.

Fig. 3.1 shows the complex $\varepsilon_r$ and $\mu_r$ spectra of the $SrFe_{2-x}Zn_xW$ ($x$ = 0.0, 0.5, 1.0, and 2.0) composites with the $V_f$ of 90% as a function of microwave frequency in the Ku-band of 0.5–18 GHz. From Fig. 3.1(a), one can see that the real parts of $\varepsilon'$ are continuously decreased with increasing frequency up to ~10 GHz. This behavior commonly occurs in carbon-based materials and magnetic materials [20]. The reason for this phenomenon arises from the polarization of electric dipole lagging behind the change of the electric field [21, 22]. Interestingly, the oscillation behavior of $\varepsilon_r$ data is observable above ~10 GHz, which is similar to previous reports [23, 24]. However, the occurrence of these results is unclear at this moment and requires further more detailed investigation.

It is also noteworthy that the real and imaginary parts of $\varepsilon_r$ values for composite samples with the $V_f$ of 90% are continuously decreased with increasing $x$, the amount of the Zn substituent, which is most probably due to a continuous decrease in the concentration of $Fe^{2+}$ ions in $SrFe_{2-x}Zn_xW$ samples. The reason is that a polarization by a local displacement of electrical charge carriers can be reduced due to decreased electron hopping between $Fe^{2+}$ and $Fe^{3+}$ ions. A similar behavior has been reported for Al-substituted W-type hexaferrites of $BaCo_2Fe_{16-x}Al_xO_{27}$ in which less electron hopping may occur [25]. Also, according to Fengying *et al.* [3], who reported the microwave absorbing properties of $Ba_{0.9}RE_{0.1}Co_2Fe_{16}O_{27}$ (RE = La, Nd, Sm), the substitution of $RE^{3+}$ ion for the $Ba^{2+}$ sites leads to a change of $Fe^{3+}$ to $Fe^{2+}$ to maintain

charge valence ($Ba^{2+} + Fe^{3+} \rightarrow Re^{3+} + Fe^{2+}$), resulting in the enhancement of the electron hopping between $Fe^{2+}$ and $Fe^{3+}$.

On the other hand, from Fig. 3.1(b), one can see that the real and imaginary parts of $\mu_r$ spectra are initially decreased with increasing frequency up to ~2 GHz. With further increasing frequency, both $\mu'$ and $\mu''$ spectra become almost constant with a small repeated fluctuation in the frequency range of 2-18 GHz. In addition, both the real and imaginary parts of $\mu_r$ spectra are continuously increased from $x$ = 0 to 1.0, and then decreased with further increasing of $x$ to 2.0. In other words, compared with fully Zn-substituted SrW-type hexaferrite of $SrZn_2W$, partially Zn-substituted SrW-type hexaferrites exhibit higher real and imaginary parts of $\mu_r$. The dependence of $\mu'$ on the amount of Zn substituent, $x$, can be understood on the basis of increased $M_s$ together with decreased anisotropy field ($H_a$) as discussed in our previous paper [13]. According to Snoek's law, $\mu_r$ is proportional to $M_s$ and inversely proportional to $H_a$. This law can be written as follows,

$$\mu' - 1 = \frac{4\pi M_s}{3} \frac{1}{H_a}$$

where $\mu_i'$ is the real part of initial permeability. The proportionality between $\mu_i'$ and $M_s$ has also been found for other hexaferrites such as $BaZn_{2-x}Co_xFe_{16}O_{27}$ [26] and $BaZn_{2-x}Cu_xFe_{12}O_{22}$ [27]. In Fig. 3.1(b), the multiple resonance peaks are observed at frequencies lower than 1 GHz. This result might come from different types of ferromagnetic resonances such as domain wall resonance and spin or magnetic domain rotation in polycrystalline hexaferrites [14]. However, the ferromagnetic resonance peaks of $SrFe_{2-x}Zn_xW$ are undetectable since the ferromagnetic resonance may exist over the Ku-band because of strong $c$-axis anisotropy for the divalent ions

such as $Fe^{2+}$, $Zn^{2+}$ and $Ni^{2+}$ [7, 28, 29] Meanwhile, the $BaCo_2W$ has a planar anisotropy because the substitution of $Co^{2+}$ for the $Fe^{2+}$ sites can change the crystalline anisotropy from *c*-axis uniaxial to *c*-plane planar anisotropy [4].

Fig. 3.2 shows the dielectric tangent loss ($\tan\delta_e$) and magnetic tangent loss ($\tan\delta_m$) of the SrFeZnW composites with the $V_f$ of 30, 50, 70, and 90% as a function of frequency in the Ku-band. These graphs are derived from the formula of $\tan\delta_e = \varepsilon''/\varepsilon'$ and $\tan\delta_m = \mu''/\mu'$, respectively. From Fig. 3.2(a), it can be seen that higher $\tan\delta_e$ values are obtainable from the SrFeZnW composites with $V_f$ of 50 and 70% compared with those with $V_f$ of 30 and 90%, and thus enhanced capability of microwave absorption is expected for these samples. However, from Fig. 3.2(b), it is clearly observed that the $\tan\delta_m(f)$ curve is very similar to the $\mu''(f)$ curve in Fig. 3(b), and hence the $\tan\delta_m$ values are decreased with increasing frequency up to ~2 GHz. When the frequency is further increased above ~2 GHz, the $\tan\delta_e$ values are much larger than the $\tan\delta_m$ values, suggesting that, in this frequency region, the microwave absorption of SrFeZnW composites originates mainly from $\tan\delta_e$ rather than $\tan\delta_m$. Particularly, it should be noted that, although SrW hexaferrites are known as magnetic materials, the $\tan\delta_e$ (i.e., dielectric loss) in unsubstituted and partially Zn-substituted SrW hexaferrites is the major source of energy dissipation due to improved $\varepsilon'$ and $\varepsilon''$ values which are comparable to dielectric materials [30].

It is well known that the $\varepsilon''$ mainly arises from conductivity loss and polarization loss [31], where polarization can be classified into dipole, interfacial, ionic, and electronic polarization [32]. According to free electron theory ($\varepsilon'' = 1/2\varepsilon_o\rho\pi f$) [33], higher conductivity results in larger $\varepsilon''$. However, ionic and electronic polarization are negligible in microwave absorption since these polarizations are detectable only at a much higher frequency region ($10^3$-$10^6$ GHz) [34, 35]. On the other hand,

interfacial polarization loss occurs at the interfaces between filler particles and epoxy resin in the MAM composites, and thus non-uniform distribution of space charges at the interfaces will enhance $\varepsilon''$ [36]. In order to identify the dielectric loss mechanism of $SrFe_{2-x}Zn_xW$ composites, the Debye relaxation was considered. The relationship between $\varepsilon'$ and $\varepsilon''$ can be expressed as follows [32, 33],

$$\varepsilon_r = \varepsilon_\infty + \frac{\varepsilon_s - \varepsilon_\infty}{1 + j2\pi f} = \varepsilon' - j\varepsilon'' \tag{3.1}$$

where $\varepsilon_s$ is static permittivity, $\varepsilon_\infty$ is relative dielectric permittivity at the high-frequency limit, ω is angular frequency, and τ is relaxation time. From Eq. (3.1), $\varepsilon'$ and $\varepsilon''$ can be deduced by

$$\varepsilon'(f) = \varepsilon_\infty + \frac{\varepsilon_s - \varepsilon_\infty}{(2\pi f)^2 \tau^2} \tag{3.2}$$

$$\varepsilon''(f) = \varepsilon_\infty + \frac{2\pi f \tau(\varepsilon_s - \varepsilon_\infty)}{1 + (2\pi f)^2 \tau^2} \tag{3.3}$$

According to Eqs. (3.2) and (3.3), the relationship between ε′ and ε″ can be described by

$$(\varepsilon' - \frac{\varepsilon_s - \varepsilon_\infty}{2})^2 + (\varepsilon'')^2 = (\frac{\varepsilon_s - \varepsilon_\infty}{2})^2 \tag{3.4}$$

Based on Eq. (3.4), if there is a polarization relaxation, the plot of ε′ and ε″ should be a single semicircle, which is defined as the Cole-Cole semicircle, and each semicircle corresponds to one Debye relaxation. For the SrFeZnW composites with the $V_f$ values of 30, 50, 70, and 90%, Cole-Cole semicircles are plotted in Fig. 3.2(c).

The shapes of the Cole-Cole plots are imperfect semicircles, implying that the relaxation is a multi-relaxation process [37]. In other words, when several relaxations are coexisting, each separate relaxation would deviate from an ideal Debye relaxation. In addition, one can see that a clear difference is observed for the SrFeZnW composite with the $V_f$ of 30%, the Cole-Cole shape is close to a straight line, which is mainly attributable to a weak polarization loss compared with those with $V_f$ of 50, 70, and 90%. It can also be seen that the Cole-Cole semicircles become larger and more enhanced with increasing $V_f$ in the composites, implying that, with increasing $V_f$, the interfacial polarization is increased, and thus the $\varepsilon''$ value is enhanced.

For the $SrFe_2W$ composites with the $V_f$ values of 30, 50, 70, and 90%, their $\varepsilon_r$ and $\mu_r$ spectra are plotted in Fig. 3.3 as a function of frequency in the region of 0.5–18 GHz. All real and imaginary parts of $\varepsilon'$, $\varepsilon''$, $\mu'$, and $\mu''$ are decreased with decreasing hexaferrite filler $V_f$ (or with increasing the epoxy-resin matrix fraction). The reason is that the real and imaginary parts of $\varepsilon_r$ and $\mu_r$ ($\varepsilon' \approx 3$, $\varepsilon'' \approx 0$, $\mu' \approx 1$, and $\mu'' \approx 0$) of epoxy resin, which were independently measured though not presented, are much lower than those of the $SrFe_2W$ hexaferrite.

According to the transmission line theory, the normalized input impedance $Z_{in}$ of a single layer microwave absorber backed by a perfect conductor is given by

$$\frac{Z_{in}}{Z_0} = \sqrt{\frac{\mu_r}{\varepsilon_r}} \tanh\left[ j(2\pi fd / c)\sqrt{\mu_r \varepsilon_r} \right] \tag{3.5}$$

where $Z_0 = \sqrt{\mu_0 / \varepsilon_0}$ is the characteristic impedance of free space. $c$ is the speed of light, $f$ is the frequency of the microwave, and $d$ is the thickness of the absorber.

Impedance matching between the microwave absorber and free space is important for the achievement of superior microwave absorption properties. The *RL* of a single layer microwave absorber backed by a conductive metal plate, which is the absorption of the incident microwave in the absorber, is related to $Z_{in}$ as the following,

$$\text{Reflection loss (dB)} = 20\log\left|\frac{Z_{in} - Z_0}{Z_{in} + Z_0}\right| \tag{3.6}$$

The *RL* values were calculated by inserting the $\varepsilon_r$ and $\mu_r$ spectra values of samples shown in Figs. 3.1 and 3.3 into Eqs. (3.5) and (3.6), and represented as the *RL* maps in Figs. 3.4-3.7 up to the thicknesses of 4 mm. In the *RL* maps, the regions with *RL* $\leq -10$ dB (90% absorption of incident microwave) are enclosed with black lines. In Figs. 3.4-3.7, it can also be seen that, as the $V_f$ decreases, the areas with *RL* $\leq -10$ dB are shifted to higher thickness regions at the same composition. This is due to the quarter wavelength principle which can be expressed as follows,

$$d = \frac{\lambda}{4} = \frac{c}{4f\sqrt{\mu_r \varepsilon_r}} \tag{3.7}$$

where $d$ is the thickness of the absorber, $\lambda$ is the wavelength of the microwave, $f$ is the frequency of the microwave, and $c$ is the speed of light. According to Eq. (3.7), thinner thickness or lower matching frequency can be obtained from an absorber with higher refractive index. In addition, the $SrFe_{2-x}Zn_xW$ ($x$ = 0.0, 0.5, and 1.0) composites have thinner thickness area of *RL* $\leq -10$ dB (90% absorption of incident microwave) compared with the $SrZn_2W$ composites as shown in Figs. 3.4-3.7, which is mainly attributable to higher real and imaginary parts of $\varepsilon_r$ in $SrFe_{2-x}Zn_xW$ ($x$ = 0.0, 0.5, and 1.0) composites caused by the presence of $Fe^{2+}$ ions, resulting in higher refractive index.

The minimum *RL* value, $RL_{min}$, for each composition can be achieved when impedance matching occurs between the microwave absorber and free space. The impedance matching condition is satisfied when the input impedance of the absorber is identical to the characteristic impedance of free space. Therefore, the impedance matching condition should be taken into account for designing a microwave absorber. From Eq. (3.5), the ratio of $Z_{in}/Z_0$ can be calculated with the variables of $\mu_r$, $\varepsilon_r$, $f$, and $d$. There exist a matching frequency ($f_m$) and a matching thickness ($d_m$) which satisfies the impedance matching condition for a given $\mu_r$ and $\varepsilon_r$ spectra. Fig. 3.8 shows the real and imaginary parts of $Z_{in}/Z_0$, calculated by Eq. (3.5), and the *RL* values, calculated by Eq. (3.6), as a function of frequency for the SrFeZnW composites with the $V_f$ of 30, 50, 70, and 90%. One can see that the *RL* value becomes a minimum at the matching frequency, $f_m$, where the real part of $Z_{in}/Z_0$ approaches 1 and the imaginary part of $Z_{in}/Z_0$ approaches 0. For the SrFeZnW composites with the $V_f$ of 70%, impedance matching occurs at a $f_m$ of 5.7 GHz with a $d_m$ value of 2.40 mm, at which the minimum *RL* value of −69.9 dB was obtained as listed in Table 3.1. However, for the $V_f$ values of 30 and 90%, it was impossible to achieve good impedance matching, and thus relatively poor absorption properties of *RL* values were obtained. Consequently, it is obvious that the partial substitution of $Zn^{2+}$ ion for the $Fe^{2+}$ site in SrW-type hexaferrites can enhance the absorption properties with reduced filler $V_f$ from 90 to 70%.

The $RL_{min}$ spectra of the SrFeZnW composites were calculated at their matching thicknesses, and presented in Fig. 3.9. This figure shows that while their $RL_{min}$ values of the composite samples with the $V_f$ values of 30 and 90% are relatively higher, those of the composite sample with $V_f$ of 50 and 70% are much lower since it has a good impedance matching as shown in Fig. 3.8(b) and (c). In general, higher real and

imaginary parts of $\varepsilon_r$ and $\mu_r$ are desirable for high performance MAM since $\varepsilon_r$ and $\mu_r$ can be controlled by varying $V_f$ to satisfy the good impedance matching. However, extraordinary high (or low) real and imaginary parts of $\varepsilon_r$ and $\mu_r$ (for instance, the composite samples with $V_f$ of 30 and 90%) induce a serious impedance mismatch due to incident microwave reflections on the surface of the microwave absorber.

Now, our results are compared with previous reports on other fully Zn-substituted Sr(or Ba)$Zn_2$W-type hexaferrites [38, 39]. According to A.R. Farhadizadeh *et al.* [39], the $RL_{min}$ value of $SrZn_2W$ composite with the $V_f$ of 90% was −10.2 dB at 10.3 GHz and 4.5 mm. For a direct comparison, the matching frequency of our $SrZn_2W$ composite with the $V_f$ of 90% is adjusted around 10 GHz. As a result, it is confirmed that a 1.5 mm-thick $SrZn_2W$ exhibited the *RL* value of −15.4 dB at 10 GHz. However, it is difficult to compare deeply microwave absorption properties with our data because they simply calculated the *RL* value without showing the real and imaginary parts of $\varepsilon_r$ and $\mu_r$. On the contrary, J. Zhang *et al.* [38] reported that the $RL_{min}$ value of $BaZn_2W$ was −17 dB at 9 GHz and 3.5 mm. Since a $V_f$ was not indicated in this report, the microwave absorption properties are compared with the most similar real and imaginary parts of $\varepsilon_r$ and $\mu_r$ values among our samples ($SrZn_2W$ composites with the $V_f$ of 30%). As a result, the matching frequency of $SrZn_2W$ is modified around 9 GHz. Thus, a 3.4 mm-thick $SrZn_2W$ exhibited *RL* of −9.5 dB at 9 GHz. This result is mainly due to a difference in the real and imaginary parts of $\varepsilon_r$ values. The $BaZn_2W$ composite showed the $\varepsilon'$ of 4.7, $\varepsilon''$ of 0.25, $\mu'$ of 1.05 and $\mu''$ of 0.5 at 9 GHz while our $SrZn_2W$ composite with the $V_f$ of 30% has an $\varepsilon'$ of 6.3, $\varepsilon''$ of 1.45, $\mu'$ of 1.04, and $\mu''$ of 0.1 at 9 GHz. Hence, the real and imaginary parts of $\varepsilon_r$ for our $SrZn_2W$ composite are too high to satisfy impedance matching, and thus the *RL* values are higher than −10 dB in the Ku-band.

In order to find an optimal absorber thickness, the thickness dependence of the *RL* values was calculated for all composite samples, and plotted for $SrFe_{2-x}Zn_xW$ ($x$ = 0.5 and 1.0) composites as representatives in Fig. 3.10. The calculations were carried out with a step of 0.05 mm. According to Eq. (3.7), the thickness is inversely proportional to peak frequency. Thus, the hump of *RL* curve has been shifted toward lower frequency regions with increasing the thickness. This result is a typical behavior of the thickness dependence of the *RL* value as observed for another hexaferrite [40], indicating that the $RL_{min}$ value can be easily adjusted by varying the thickness of MAMs at an aimed frequency.

It must be interesting to compare the bandwidths of our samples with previously reported values in the two distinctive regions of 3.4-3.8 and 5.9-7.1 GHz [15, 41-49]. The microwave absorption properties are summarized in Table 3.2. It can be seen that in order to have wider bandwidth, impedance matching should occur near the aimed frequency regions as shown in Table 3.2. Moreover, according to Eq. (3.7), both real and imaginary parts of $\varepsilon_r$ and $\mu_r$ values (and thus refractive index) must be very high to achieve bandwidth including the frequency region of 3.4-3.8 GHz. From Table 3.2, one can see that it is impossible to achieve the bandwidth in the region of 3.4-3.8 GHz from previous reports because of lower real and imaginary parts of $\varepsilon_r$ and $\mu_r$ except partially Zn-substituted $Ba_2Y$-type hexaferrites of $Ba_2Fe_{2-x}Zn_xFe_{12}O_{22}$ ($x$ = 0.5, 1.0, 1.5, and 2.0) [15].

To find the most appropriate absorber in two distinctive frequency regions of 3.4-3.8 and 5.9-7.1 GHz, two different $SrFe_{2-x}Zn_xW$ composites of $x$ = 0.5 and 1.0 for the region of 3.4-3.8 GHz, and two different $SrFe_{2-x}Zn_xW$ composites of $x$ = 1.0 and 2.0 for the region of 5.9-7.1 GHz are selected from Table 3.2. Their *RL* values are plotted as a function of frequency in two different frequency regions of 3.4-3.8 and

5.9-7.1 GHz in Fig. 3.11(a) and (b), respectively. For a comparison, previously reports *RL* values as the function of frequency for $Ba_2Fe_{2-x}Zn_xY$-type hexaferrite-epoxy resin composite [15] and BaCoZnW-type hexaferrite [43] are also presented in this figure. From Fig. 3.11(a), it is obvious that the $SrFe_{1.5}Zn_{0.5}W$ composite with the $V_f$ of 90% is the most appropriate in the region of 3.4-3.8 GHz from the viewpoint of absorbance with RL below −10 dB, thickness, and weight although all three different composites are applicable in this frequency region. On the other hand, in the frequency region of 5.9-7.1 GHz, the SrFeZnW composite with the $V_f$ of 70% is the most appropriate from the same viewpoint although all four different composites are applicable.

In general, carbon-based materials i.e., (carbon nanotubes, carbon black, carbon nanofiber, and graphite) are well known as lightweight MAMs with lower $V_f$ due to their unique structure and excellent $\varepsilon_r$ spectra [47-49]. Generally, the $\varepsilon_r$ spectra for these carbon-based materials are varied by the amount of loaded filler [47]. This behavior is mainly attributable to a change in electrical conductivity [50]. Although, carbon-based materials have relatively higher $\varepsilon_r$ spectra, its real application is difficult due to their real and imaginary parts of $\mu_r$ value. Their $\mu_r$ spectra are considered to be close to those of the composite matrix, and thus, it is difficult to expect higher *RL* value from carbon-based materials because the refractive index is dependent on the product between $\varepsilon_r$ and $\mu_r$ according to Eq (3.7), suggesting that it is very hard to fabricate a high-performance MAM composed of a single type carbon-based material.

Consequently, the substitution of $Zn^{2+}$ for the $Fe^{2+}$ sites in the SrW-type hexaferrites exhibit higher *RL* values with wider bandwidth in the frequency regions of 3.4-3.8 and 5.9-7.1 GHz compared with other MAMs. Although higher *RL* values

are obtainable from other hexaferrites and carbon-based materials, those are inadequate for real application due to much smaller bandwidth. These results strongly support that the substitution of $Zn^{2+}$ for the $Fe^{2+}$ site in the SrW-type hexaferrites is very effective for lowering the *RL* value with wider bandwidth and thinner thickness, *d* (1.93-3.05 mm).

## 3.4 Summary

The complex permittivity, permeability, and microwave absorption properties of $SrFe_{2-x}Zn_xW$ composites with the $V_f$ of 30, 50, 70, and 90% in the frequency range of 0.5–18 GHz were investigated. The partial substitution of $Zn^{2+}$ greatly increased the complex permittivity which is attributable to the replacement of $Fe^{2+}$ ions and the electron hopping between $Fe^{2+}$ and $Fe^{3+}$ ions. The complex permeability values were also slightly increased compared to the composite of fully Zn-substituted W-type hexaferrite. Owing to the increased real and imaginary parts of relative complex permittivity and permeability, the composites of partially Zn-substituted W-type hexaferrites exhibited lower *RL* values with wider bandwidth. Among all samples, a 2.8 mm-thick $SrFe_{1.5}Zn_{0.5}W$ composite with the $V_f$ of 90% exhibited the most appropriate for application in the frequency region of 3.4-3.8 GHz, having the reflection loss (*RL*) of −46 dB at 3.6 GHz with the bandwidth of 0.43 GHz (3.38-3.81 GHz) below −10 dB, while a 2.15 mm-thick SrFeZnW composite with the $V_f$ of 70% showed the most appropriate for application in the frequency region of 5.9-7.1 GHz, possessing the *RL* value of −23.7 dB at 6.6 GHz with bandwidth of 1.38 GHz (5.85-7.23 GHz) below −10 dB. Therefore, partially Zn-substituted SrW-type hexaferrites are very promising candidates applicable to 5G communications.

**Table 3.1.** The list of $d_m$, $f_m$, *RL*, and bandwidth (below ≤ −10 dB) of $SrFe_{2-x}Zn_xW$ ($x$ = 0.0, 0.5, 1.0, and 2.0) composites with various $V_f$ values.

| Zn content (x) | $V_f$ (%) | $d_m$ (mm) | $f_m$ (GHz) | *RL* (dB) | Bandwidth ≤ −10 dB (GHz) |
|---|---|---|---|---|---|
| 0.0 | 90 | 2.64 | 3.7 | −22.2 | 0.50 (3.43-3.93 GHz) |
| | 70 | 1.26 | 9.9 | −52.5 | 1.67 (9.33-11 GHz) |
| | 50 | 0.87 | 17.9 | −39.2 | 1.74 (16.26-18 GHz) |
| | 30 | 3.93 | 17.3 | −62.0 | 1.42 (16.58-18 GHz) |
| 0.5 | 90 | 2.62 | 3.8 | −57.7 | 0.50 (3.58-4.08 GHz) |
| | 70 | 0.80 | 15.4 | −48.1 | 2.51 (14.13-16.64 GHz) |
| | 50 | 1.16 | 13.4 | −42.6 | 1.42 (12.55-13.97 GHz) |
| | 30 | 3.83 | 16.7 | −45.4 | 1.45 (15.87-17.32 GHz) |
| 1.0 | 90 | 3.16 | 3.5 | −25.6 | 0.52 (3.22-3.74 GHz) |
| | 70 | 2.40 | 5.7 | −69.9 | 1.27 (5.30-6.57 GHz) |
| | 50 | 1.90 | 9.3 | −60.6 | 2.17 (8.25-10.42 GHz) |
| | 30 | 1.43 | 17.9 | −21.1 | 2.24 (15.76-18 GHz) |
| 2.0 | 90 | 0.94 | 17.1 | −21.2 | 2.63 (15.37-18 GHz) |
| | 70 | 1.14 | 17.1 | −27.1 | 3.03 (14.97-18 GHz) |
| | 50 | 1.95 | 11.3 | −66.2 | 3.69 (9.72-13.41 GHz) |
| | 30 | 2.38 | 13.5 | −9.7 | |

**Table 3.2.** The list of fillers, matrices, *d*, *f*, *RL*, bandwidths covering two different frequency regions of 3.4-3.8 and 5.9-7.1 GHz (*RL* below −10 dB).

| MAM filler | Filler $V_f$ (%) | *d* (mm) | *f* (GHz) | *RL* (dB) | Bandwidth (GHz) (*RL* ≤ −10 dB) | | Ref. |
|---|---|---|---|---|---|---|---|
| | | | | | 3.4-3.8 GHz | 5.9-7.1 GHz | |
| SrW | 70 | 1.93 | 6.4 | −25.1 | | 0.95 (5.91-6.86) | Present results |
| $SrFe_{1.5}Zn_{0.5}W$ | 90 | 2.80 | 3.6 | −46.0 | 0.43 (3.38-3.81) | | |
| $SrFe_{1.5}Zn_{0.5}W$ | 70 | 2.06 | 6.1 | −23.9 | | 1.04 (5.55-6.59) | |
| SrFeZnW | 90 | 2.99 | 3.7 | −23.6 | 0.51 (3.41-3.92) | | |
| SrFeZnW | 70 | 2.15 | 6.6 | −23.7 | | 1.38 (5.85-7.23) | |
| $SrZn_2W$ | 50 | 3.05 | 6.7 | −42.1 | | 2.08 (5.80-7.88) | |
| $Ba_2Zn_2Y$ | 90 | 4.00 | 7.1 | −21.8 | 3.28 (2.98 -6.26) | | [15] |
| $Ba_2Fe_{1.5}Zn_{0.5}Y$ | 30 | 2.60 | 6.9 | −25.4 | | 2.39 (5.90-8.29) | [15] |
| BaM | 30 | 2.40 | 12.0 | −30.0 | | | [41] |
| $BaNi_{0.2}Co_{0.8}TiM$ | 50 | 2.00 | 16.0 | −47.0 | | | [42] |
| BaCoZnW | 50 | 2.40 | 8.0 | −17.0 | | 10.00 (5.50-15.50) | [43] |
| $BaCoZnAl_{0.2}Ce_{0.2}W$ | 100 | 4.37 | 6.8 | −34.7 | | 1.20 (6.20-7.40) | [44] |
| $Ba_{0.8}La_{0.2}Co_{0.9}Zn_{1.1}W$ | 49 | 2.00 | 12.6 | −39.6 | | | [45] |
| $Ba_{0.85}Sm_{0.15}Co_2W$ | 35 | 1.80 | 17.0 | −23.0 | | | [46] |
| SWCNT | 5 | 2.00 | 7.5 | −13.0 | | 1.00 (6.20-7.20) | [47] |
| MWCNT | 4 | 2.00 | 7.6 | −17.0 | | | [48] |
| CB | 10 | 3.00 | 7.1 | −18.0 | | 1.70 (6.10-7.80) | [49] |

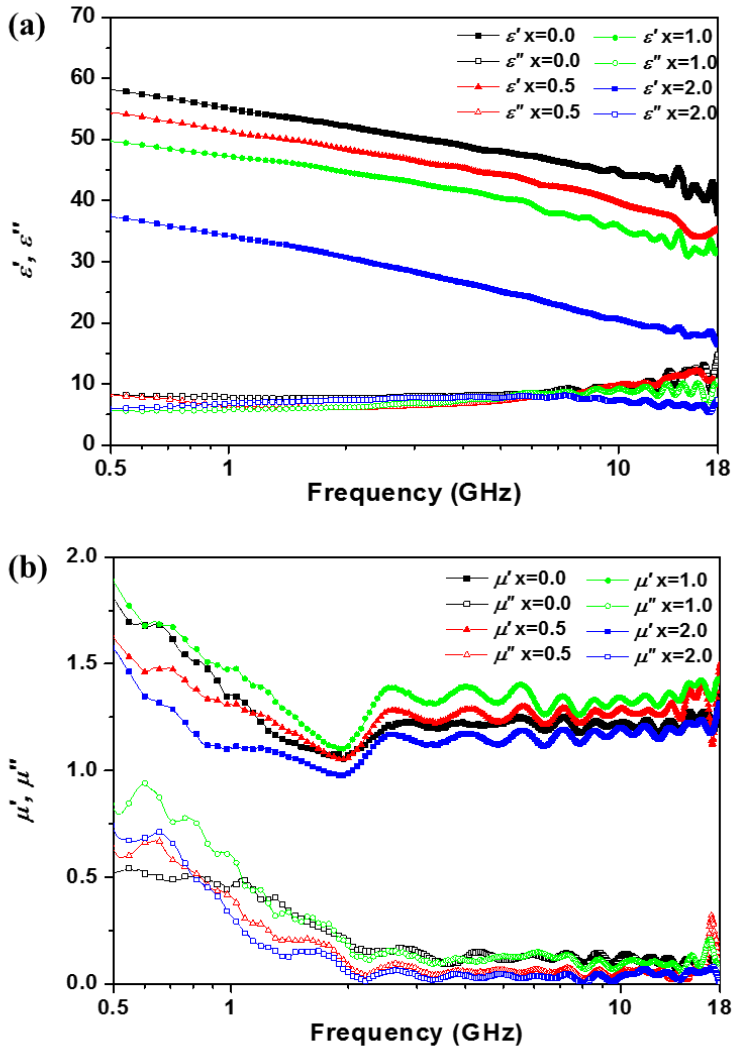


**Fig. 3.1.** The real and imaginary parts of complex permittivity in (a), and those of complex permeability in (b) for all composite samples with the $V_f$ of 90%.

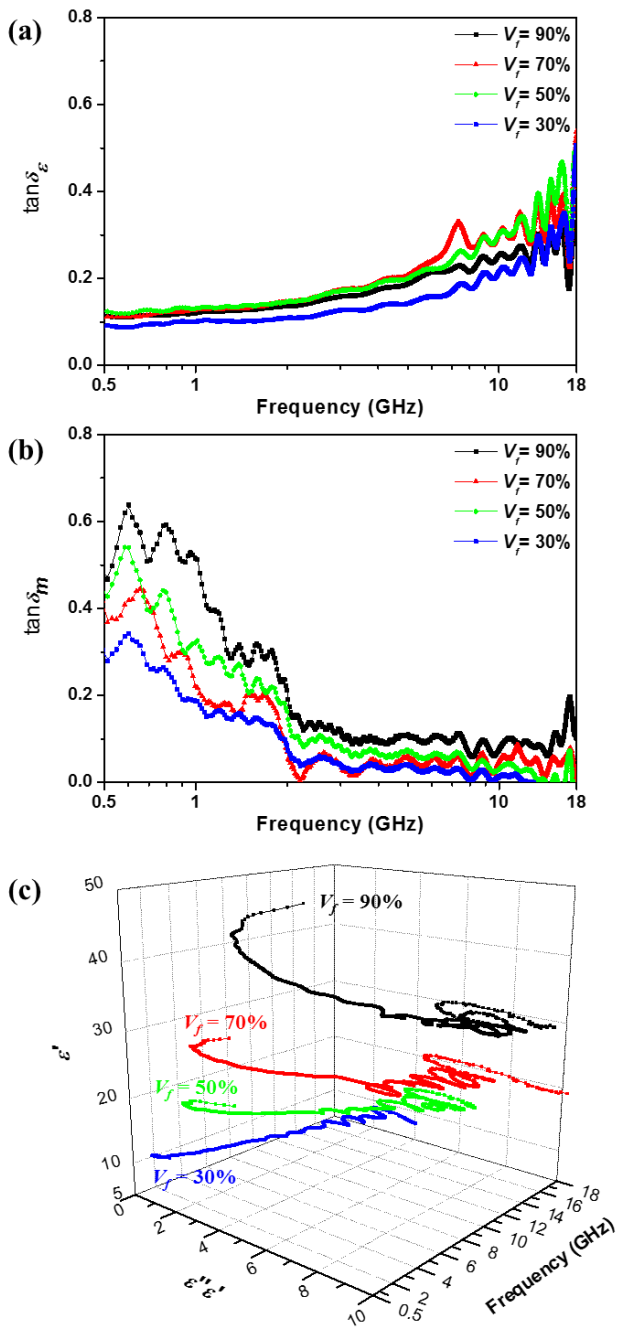


**Fig. 3.2.** (a) Dielectric loss tangent, (b) magnetic loss tangent, (c) Cole-Cole plot of the SrFeZnW composites with the $V_f$ values of 30, 50, 70, and 90%.

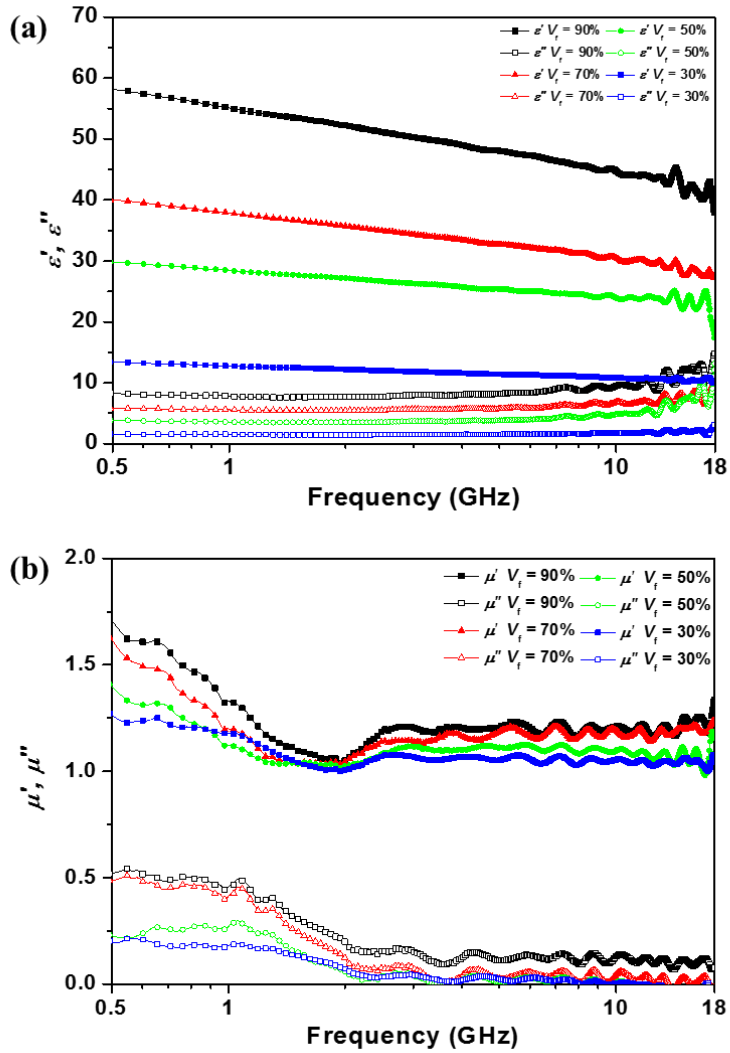


**Fig. 3.3.** The real and imaginary parts of complex permittivity in (a), and those of complex permeability in (b) for the $SrFe_2W$ composites with the $V_f$ values of 30, 50, 70, and 90%.

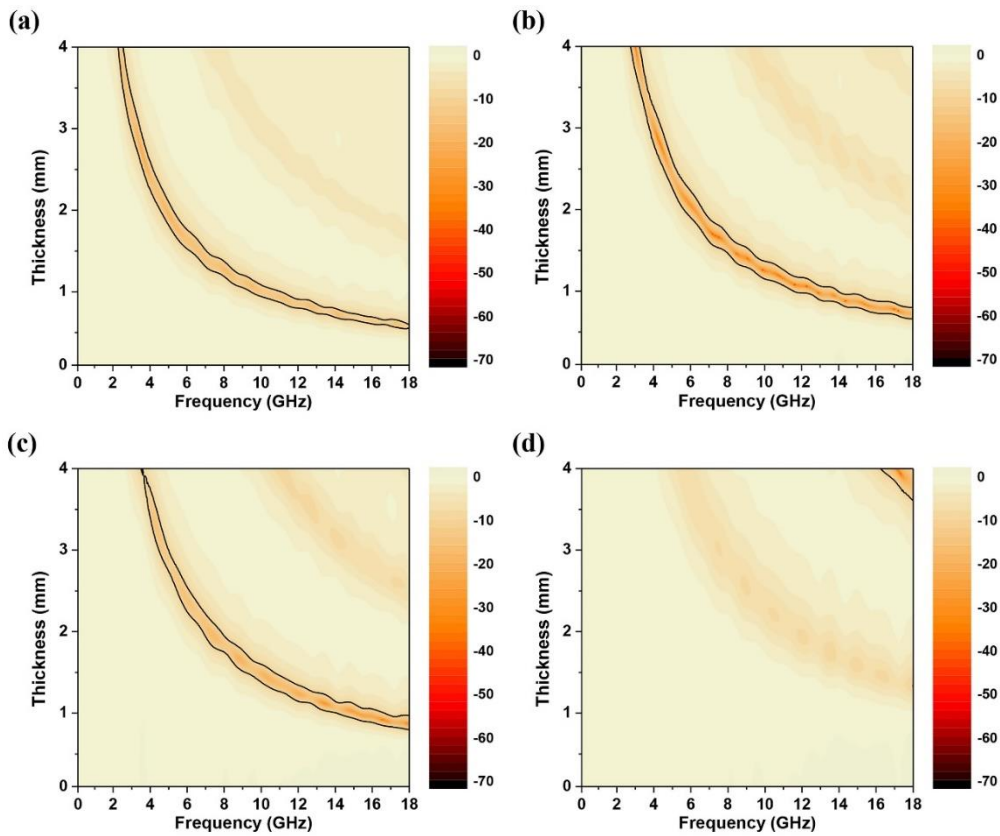


**Fig. 3.4.** *RL* maps for the $SrFe_{2-x}Zn_xW$ composites of (a) $x$ = 0.0, (b) $x$ = 0.5, (c) $x$ = 1.0, and (d) $x$ = 2.0 with the $V_f$ of 90%.

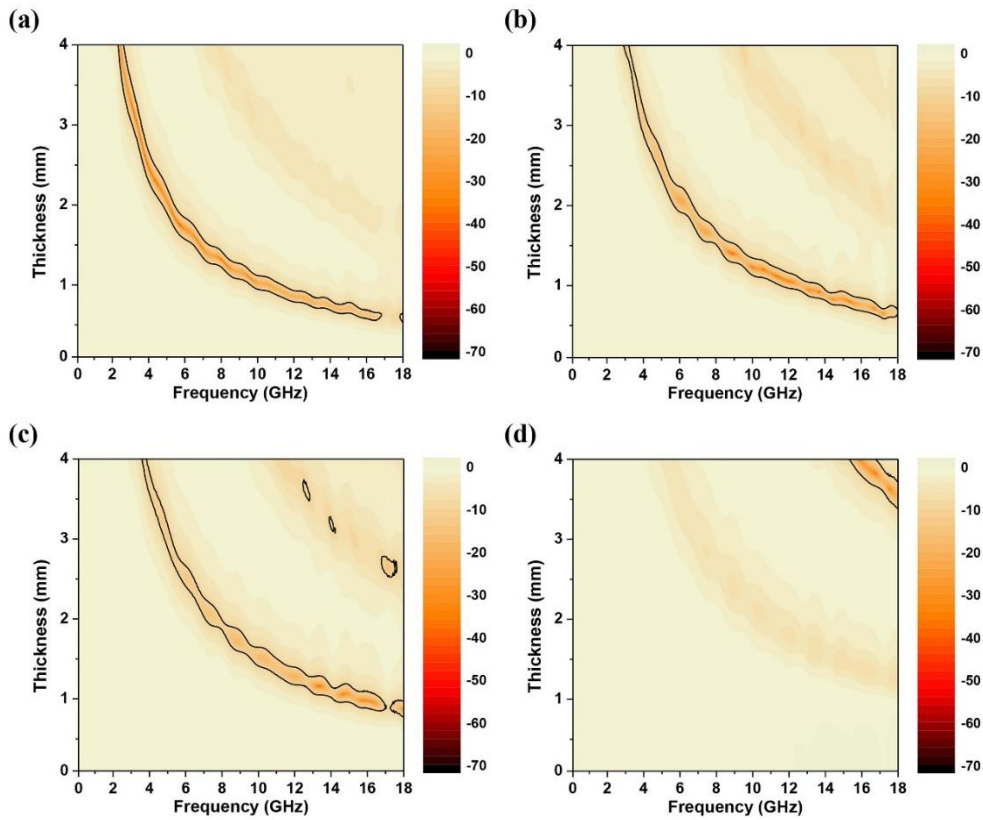


**Fig. 3.5.** *RL* maps for the $SrFe_{2-x}Zn_xW$ composites of (a) $x$ = 0.0, (b) $x$ = 0.5, (c) $x$ = 1.0, and (d) $x$ = 2.0 with the $V_f$ of 70%.

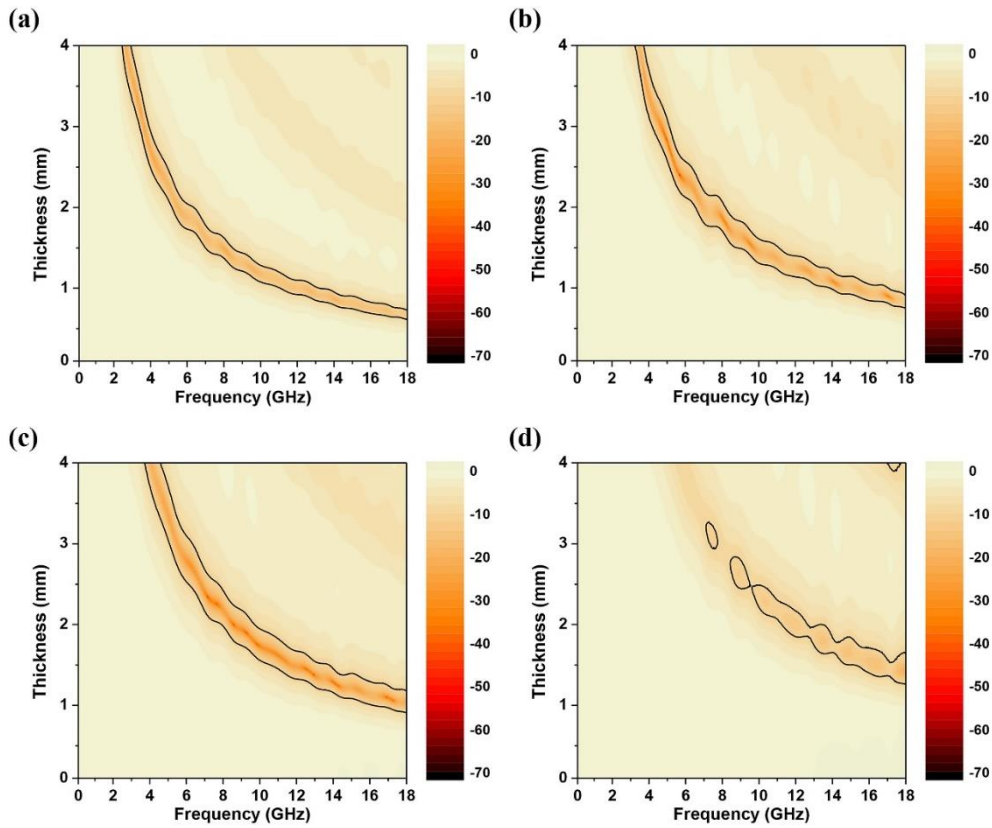


**Fig. 3.6.** *RL* maps for the $SrFe_{2-x}Zn_xW$ composites of (a) $x$ = 0.0, (b) $x$ = 0.5, (c) $x$ = 1.0, and (d) $x$ = 2.0 with the $V_f$ of 50%.

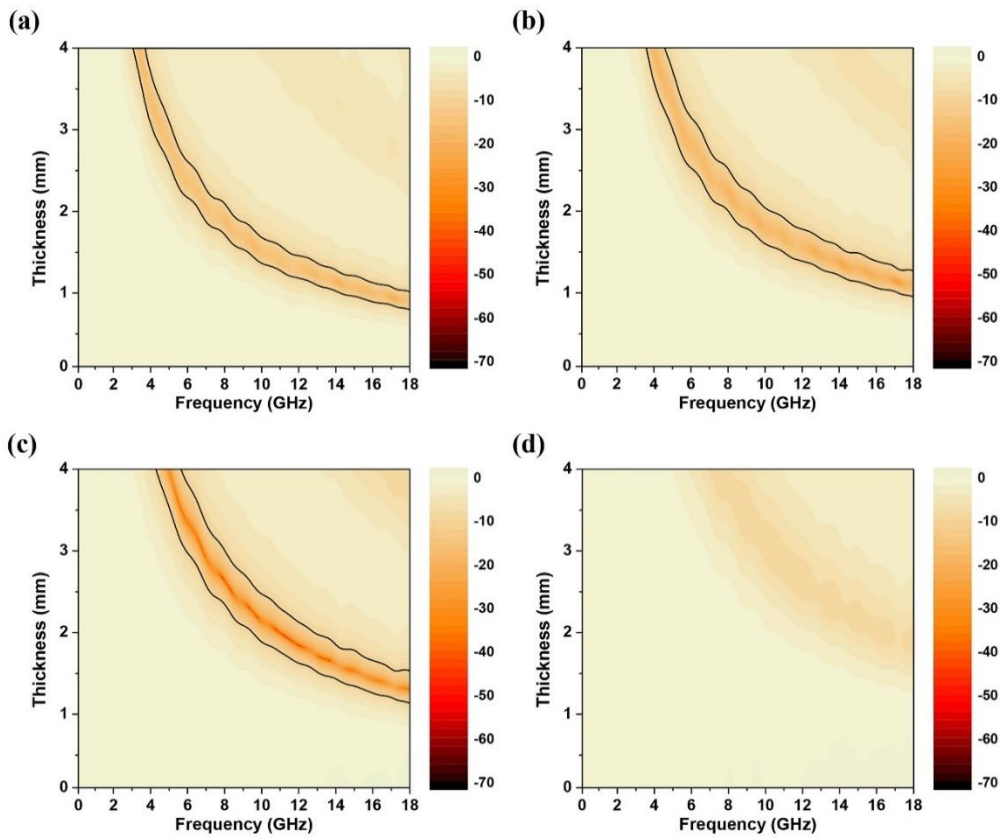


**Fig. 3.7.** *RL* maps for the $SrFe_{2-x}Zn_xW$ composites of (a) $x$ = 0.0, (b) $x$ = 0.5, (c) $x$ = 1.0, and (d) $x$ = 2.0 with the $V_f$ of 30%.

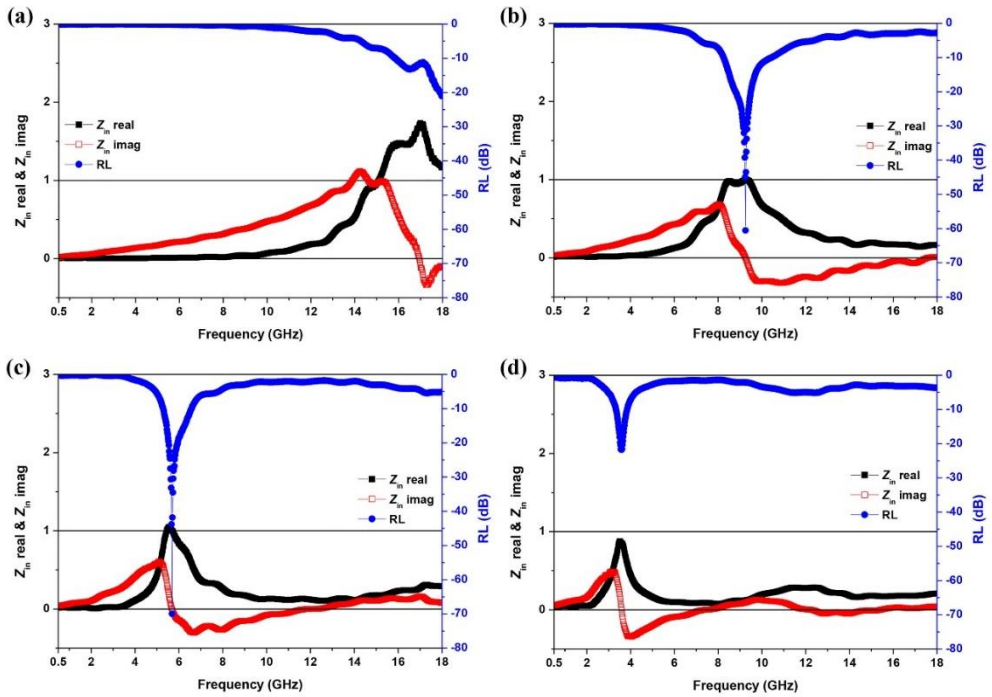


**Fig. 3.8.** Plots of the real and imaginary parts of the normalized $Z_{in}$ and *RL* as a function of frequency for the SrFeZnW composites with the $V_f$ values of (a) 30, (b) 50 (c) 70, and (d) 90%.

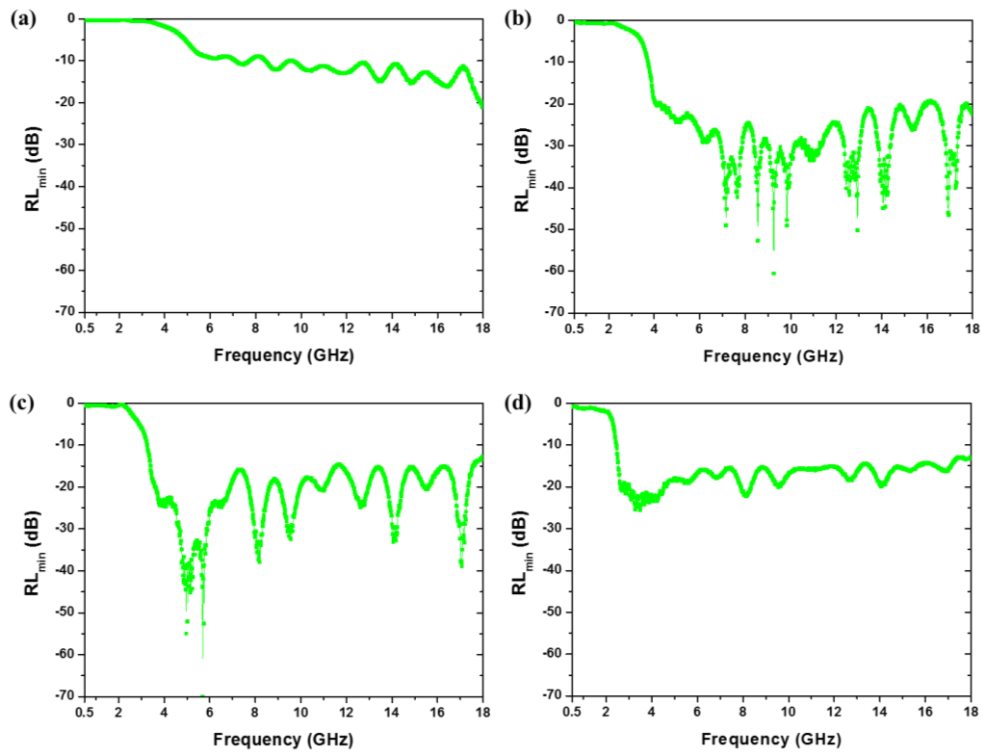


**Fig. 3.9.** Plots of $RL_{min}$ as a function of frequency for the SrFeZnW composites with the $V_f$ values of (a) 30, (b) 50, (c) 70, and (d) 90%.

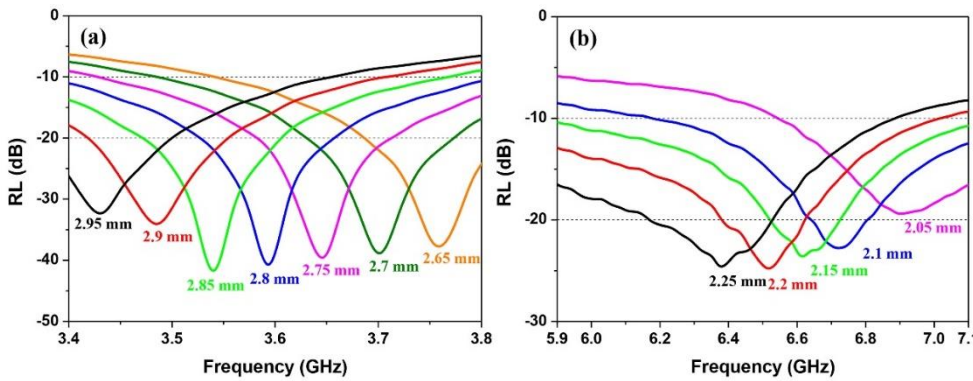


**Fig. 3.10.** *RL* as a function of frequency for (a) the $SrFe_{1.5}Zn_{0.5}W$ composites with $d$ = 2.65-2.95 mm and the $V_f$ of 90%, and for (b) the SrFeZnW composites with $d$ = 2.05-2.25 mm and the $V_f$ of 70%.

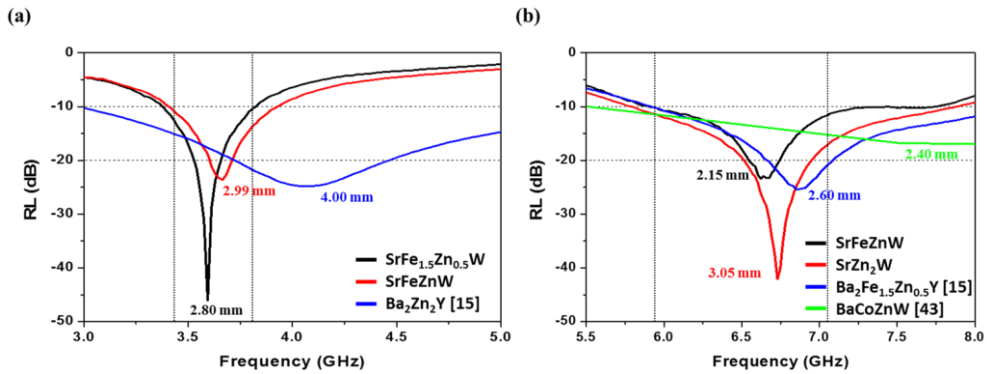


**Fig. 3.11.** *RL* as a function of frequency in two different frequency regions of (a) 3.4-3.8 and (b) 5.9-7.1 GHz for three different $SrFe_{2-x}Zn_xW$ composites of $x$ = 0.5, 1.0, and 2.0. While the *RL* curve from our previous report [15] is accurate, that from ref. [43] is approximated.

# References

[1] P. Azizi, S.M. Masoudpanah, S. Alamolhoda, Magnetic and microwave absorption properties of $SrZnCoFe_{16}O_{27}$ powders synthesized by solution combustion method, Journal of Alloys and Compounds, 739 (2018) 211-217.

[2] A. Ghasemi, G.R. Gordani, E. Ghasemi, $Co_2W$ hexaferrite nanoparticles-carbon nanotube microwave absorbing nanocomposite, Journal of Magnetism and Magnetic Materials, 469 (2019) 391-397.

[3] F.Y. Guo, G.J. Ji, J.J. Xu, H.F. Zou, S.C. Gan, X.C. Xu, Effect of different rare-earth elements substitution on microstructure and microwave absorbing properties of $Ba_{0.9}RE_{0.1}Co_2Fe_{16}O_{27}$ (RE=La, Nd, Sm) particles, Journal of Magnetism and Magnetic Materials, 324 (2012) 1209-1213.

[4] A.R. Farhadizadeh, S.A.S. Ebrahimi, S.M. Masoudpanah, Effect of $Nd^{3+}$ Substitution on the Phase Evolution and Magnetic Properties of W-Type Strontium Hexaferrite, Journal of Superconductivity and Novel Magnetism, 29 (2016) 1273-1278.

[5] M. Sun, J. Zheng, L. Liang, K. Sun, Y. Song, S. Zhao, Effect of Zn substitution on the electromagnetic and microwave absorbing properties of $BaCo_2$ hexaferrite, Journal of Materials Science-Materials in Electronics, 26 (2015) 9970-9976.

[6] Z.F. Zi, J.M. Dai, Q.C. Liu, H.Y. Liu, X.B. Zhu, Y.P. Sun, Magnetic and microwave absorption properties of W-type $Ba(Zn_xCo_{1-x})_2Fe_{16}O_{27}$ hexaferrite platelets, Journal of Applied Physics, 109 (2011) 7E536.

[7] Y.J. Kim, S.S. Kim, Microwave absorbing properties of Co-substituted $Ni_2W$ hexaferrites in Ka-band frequencies (26.5-40 GHz), Ieee Transactions on Magnetics, 38 (2002) 3108-3110.

[8] W. Jing, Z. Hong, S.X. Bai, C. Ke, C.R. Zhang, Microwave absorbing properties of rare-earth elements substituted W-type barium ferrite, Journal of Magnetism and Magnetic Materials, 312 (2007) 310-313.

[9] X. Tang, B.Y. Zhao, Q. Tian, K.A. Hu, Synthesis, characterization and microwave absorption properties of titania-coated barium ferrite composites, Journal of Physics and Chemistry of Solids, 67 (2006) 2442-2447.

[10] J. Zhang, L.X. Wang, Q.T. Zhang, Electromagnetic properties and microwave-absorption properties of $BaTiO_3/BaZn_2Fe_{16}O_{27}$ composite in 2-18 GHz, Journal of Materials Science-Materials in Electronics, 25 (2014) 5601-5605.

[11] M.R. Dadfar, S.A.S. Ebrahimi, M. Dadfar, Microwave absorption properties of 50% $SrFe_{12}O_{19}$-50% $TiO_2$ nanocomposites with porosity, Journal of Magnetism and Magnetic Materials, 324 (2012) 4204-4208.

[12] M.J. Molaei, M.R. Rahimipour, Microwave reflection loss of magnetic/dielectric nanocomposites of $BaFe_{12}O_{19}/TiO_2$, Materials Chemistry and Physics, 167 (2015) 145-151.

[13] J.H. You, S.I. Yoo, Improved magnetic properties of Zn-substituted strontium W-type hexaferrites, Journal of Alloys and Compounds, 763 (2018) 459-465.

[14] R.S. Meena, S. Bhattachrya, R. Chatterjee, Complex permittivity, permeability and microwave absorbing properties of $(Mn_{2-x}Zn_x)$U-type

hexaferrite, Journal of Magnetism and Magnetic Materials, 322 (2010) 2908-2914.

[15] J.H. You, S. Choi, S.Y. Park, S.I. Yoo, Enhanced microwave absorption properties of Zn-substituted Y-type hexaferrites, Journal of Magnetism and Magnetic Materials, 491 (2019).

[16] P. Sanchez-Olivares, P. Sanchez-Dancausa, J.L. Masa-Campos, M. Iglesias-Menendez-de-la-Vega, E. Garcia-Marin, Circular Conformal Array Antenna With Omnidirectional and Beamsteering Capabilities for 5G Communications in the 3.5-GHz Range, Ieee Antennas and Propagation Magazine, 61 (2019) 97-108.

[17] I.P. Belikaidis, A. Georgakopoulos, E. Kosmatos, V. Frascolla, P. Demestichas, Management of 3.5-Ghz Spectrum in 5G Dense Networks A Hierarchical Radio Resource Management Scheme, Ieee Vehicular Technology Magazine, 13 (2018) 57-64.

[18] W. Debaenst, A. Feys, I. Cuinas, M.G. Sanchez, J. Verhaevert, RMS Delay Spread vs. Coherence Bandwidth from 5G Indoor Radio Channel Measurements at 3.5 GHz Band, Sensors, 20 (2020) 750.

[19] E. Ni, An uncertainty analysis for the measurement of intrinsic properties of materials by the combined transmission-reflection method, Ieee Transactions on Instrumentation and Measurement, 41 (1992) 495-499.

[20] J.Y. Fang, T. Liu, Z. Chen, Y. Wang, W. Wei, X.G. Yue, Z.H. Jiang, A wormhole-like porous carbon/magnetic particles composite as an efficient broadband electromagnetic wave absorber, Nanoscale, 8 (2016) 8899-8909.

[21] S. Dong, X.H. Zhang, P.T. Hu, W.Z. Zhang, J.C. Han, P. Hu, Biomass-derived carbon and polypyrrole addition on SiC whiskers for enhancement of electromagnetic wave absorption, Chemical Engineering Journal, 359 (2019) 882-893.

[22] S. Dong, Y.X. Chen, C.Q. Hong, Synergetic impedance matching and loss ability towards ef ficient microwave absorption of $Fe_3O_4$ nanoparticles anchored on SiC whiskers via a simple solvothermal method, Journal of Alloys and Compounds, 838 (2020) 155558.

[23] H. Kaur, C. Singh, A. Marwaha, S.B. Narang, R. Jotania, S.R. Mishra, Y. Bai, K.C.J. Raju, D. Singh, M. Ghimire, P. Dhruv, A.S.B. Sombra, Elucidation of microwave absorption mechanisms in Co-Ga substituted Ba-Sr hexaferrites in X-band, Journal of Materials Science-Materials in Electronics, 29 (2018) 14995-15005.

[24] X. Liu, C. Zhao, Z. Li, A. Xia, C. Jin, H. Wei, H. Zhang, H. Li, S. Zhang, H. Long, Core-Shell Ni@Onion-Like Carbon Nanocapsules-Decorated Reduced Graphene Oxides with Enhanced Microwave Absorption Properties in GHz Range, Nano, 12 (2017) 1750085.

[25] M. Ahmad, R. Groessinger, M. Kriegisch, F. Kubel, M.U. Rana, Magnetic and microwave attenuation behavior of Al-substituted Co2W hexaferrites synthesized by sol-gel autocombustion process, Current Applied Physics, 12 (2012) 1413-1420.

[26] Z.W. Li, L.F. Chen, C.K. Ong, High-frequency magnetic properties of W-type barium-ferrite BaZn2-xCoxFe16O27 composites, Journal of Applied Physics, 94 (2003) 5918-5924.

[27] Z.W. Li, M.J. Chua, Z.H. Yang, Studies of static, high-frequency and electromagnetic attenuation properties for Y-type hexaferrites $Ba_2Cu_xZn_{2-x}Fe_{12}O_{22}$ and their composites, Journal of Magnetism and Magnetic Materials, 382 (2015) 134-141.

[28] V.G. Harris, Modern Microwave Ferrites, Ieee Transactions on Magnetics, 48 (2012) 1075-1104.

[29] U. Ozgur, Y. Alivov, H. Morkoc, Microwave ferrites, part 1: fundamental properties, Journal of Materials Science-Materials in Electronics, 20 (2009) 789-834.

[30] Y. Zhang, Y.a. Huang, X. Liang, Y. Yang, R. Zhang, R. Huang, Preparation and Microwave Absorption of Nitrogen-Doped Carbon Nanotubes With Iron Particles, Ieee Transactions on Magnetics, 54 (2018) 2300606.

[31] Y. Wei, H. Liu, S. Liu, M. Zhang, Y. Shi, J. Zhang, L. Zhang, C. Gong, Waste cotton-derived magnetic porous carbon for high-efficiency microwave absorption, Composites Communications, 9 (2018) 70-75.

[32] L.J. Yu, Y.F. Zhu, Y.Q. Fu, Waxberry-like carbon@polyaniline microspheres with high-performance microwave absorption, Applied Surface Science, 427 (2018) 451-457.

[33] X. Sun, J.P. He, G.X. Li, J. Tang, T. Wang, Y.X. Guo, H.R. Xue, Laminated magnetic graphene with enhanced electromagnetic wave absorption properties, Journal of Materials Chemistry C, 1 (2013) 765-777.

[34] F. Wan, F. Luo, H.Y. Wang, Z.B. Huang, W.C. Zhou, D.M. Zhu, Effects of carbon black (CB) and alumina oxide on the electromagnetic- and

microwave-absorption properties of SiC fiber/aluminum phosphate matrix composites, Ceram. Int., 40 (2014) 15849-15857.

[35] F.B. Meng, H.G. Wang, F. Huang, Y.F. Guo, Z.Y. Wang, D. Hui, Z.W. Zhou, Graphene-based microwave absorbing composites: A review and prospective, Composites Part B-Engineering, 137 (2018) 260-277.

[36] H. Wang, F. Meng, J. Li, T. Li, Z. Chen, H. Luo, Z. Zhou, Carbonized Design of Hierarchical Porous Carbon/$Fe_3O_4$@Fe Derived from Loofah Sponge to Achieve Tunable High-Performance Microwave Absorption, Acs Sustainable Chemistry & Engineering, 6 (2018) 11801-11810.

[37] P. Xie, H. Li, B. He, F. Dang, J. Lin, R. Fan, C. Hou, H. Liu, J. Zhang, Y. Ma, Z. Guo, Bio- gel derived nickel/ carbon nanocomposites with enhanced microwave absorption, Journal of Materials Chemistry C, 6 (2018) 8812-8822.

[38] J. Zhang, Interference effects on microwave absorbing properties of W-type $BaZn_2Fe_{16}O_{27}$ prepared by solid method, Journal of Materials Science-Materials in Electronics, 30 (2019) 8437-8444.

[39] A.R. Farhadizadeh, S.A.S. Ebrahimi, S.M. Masoudpanah, Magnetic and microwave absorption properties of ZnCo-substituted W-type strontium hexaferrite, Journal of Magnetism and Magnetic Materials, 382 (2015) 233-236.

[40] S.B. Narang, K. Pubby, C. Singh, Thickness and Composition Tailoring of K- and Ka-Band Microwave Absorption of $BaCo_xTi_xFe_{(12-2x)}O_{19}$ Ferrites, Journal of Electronic Materials, 46 (2017) 718-728.

[41] Z. Torabi, A. Arab, F. Ghanbari, Structural, Magnetic and Microwave Absorption Properties of Hydrothermally Synthesized (Gd, Mn, Co) Substituted Ba-Hexaferrite Nanoparticles, Journal of Electronic Materials, 47 (2018) 1259-1270.

[42] P. Meng, K. Xiong, L. Wang, S. Li, Y. Cheng, G. Xu, Tunable complex permeability and enhanced microwave absorption properties of $BaNi_xCo_{1-x}TiFe_{10}O_{19}$, Journal of Alloys and Compounds, 628 (2015) 75-80.

[43] Y.P. Wu, C.K. Ong, Z.W. Li, L. Chen, G.Q. Lin, S.J. Wang, Microstructural and high-frequency magnetic characteristics of W-type barium ferrites doped with $V_2O_5$, Journal of Applied Physics, 97 (2005).

[44] M.J. Iqbal, R.A. Khan, S. Takeda, S. Mizukami, T. Miyazaki, W-type hexaferrite nanoparticles: A consideration for microwave attenuation at wide frequency band of 0.5-10 GHz, Journal of Alloys and Compounds, 509 (2011) 7618-7624.

[45] L.W. Deng, L. Ding, K.S. Zhou, S.X. Huang, Z.W. Hu, B.C. Yang, Electromagnetic properties and microwave absorption of W-type hexagonal ferrites doped with $La^{3+}$, Journal of Magnetism and Magnetic Materials, 323 (2011) 1895-1898.

[46] L.X. Wang, J. Song, Q.T. Zhang, X.G. Huang, N.C. Xu, The microwave magnetic performance of $Sm^{3+}$ doped $BaCo_2Fe_{16}O_{27}$, Journal of Alloys and Compounds, 481 (2009) 863-866.

[47] Z.F. Liu, G. Bai, Y. Huang, F.F. Li, Y.F. Ma, T.Y. Guo, X.B. He, X. Lin, H.J. Gao, Y.S. Chen, Microwave absorption of single-walled carbon nanotubes/soluble cross-linked polyurethane composites, Journal of Physical Chemistry C, 111 (2007) 13696-13700.

[48] Z.J. Fan, G.H. Luo, Z.F. Zhang, L. Zhou, F. Wei, Electromagnetic and microwave absorbing properties of multi-walled carbon nanotubes/polymer composites, Mat Sci Eng B-Solid, 132 (2006) 85-89.

[49] S.K. Kwon, J.M. Ahn, G.H. Kim, C.H. Chun, J.S. Hwang, J.H. Lee, Microwave absorbing properties of carbon black/silicone rubber blend, Polymer Engineering and Science, 42 (2002) 2165-2171.

[50] F. Nanni, P. Travaglia, M. Valentini, Effect of carbon nanofibres dispersion on the microwave absorbing properties of CNF/epoxy composites, Composites Science and Technology, 69 (2009) 485-490.

# Chapter 4

# Microwave absorption properties of Zn-substituted W-type hexaferrites in the Ka-band (26.5-40 GHz)

## 4.1 Introduction

With the development of 5G wireless communication devices operating in the microwave region, electromagnetic interference has become a serious pollution problem since it can harm human or animal health and surrounding electronic systems [1-3]. Therefore, to address this problem, a tremendous effort has been made for the development of high-performance microwave absorbers possessing high absorption efficiency with broadband, lightweight, and thin thickness simultaneously [4]. Since the microwave absorption properties of microwave absorption materials (MAMs) are mainly determined by the relative complex permittivity ($\varepsilon_r = \varepsilon' - j\varepsilon''$) and permeability ($\mu_r = \mu' - j\mu''$), and their thickness values are inversely proportional to their refractive indices ($n = \mathrm{Re}\sqrt{\mu_r \varepsilon_r}$), researchers have focused on the improvement of their real and imaginary parts of $\varepsilon_r$ and $\mu_r$ for real applications.

In general, MAMs are classified into two different types: (1) magnetic materials such as ferromagnetic materials [5-9], spinel ferrites [10], and hexagonal ferrites [11-15], and (2) dielectric materials such as $Al_2O_3$ [16], $BaTiO_3$ [17], polymers [18, 19], and carbon-based materials [20-24]. Among MAMs, both spinel and hexagonal ferrites have been most widely used for real applications. While spinel ferrites are

normally used at the frequency region below 1 GHz due to their relatively lower ferromagnetic resonance (FMR) frequencies [25], hexaferrites are regarded as promising materials for microwave absorbers above 1 GHz due to their higher FMR frequencies.

Hexaferrites can be categorized into six different types: M, X, U, Y, Z, and W [26]. Among these, M- and W-type hexaferrites are the most promising materials as microwave absorbers since their FMR frequencies are as high as 38~56 [27-30] and 30~60 GHz [27, 31, 32], respectively. Most of researchers have focused on M-type hexaferrites owing to their excellent chemical stability in addition to their high FMR frequencies. However, W-type hexaferrites must be promising candidates for MAMs since they also possess high $M_s$ values, high $H_a$, and high FMR frequency comparable to M-type hexaferrites.

Up to date, since unsubstituted Sr or BaW-type hexaferrites are metastable phases in air, researchers have mainly focused on the microwave absorption properties of W-type hexaferrites, stabilized by fully substituting various divalent cations such as $Co^{2+}$ [33], $Mn^{2+}$ [34], and $Mg^{2+}$ [35] for the $Fe^{2+}$ sites. Moreover, most of literature report the microwave absorption properties of W-type hexaferrites in the Ku-band region (i.e., 0.5-18 GHz), which is much lower than their FMR frequencies. Literature reporting microwave absorption properties of W-type hexaferrites in the Ka-band (26.5-40 GHz) is hardly found. To the best of our knowledge, only one paper from Y. Kim *et al*. [36] is available for $BaNi_{2-x}Co_xW$ hexaferrites in the Ka-band. They reported the $RL_{min}$ value of −45 dB at 31.9 GHz with the bandwidth of 26.5-33 GHz below −20 dB and the thickness of 0.9 mm for the composite sample composed of 80 wt% $BaNi_{1.6}Co_{0.4}Fe_{16}O_{27}$–silicone rubber. Therefore, in order to develop a new high-performance microwave absorber of W-type hexaferrite in the

Ka-band, we selected the composite samples composed of partially Zn-substituted SrW-type hexaferrites within the epoxy resin matrix in this study. The reason for this selection is as follows; First, according to our previous study on Zn-substituted SrW-type hexaferrites [37], with increasing $x$ up to 1.0 in $SrFe_{2-x}Zn_xW$, the $M_s$ values are almost linearly increased while the $H_a$ values are abruptly decreased. With further increase of $x$ up to 2.0, the $M_s$ value is largely decreased while the $H_a$ value is slightly decreased. Therefore, the real parts of $\mu_r$ are expected to continuously increase up to $x$ =1.0 since they are proportional to the ratio of $M_s/H_a$. Second, higher real and imaginary parts of complex permittivity are expected due to an increased electric conductivity through electron hopping between $Fe^{2+}$ and $Fe^{3+}$ ions [38]. In particular, since 28 GHz is regarded as a future frequency for 5G communication [39-41], we also tried to develop a thin broadband microwave absorber covering the frequency region of 27-29 GHz.

## 4.2 Experimental

Various SrW-type hexaferrites with the nominal compositions of x = 0.0, 0.25, 0.5, 1.0, and 2.0 in SrFe2-xZnxW were synthesized by solid-state reaction in the reduced oxygen atmosphere. The precursors were SrCO3 (99.9% Kojundo Korea Co.), Fe2O3 (99.9% Kojundo Korea Co.), and ZnO (99.9% Kojundo Korea Co.). The precursors were weighed, ball-milled with zirconia balls in ethanol for 24 h, and dried in an oven at 45℃. As-dried powders were calcined at 1150 ℃ for 8 h in air, ball-milled again for 24 h, and uniaxially pressed into pellets (15 mm diameter and 2 mm thickness) under the pressure of 180 kg/cm2. As-pressed pellets with the compositions of x = 0.0, 0.25, 0.5, and 1.0 were put into a tube furnace, sintered at

1315, 1290, 1280, and 1250 ˚C for 2 h, respectively, in the oxygen partial pressure (PO2) of 10-3 atm with flowing 0.1% O2-N2 mixture gas, and subsequently furnace-cooled. The gas flow was controlled by a mass flow controller with a flow rate of 0.5 l/min. On the other hand, the fully Zn-substituted sample of SrZn2W having x = 2.0 was sintered at 1300 ℃ for 2 h and furnace-cooled in air.

In order to evaluate the microwave absorption properties of composite samples, our specimens were prepared by the following procedures; At first, each hexaferrite filler was mixed with the epoxy-resin matrix to have its Vf values of 30, 60, and 90 %, and then each powder mixture was pressed into a thin rectangular plate (7.11 mm ×3.56 mm × ~1.0 mm), and subsequently hardened at 175 ˚C for 1 h in air. The thickness of rectangular plates was controlled to have the value less than 1.0 mm to prevent a negative permeability caused by a sample-size resonance during the microwave property measurements [42].

The measurements of complex permittivity and permeability were carried out for our specimens using the VNA (Agilent PNA N5525A). Their complex permittivity and permeability values were calculated from S-parameters in the Ka-band frequency region of 26.5-40 GHz by using a transmission and reflection method based on the algorithm developed by Nicolson and Ross [43].

## 4.3 Results and discussion

In this section, we first present the real and imaginary parts of both $\varepsilon_r$ and $\mu_r$ as a function of frequency in the region of 26.5-40 GHz for our samples composed of $SrFe_{2-x}Zn_xW$ ($x$ = 0.0, 0.25, 0.5, 1.0, and 2.0)-epoxy resin composites (hereafter,

$SrFe_{2-x}Zn_xW$ composites) with the $V_f$ values of 30, 60, and 90%. Next, their dielectric and magnetic loss tangents are presented to discuss the mechanism of microwave absorption properties. Third, their reflection losses (*RL*), calculated by transmission line theory [44], are presented as the function of frequency and sample thickness. On the basis of these data, we discuss the effect of $Zn^{2+}$ substitution for the $Fe^{2+}$ site on the microwave absorption properties of our samples in the Ka-band. Finally, we describe a successful fabrication of the thin broadband absorber for 5G communication in the frequency region of 27-29 GHz. Meanwhile, since the powder XRD patterns and dc magnetic properties of $SrFe_{2-x}Zn_xW$ hexaferrites have been reported in our previous paper [37], those are not presented in this paper.

The real and imaginary parts of $\varepsilon_r$ and $\mu_r$, are shown in Figs. 1 and 2, respectively, as the function of frequency for our composite samples. Here, it should be noted that the real parts of $\varepsilon'$ and $\mu'$ stand for the storage ability of electromagnetic energy, and the imaginary parts of $\varepsilon''$ and $\mu''$ stand for the loss of electromagnetic energy. From Fig. 1(a)-(c), we can see that the real parts of $\varepsilon_r$ continuously decrease with increasing $x$ (i.e., the amount of $Zn^{2+}$ substituent for the $Fe^{2+}$ site), which can be explained by a continuous reduction in electron hopping between $Fe^{2+}$ and $Fe^{3+}$ ions [45]. For $SrFe_{2-x}Zn_xW$-type hexaferrite ($0.0 \leq x \leq 2.0$) composites, this continuous decrease in the $\varepsilon'$ spectra with increasing $x$ in the Ka-band has already been observed in the Ku-band [46]. This behavior has also been reported for Zn-substituted $Ba_2Fe_{2-x}Zn_xY$-type hexaferrite ($0.5 \leq x \leq 2.0$) composites in the Ku-band [38]. However, in the case of the $\varepsilon''$ spectra, the same behavior is observable only for the $SrFe_{2-x}Zn_xW$ composites with $V_f$ of 90%. Among the samples with lower $V_f$ values of 30%, while the composite samples of $x$ = 0 and 2.0 exhibit the same behavior, other composite samples with $x$ = 0.25, 0.5, and 1.0 exhibit somewhat complicated deviation in their

$\varepsilon''$ spectra. Among the samples with $V_f$ value of 60%, only the composite sample of $x = 0.25$ show a significant deviation in its $\varepsilon''$ spectrum.

As shown in Figs. 1 and 2, there is a trend of decreasing $\varepsilon_r$ and $\mu_r$ with decreasing $V_f$ (i.e., increasing the amount of epoxy resin). To understand this behavior, we also measured the real and imaginary parts of $\varepsilon_r$ and $\mu_r$ in the Ka-band for pure epoxy resin sample and plotted the data in Fig 3. This figure shows that the real and imaginary parts of $\varepsilon_r$ and $\mu_r$ are independent of frequency, and their values are $\varepsilon' \approx 3.1$, $\varepsilon'' \approx 0.15$, $\mu' \approx 1.05$, and $\mu'' \leq 0.01$. Thus, this decreasing tendency in both $\varepsilon_r$ and $\mu_r$ with decreasing $V_f$ is ascribable to a continuous increase in the relative fraction of epoxy resin since its real and imaginary parts of $\varepsilon_r$ and $\mu_r$ are much lower than those of $SrFe_{2-x}Zn_xW$ hexaferrites. Because the electrical resistivity of the composites abruptly increases due to the epoxy resin [47], the space-charge polarization of the composites might be gradually reduced with increasing the fraction of the epoxy resin, leading to the decreasing tendency in $\varepsilon_r$ with decreasing $V_f$. A similar decreasing tendency in $\varepsilon_r$ with decreasing $V_f$ has been reported for core-shell carbonyl iron@epoxy composites by X. Guo *et al*. [5]. On the other hand, the real and imaginary parts of $\mu_r$ values also decrease with increasing the amount of epoxy resin, which is explainable simply by a continuous decrease in the amount of hexaferrite filler. Another important quantities determining the microwave absorption properties are the dielectric ($\tan\delta_\varepsilon = \varepsilon''/\varepsilon'$) and magnetic loss tangents ($\tan\delta_\mu = \mu''/\mu'$). As shown in Fig. 3(c) and (d), the $\tan\delta_\varepsilon$ values of epoxy resin are arround five times larger than that of $\tan\delta_\mu$, implying that the micrwoave absorption mechanism of epoxy resin matrix is mainly attributable to the dielectric tangent loss in this frequency region.

Referring to our previous report [46] on Zn-substituted SrW-type hexaferrite composites in the Ku-band, the real and imaginary parts of $\mu_r$ continuously increase with increasing $x$ from 0.0 to 1.0 and then decrease with further increasing $x$ up to 2.0. This behavior was expected to occur in the Ka-band as well. From Fig. 2(a)-(c), one can see that this behavior occurs obviously for the samples with $V_f$ of 90% in the frequency region of 26.5-33 GHz. This behavior is believed to originate from increasing $M_s$ together with decreasing the magnetic anisotropy field, $H_a$, according to Snoek's law given by

$$\mu_i' - 1 = \frac{4\pi M_s}{3}\frac{1}{H_a} \qquad (1)$$

where the real part of initial permeability ($\mu_i'$) is proportional to $M_s$ while it is inversely proportional to $H_a$. However, unlike the behavior in the Ku-band [46], the dependence of $\mu_i'$ on $x$ becomes complicated due to the existence of FMR peaks and epoxy resin as shown in Fig. 2(a)-(c). A significant deviation from the proportionality between $\mu_i'$ and $M_s/H_a$ can be observed for the samples of $x$ = 1.0 and 2.0 with $V_f$ of 90% in the frequency region 33-40 GHz due to the existence of FMR peaks as previously mentioned. On the other hand, in the case of $SrFe_{2-x}Zn_xW$ composites with $V_f$ of 30 and 60%, the deviation from the proportionality between $\mu_i'$ and $M_s/H_a$ becomes more significant with decreasing $V_f$, which might originate from the increased of the epoxy resin since the $\mu'$ value of the epoxy resin matrix (see Fig. 3) becomes comparable to those of hexaferrite fillers.

From Fig. 2(a)-(c), the FMR peaks are unobservable for $SrFe_{2-x}Zn_xW$ composites with $x$ = 0.0, 0.25, and 0.5, which is in good agreement with previous literature [31] reporting that the FMR frequency of $SrZnCoFe_{16}O_{27}$ W-type hexaferrite is over 40

GHz. In these figures, however, the FMR peaks are clearly observed at around 37 ±0.1 and 35.5 ±0.1 GHz for $SrFe_{2-x}Zn_xW$ hexaferrites with $x$ = 1.0 and 2.0, respectively, regardless of their $V_f$ values. The FMR frequency ($f_r$) of a hexaferrite having the uniaxial magnetocrystalline anisotropy along the c-axis is related with $H_a$ by the following equation;

$$f_r = \frac{\gamma}{2\pi} H_a \qquad (2)$$

where $\gamma$ is the gyromagnetic ratio [48]. Referring to our previous report [37], the $H_a$ values of $SrFe_{2-x}Zn_xW$ are continuously decreased with increasing $x$, This behavior is ascribable to the nonmagnetic $Zn^{2+}$ ions which can weaken the super-exchange coupling of magnetic ions and spin-orbit coupling interaction. Thus, it can be deduced that a decrease in $H_a$ with increasing $x$ shifts $f_r$ to lower frequency region. These results are similar to previous report on $BaNi_{2-x}Co_xW$-type hexaferrites by Y. Kim *et al*. [36] in that with increasing the amount of Co substituent for the $Ni^{2+}$ site, the uniaxial magnetocrystalline anisotropy is gradually weakened, and finally easy axis changes from the *c*-axis to the *c*-plane [49], resulting in a gradual decrease in FMR frequency [36].

It is noteworthy that the FMR frequencies of $SrFe_{2-x}Zn_xW$ hexaferrites ($x$ = 1.0 and 2.0) are 42.3 and 40.9 GHz, respectively, if these are calculated by multiplying their $H_a$ values of 15.1 and 14.6 kOe, respectively, estimated by using the law of approach to saturation in our previous paper [37], with the $\frac{\gamma}{2\pi}$ value of 2.8 GHz/kOe. Since these FMR values are larger than 40 GHz, the FMR peaks must be unobservable in the Ka-band. However, as shown in Fig. 2, the FMR frequencies are clearly observable for $SrFe_{2-x}$ $Zn_xW$ hexaferrites with $x$ = 1.0 and 2.0. This

discrepancy may be understood as follows. The $H_a$ values evaluated by the law of approach are dependent on their field range of reversible magnetization curves used for calculation. On the other hand, our $H_a$ values calculated by measured FMR frequencies of 37 ±0.1 and 35.5 ±0.1 GHz for $SrFe_{2-x}Zn_xW$ hexaferrites with $x$ = 1.0 and 2.0, respectively, and the $\frac{\gamma}{2\pi}$ value of 2.8 GHz/kOe are 13.2 and 12.7 kOe, respectively, which are around 14% lower than the above values. Consequently, we believe that these $H_a$ values, calculated from measured FMR frequencies, are more accurate than the previous $H_a$ values evaluated by the law of approach, which might be overestimated due to the selection of field range for calculation. Although these $H_a$ values from the FMR peaks are lower than those evaluated by the law of approach, the tendency of decreasing $H_a$ with increasing $x$ is in good agreement.

Fig. 4(a) and (b) shows the $\tan\delta_\varepsilon$ and $\tan\delta_\mu$ values, respectively, as a function of frequency in the Ka-band for the $SrFe_{2-x}Zn_xW$ composites with $V_f$ of 30%. These data were calculated on the basis of the real and imaginary parts of $\varepsilon_r$ and $\mu_r$ shown in Figs. 1 and 2. In accordance with our expectation from almost frequency-independent $\varepsilon'$ and $\varepsilon''$ values in Fig. 1(a), one can see from Fig. 4(a) that the $\tan\delta_\varepsilon$ values are almost frequency-independent for all $SrFe_{2-x}Zn_xW$ composites. On the other hand, the $\tan\delta_\mu$ values of $SrFe_{2-x}Zn_xW$ ($x$ = 0.0, 0.25, and 0.5) composites increase rapidly from ~30 GHz. For $SrFe_{2-x}Zn_xW$ ($x$ = 1.0 and 2.0) composites, the $\tan\delta_\mu$ values are increased up to their FMR frequencies, and then decreased as shown in Fig. 4(b). To identify a dominant source affecting the microwave absorption, researchers have generally compared $\tan\delta_\varepsilon$ with $\tan\delta_\mu$ values [50, 51]. Interestingly, only the $\tan\delta_\varepsilon$ values of the $SrZn_2W$ ($x$ = 2.0) composite are higher than its $\tan\delta_m$ values in the whole measured frequency region. For the other samples, the $\tan\delta_\varepsilon$

values are larger than the tan$\delta_\mu$ ones below ~33 GHz. With increasing frequency, the tan$\delta_\mu$ values are increased and eventually become larger than the tan$\delta_\varepsilon$ values for the other composites. However, it must be inappropriate to simply compare the values of tan$\delta_\mu$ with those of tan$\delta_\varepsilon$ for the determination of a dominant loss mechanism since the imaginary parts of $\varepsilon_r$ are one order of magnitude larger than the imaginary parts of $\mu_r$ for our $SrFe_{2-x}Zn_xW$ composites, suggesting that dielectric loss is dominant in our samples. Although SrW hexaferrties are known as magnetic materials, our unsubstituted and partially Zn-substituted SrW hexaferrites exhibit greatly higher values of the real and imaginary parts of $\varepsilon_r$ which are comparable to dielectric materials [52].

On the other hand, it is well known that the imaginary parts of $\varepsilon_r$ mainly come from polarization loss and conductivity loss [53]. According to free-electron theory [51], high conductivity can increase $\varepsilon''$. Also, the interfacial polarization loss occurs at the interfaces between filler and matrix in the composites, and thus non-uniform distribution of space charge at the interface can enhance $\varepsilon''$ [21]. It is reported that the Cole-Cole plot of $\varepsilon''$ versus $\varepsilon'$ shows a circle shape if $\varepsilon''$ mainly originates from polarization loss while it shows a linear shape if $\varepsilon''$ mainly originates from conductivity loss [54, 55]. Therefore, the tan$\delta_\varepsilon$ in our samples is mainly attributable to interfacial polarization since the Cole-Cole shapes are multi-circles as shown in Fig. 4(c).

In general, the magnetic loss originates from hysteresis loss, eddy current loss, domain wall resonance, and FMR [56]. The hysteresis loss in our samples is negligible since the magnetic amplitude of incident microwave is very small [57, 58]. The domain wall resonances of hexaferrites and spinel ferrites are reported to occur at a frequency around 1-2 GHz [57, 58] and 10-100 MHz [59], respectively,

suggesting that the magnetic loss due to domain wall resonance needs not to be taken into account in the Ka band. If the main mechanism of magnetic loss is from the eddy current loss, the values of $\mu''(\mu')^{-2}(f)^{-1}$ should be independent of frequency [60]. From Fig. 4(d), it is obvious that the values of $\mu''(\mu')^{-2}(f)^{-1}$ are almost constant with frequency, representing that the eddy current loss is the dominant source for magnetic loss in relatively lower frequency up to ~30 GHz. On the other hand, since the values of $\mu''(\mu')^{-2}(f)^{-1}$ significantly increase above ~30 GHz due to the FMR effect, the magnetic loss above ~30 GHz originates not only from eddy current loss but also from FMR loss. Consequently, while the source of magnetic loss in our composite samples must be due to the eddy current loss in relatively lower frequency region, the mechanisms of magnetic loss in relatively higher frequency region are attributable to both the eddy current loss and FMR.

Although the electric loss tangent, $\tan\delta_\varepsilon$, and the magnetic loss tangent, $\tan\delta_\mu$, are important factors related to microwave absorption ability, higher $\tan\delta_\varepsilon$ and/or $\tan\delta_\mu$ values do not always guarantee excellent microwave absorption properties. To fully understand the critical factors determining microwave absorption properties, impedance matching should be taken into account. According to the transmission line theory, the normalized input impedance $Z_{in}$ is given by

$$Z_{\text{in}} = Z_0\sqrt{\frac{\mu_r}{\varepsilon_r}}\tanh\left[\, j(2\pi fd/c)\sqrt{\mu_r\varepsilon_r}\,\right] \qquad (3)$$

where $Z_0 = \sqrt{\mu_0/\varepsilon_0}$ is the characteristic impedance of free space. $c$ is the speed of light, $f$ is the frequency of the microwave, and $d$ is the thickness of the absorber. The reflection loss, *RL* value (i.e., the microwave absorption ability of an incident

microwave by a single-layer absorber) can be calculated by inserting the $Z_{in}/Z_o$ ratio from Eq. (3) into the following equation,

$$\text{Reflection loss (dB)} = 20\log\left|\frac{Z_{in} - Z_0}{Z_{in} + Z_0}\right| \qquad (4)$$

One can see from Eq. (4) that the *RL* value becomes negatively infinite when the input impedance and impedance of free space are equal, which corresponds to a perfect absorption of the incident microwave. Therefore, impedance matching is an important factor in designing a microwave absorber.

To characterize the microwave absorption properties of $SrFe_{2-x}Zn_xW$ composites, we calculated their *RL* values by inserting their $\varepsilon_r$ and $\mu_r$ data shown in Figs. 1 and 2 into Eqs. (3) and (4). The *RL* values of −10 and −20 dB represent the microwave absorption efficiency of 90 and 99%, respectively. Evaluated *RL* values for the $SrFe_{2-x}Zn_xW$ composites with $V_f$ of 30 are displayed on the *RL* maps in Fig. 5. In these *RL* maps, the regions of $RL \leq -20$ dB are enclosed by black dots. From Fig. 5(f), as *x* increases in the $SrFe_{2-x}Zn_xW$ composites with the same $V_f$ of 30%, the region with $RL \leq -20$ dB shifts to thicker $d_m$. This behavior can be explained by the following quarter wavelength principle;

$$d = \frac{\lambda}{4} = \frac{c}{4f\,\mathrm{Re}\sqrt{\mu_r\varepsilon_r}} \qquad (5)$$

where *d* is the thickness of the absorber, $\lambda$ is the wavelength of the microwave, *f* is the frequency of the microwave, and *c* is the speed of light. According to Eq. (5), one can see that the smaller refractive index (*n*), which is equal to $\mathrm{Re}\sqrt{\mu_r\varepsilon_r}$), results in thicker matching thickness, $d_m$. The real and imaginary parts of $\varepsilon_r$ are

continuously decreased with increasing $x$ due to a reduced electron hopping between $Fe^{2+}$ and $Fe^{3+}$ ions as previously mentioned in Fig. 1. However, the real and imaginary parts of $\mu_r$ are around one order of magnitude less than those of $\varepsilon_r$, and hence these have a negligible effect on the matching thickness, $d_m$.

The filler volume fraction, $V_f$, matching frequency, $f_m$, matching thickness, $d_m$, and bandwidth for our composites are summarized in Table 1, among all samples, the $SrFe_{2-x}Zn_xW$ composites with $V_f$ of 30% commonly exhibit the minimum reflection loss, $RL_{min}$, lower than −50 dB. However, only the $SrFe_{1.75}Zn_{0.25}W$ ($x$ = 0.25) composite has the bandwidth covering the region of 27-29 GHz. This sample possesses the lowest $RL_{min}$ value of −68.4 dB for the thickness of 0.64 mm as shown in Table 1. Consequently, it is clear that the partial substitution of $Zn^{2+}$ ion for the $Fe^{2+}$ ion site in $SrFe_{2-x}Zn_xW$ can effectively reduce the filler volume fraction, $V_f$, from 90 to 30% with improved microwave absorption property.

The $RL_{min}$ spectra of the $SrFe_{2-x}Zn_xW$ composites with $V_f$ of 30, 60, and 90% were calculated at their matching thicknesses, $d_m$, and presented in Fig. 6. This figure represents that while $SrFe_{2-x}Zn_xW$ composites with $V_f$ of 30% have excellent microwave absorption properties with $RL \leq -20$ dB not only in the range of 27-29 GHz but also overall measured frequency region in (a), $SrFe_{2-x}Zn_xW$ composites with $V_f$ of 60 and 90% show poor microwave absorption properties with $RL \geq -20$ dB overall measured frequency region in (b) and (c), respectively. As previously mentioned, the impedance matching condition is one of the important factors for good microwave absorption property. Therefore, excellent microwave absorption properties with $RL \leq -20$ dB in (a) may be due to good impedance matching while poor microwave absorption property with $RL \geq -20$ dB in (b) and (c) may be due to their impedance mismatch. To further confirm the degree of impedance matching,

the normalized real and imaginary parts of the input impedance $Z_{in}$, calculated by Eq. (3), together with the *RL* values calculated by Eq. (4) as a function of frequency are represented for the $SrFe_{1.75}Zn_{0.25}W$ composites with $V_f$ of 30, 60, and 90% in Fig. 7. Theoretically, from Eq. (3), a perfect impedance matching can be obtained when the normalized real part of the input impedance is 1 and the normalized imaginary part of the input impedance is 0. As can be seen in Fig. 7(a), the peak of the *RL* spectrum appears near 28 GHz, representing that impedance matching occurs near this frequency. However, the $SrFe_{1.75}Zn_{0.25}W$ composites with $V_f$ of 60 and 90% exhibit poor microwave absorption ability with $RL > -20$ dB overall measured frequency region due to a severe impedance mismatch as shown in Fig. 7(b)-(c). Consequently, it is clear that impedance matching is dramatically enhanced with decreasing $V_f$. In general, higher real and imaginary parts of $\varepsilon_r$ and $\mu_r$ are required in order to have strong microwave absorption. If these values become exceedingly high, impedance mismatch can be induced due to an excessive reflection of incident microwave at the surface of the microwave absorber.

Unfortunately, it is very difficult to find the $f_m$ and $d_m$ values by numerical calculation because of many other variables included in Eq. (3). Therefore, an impedance matching solution map is very useful for determining appropriate values of $\varepsilon_r$ and $\mu_r$ [61]. As a representative, the impedance matching solution maps are represented for the $SrFe_{1.75}Zn_{0.25}W$ composites in Fig. 8. In this plot, after the real and imaginary parts of $\varepsilon_r$ and $\mu_r$ of material are measured, the $\tan\delta_\varepsilon$ values are calculated, the imaginary part of $\mu_r$ is plotted as a function of the real parts of $\mu_r$, and the real part of $\varepsilon_r$ is plotted as a dotted line. The perfect impedance matching is satisfied at the point where the $\mu_r$, $\varepsilon'$, and $d/f$ values intersect each other, and thus the $RL_{min}$ value is obtainable at this condition. On the other hand, if there is no point of

their common intersection, the impedance matching solution map can be used to determine how the real and imaginary parts of $\varepsilon_r$ and $\mu_r$ should be adjusted to satisfy the impedance matching condition. Fig. 8 also shows that the impedance matching characteristic is gradually degraded with increasing $V_f$, which is due to an excessive increase in $\varepsilon'$ (red line). In other words, for the composite with $V_f$ of 30%, its $\varepsilon'$ and $\mu'$ values are appropriate for a good impedance matching at 28 GHz as shown in Fig. 8(a). On the contrary, it is impossible to achieve the good impedance matching when the $\varepsilon'$ values are too large as shown in Fig. 8(b)-(c). These results clearly reveal that, while excessively high $\varepsilon_r$ values, caused by the partial substitution of $Zn^{2+}$ for the $Fe^{2+}$ site, are inappropriate for impedance matching (here, $V_f$ of 60 and 90%), moderately high $\varepsilon_r$ values by reducing $V_f$ to 30% is appropriate for the good impedance matching, leading to excellent microwave absorption property. According to these results, improved real and imaginary parts of $\varepsilon_r$ and $\mu_r$ by the partial substitution of $Zn^{2+}$ for the $Fe^{2+}$ site enabled to reduce $V_f$ and enhance bandwidth without a serious degradation of microwave absorption with the thickness of $d$ = 0.64 mm, supporting that partial Zn-substituted $SrFe_{2-x}Zn_xW$ composites are appropriate as the microwave absorption materials for 5G communication.

In order to find the optimal sample thickness $d$, exhibiting a broadband covering the frequency region 27-29 GHz, the three-dimensional plot of the *RL* maps for the thickness region of 0.1-2.5 mm, the $d$ dependence of the *RL* value, calculated thickness ($d_{cal}$, $\lambda/4$), and matching thickness, $d_m$, are plotted in Fig. 9(a), (b), and (c), respectively, for the $SrFe_{1.75}Zn_{0.25}W$ composite with $V_f$ of 30% as a representative of our samples. The *RL* calculations as a function of $d$ were carried out with a step of 0.01 mm (0.61-0.66 mm). The *RL* humps in Fig. 9(b) shift to a higher frequency region with decreasing $d$, which is attributed to the quarter wavelength principle.

Here, it is noteworthy that the *RL* humps are tunable by adjusting *d* at a given frequency [62]. In addition, as shown in Fig. 9(b) and (c), the $d_m$ values exhibiting the largest *RL* humps at the given $f_m$ values are well located on the line of $d_{cal}$ versus frequency, representing that the $RL_{min}$ values can be obtained when the $d_m$ and $f_m$ values satisfy the quarter wavelength principle.

For a comparison with previously reported MAMs in the frequency region of 27-29 GHz, the microwave absorption properties of $SrFe_{2-x}Zn_xW$ (x =0.25, 1.0, 2.0) composites are listed in Table 2 together with those of other MAMs [36, 63-71]. A direct comparison with other MAMs is very difficult because the matching frequency $f_m$ is normally different from each other. Thus, in addition to the $RL_{min}$ values, we focused on the values of bandwidth, *d*, and $V_f$ in the frequency region of 27-29 GHz that are very important factors for real 5G communication. Compared with Co-substituted $BaNi_2W$-type hexaferrite composites reported by Y. Kim *et al.* [36], our $SrFe_{1.75}Zn_{0.25}W$ composite has lower $RL_{min}$ value with thinner $d_m$ and smaller $V_f$, which is attributed to higher refractive index, *n*. Unfortunately, a full comparison with their results is unavailable because the $\varepsilon_r$ spectra as a function of frequency were not presented in their literature. On the other hand, in the case of M-type hexaferrite composites with relatively lower $V_f$ values ranging from 30 to 50% [64, 65, 68], it may be impossible to obtain wider bandwidth in the region of 27-29 GHz with $RL < -20$ dB as shown in Table 2. In contrast, the BaM-type hexaferrite composite [63] exhibits wider bandwidth and lower $RL_{min}$ value among all M-type hexaferrites in Table 2. However, the *d* and $V_f$ values are 0.8 mm and 90%, respectively, which are about 125% and 300% higher compared with those of our $SrFe_{1.75}Zn_{0.25}W$ composite. Consequently, it is obvious that the $SrFe_{1.75}Zn_{0.25}W$ composite with $V_f$ of 30% exhibits the lowest $RL_{min}$ value with thinner *d* and lower $V_f$ (lightweight) in the region

of 27-29 GHz among all values ever reported for MAMs.

Finally, for our $SrFe_{2-x}Zn_xW$ composite samples, we illustrated the microwave absorption mechanism in Fig 10. Since the electron hopping between $Fe^{2+}$ and $Fe^{3+}$ ions is responsible for the electric polarization, the complex permittivity in unsubstituted and partially Zn-substituted SrW composites is proportional to the concentration of $Fe^{2+}$ ions. The dielectric loss is mainly due to the interfacial polarization between hexaferrite and epoxy resin. On the other hand, the real parts of complex permeability are proportional to the ratio of $M_s/H_a$ according to Snoek's law. While the magnetic loss is mainly caused by the eddy current loss in relatively lower frequency region away from natural resonance frequency, it is also caused by the ferromagnetic resonance in relatively higher frequency close to natural resonance frequency.

## 4.4 Summary

In this study, the frequency dependence of complex permittivity and permeability of the $SrFe_{2-x}Zn_xW$ ($x$ = 0.0, 0.25, 0.5, 1.0, and 2.0) composites with $V_f$ of 30, 60, and 90%, were measured to estimate their microwave absorption properties in the Ka-band (26.5-40 GHz). The partial substitution of $Zn^{2+}$ ion for the $Fe^{2+}$ ion site turned out to be very effective for the enhancement of the $\varepsilon_r$ and $\mu_r$ components due to the electron hopping between $Fe^{2+}$ and $Fe^{3+}$ ions and improved ratio of $M_s/H_a$, respectively. Among all samples, a 0.64 mm-thick $SrFe_{1.75}Zn_{0.25}W$ composite with $V_f$ of 30% exhibited the highest performance absorber in the region of 27-29 GHz, possessing the $RL_{min}$ value of −68.4 dB at 28 GHz with the bandwidths of 5.16 GHz (26.50-31.66 GHz) and 2.48 GHz (26.50-28.98 GHz) below −10 and −20 dB,

respectively. Further improvement of microwave absorption properties may be possible by optimizing the composition $x$ (i.e., the amount of Zn substitution), its $V_f$, the kind and amount of polymer matrix, and sample fabrication processing for measurement. In conclusion, partial Zn-substituted of $SrFe_{2-x}Zn_xW$ composites must be very promising candidates as a thin broadband microwave absorber for 5G communication near 28 GHz.

**Table 4.1.** The list of $V_f$, $f_m$, $d_m$, $RL_{min}$, and bandwidths (below −10 and −20 dB) of $SrFe_{2-x}Zn_xW$ ($x$ = 0.0, 0.25, 0.5, 1.0, and 2.0) composites.

| Zn content ($x$) | $V_f$ (%) | $f_m$ (GHz) | $d_m$ (mm) | $RL$ (dB) | Bandwidth (≤−10 dB, GHz) | Bandwidth (≤−20 dB, GHz) |
|---|---|---|---|---|---|---|
| 0.0 | 90 | 27.7 | 0.38 | -9.0 | - | - |
| | 60 | 29.3 | 0.42 | -20.9 | 4.74 (27.08-31.82) | 0.51 (29.16-29.67) |
| | 30 | 34.9 | 0.46 | -55.2 | 7.15 (32.19-39.34) | 1.75 (33.97-35.72) |
| 0.25 | 90 | 29.6 | 0.40 | -11.0 | 2.80 (28.07-30.87) | - |
| | 60 | 31.5 | 0.42 | -15.9 | 5.45 (28.70-34.15) | - |
| | 30 | 28.0 | 0.64 | -68.4 | 5.16 (26.50-31.66) | 2.48 (26.50-28.98) |
| 0.5 | 90 | 31.6 | 0.40 | -12.6 | 3.13 (26.50-29.63) | - |
| | 60 | 28.8 | 0.52 | -17.0 | 5.23 (26.50-31.73) | - |
| | 30 | 36.9 | 0.52 | -53.7 | 6.85 (33.15-40.00) | 2.8 (35.63-38.43) |
| 1.0 | 90 | 26.5 | 0.51 | -13.4 | 3.34 (26.50-29.84) | - |
| | 60 | 26.5 | 0.59 | -22.7 | 3.07 (26.50-29.57) | 0.38 (26.50-26.88) |
| | 30 | 32.3 | 0.65 | -55.7 | 11.10 (28.90-40.00) | 2.27 (31.18-33.45) |
| 2.0 | 90 | 29.7 | 0.68 | -12.2 | 7.26 (26.50-33.76) | - |
| | 60 | 29.0 | 0.75 | -19.7 | 6.93 (26.50-33.43) | - |
| | 30 | 34.2 | 0.79 | -51.1 | 9.90 (30.10-40.00) | 6.94 (33.06-40.00) |

**Table 4.2.** The list of fillers, matrices, $V_f$, $f$, $d$, $RL$, and bandwidths covering the region of 27-29 GHz for our composites of $x$ = 0.25, 1.0, 2.0 and various MAMs reported in the literature. The data from ref. [36, 63-71] are approximated.

| MAM filler | Matrices | $V_f$ (%) | $f$ (GHz) | $d$ (mm) | $RL$ (dB) | Bandwidth (GHz) covering the region of 27-29 GHz | | Ref. |
|---|---|---|---|---|---|---|---|---|
| | | | | | | $RL \leq -10$ dB | $RL \leq -20$ dB | |
| $SrFe_{1.75}Zn_{0.25}W$ | Epoxy resin | 30 | 28.0 | 0.64 | −68.4 | 5.16 (26.50-31.66) | 2.48 (26.50-28.98) | present results |
| $SrFeZnW$ | Epoxy resin | 30 | 28.1 | 0.77 | −24.3 | 5.62 (26.50-32.12) | 1.60 (27.46-29.06) | |
| $SrZn_2W$ | Epoxy resin | 30 | 27.8 | 1.01 | -23.2 | 6.47 (26.50-32.97) | 1.71 (26.86-28.57) | |
| $BaNi_{1.6}Co_{0.4}W$ | Silicone rubber | 50 | 31.9 | 0.9 | −45.0 | 7.58 (26.50-34.08) | 6.21 (26.85-33.06) | [36] |
| $BaM$ | Polyvinyl alcohol | 90 | 28.1 | 0.80 | −40.0 | 6.17 (24.67-30.84) | 2.30 (27.60-29.90) | [64] |
| $BaCo_{0.5}Ti_{0.5}M$ | Silicone rubber | 50 | 31.4 | 0.70 | −30.0 | 11.08 (27.30-38.38) | 7.02 (29.15-36.17) | [65] |
| $BaZr_{0.3}M$ | Paraffin wax | 45 | 27.7 | 1.05 | −25.0 | 10.04 (26.50-36.54) | 1.29 (27.22-28.51) | [66] |
| $Ba_{0.6}La_{0.2}Na_{0.2}Fe_{10}CoTiM$ | Polyvinyl alcohol | 90 | 30.0 | 2.00 | −31.8 | 3.17 (28.67-31.84) | 1.52 (29.48-31.00) | [67] |
| $Sr_{0.85}La_{0.15}(MnZr)_{0.5}M$ | Polyvinyl alcohol | 90 | 27.6 | 2.50 | −32.9 | 6.79 (26.50-33.29) | 1.19 (27.16-28.35) | [68] |
| $Sr(MnTi)_2M$ | Thermal plastic resin | 30 | 28.0 | 2.00 | −16.0 | 1.93 (27.00-28.93) | - | [69] |
| $Ni_{0.7}Co_{0.3}Fe_{0.3}O_4$ | Polyvinyl alcohol | 90 | 28.9 | 3.50 | −24.0 | 4.06 (27.32-31.38) | 1.08 (28.38-29.46) | [70] |
| $Ba_{0.5}La_{0.25}Na_{0.25}CoZrM$ | Polyvinyl alcohol | 90 | 27.0 | 5.80 | −37.4 | 2.41 (26.50-28.91) | 1.23 (26.50-27.63) | [71] |
| $Sr_{0.75}La_{0.25}M$ | Polyvinyl alcohol | 90 | 27.8 | 2.90 | −18.6 | 1.85 (26.80-28.65) | - | [72] |

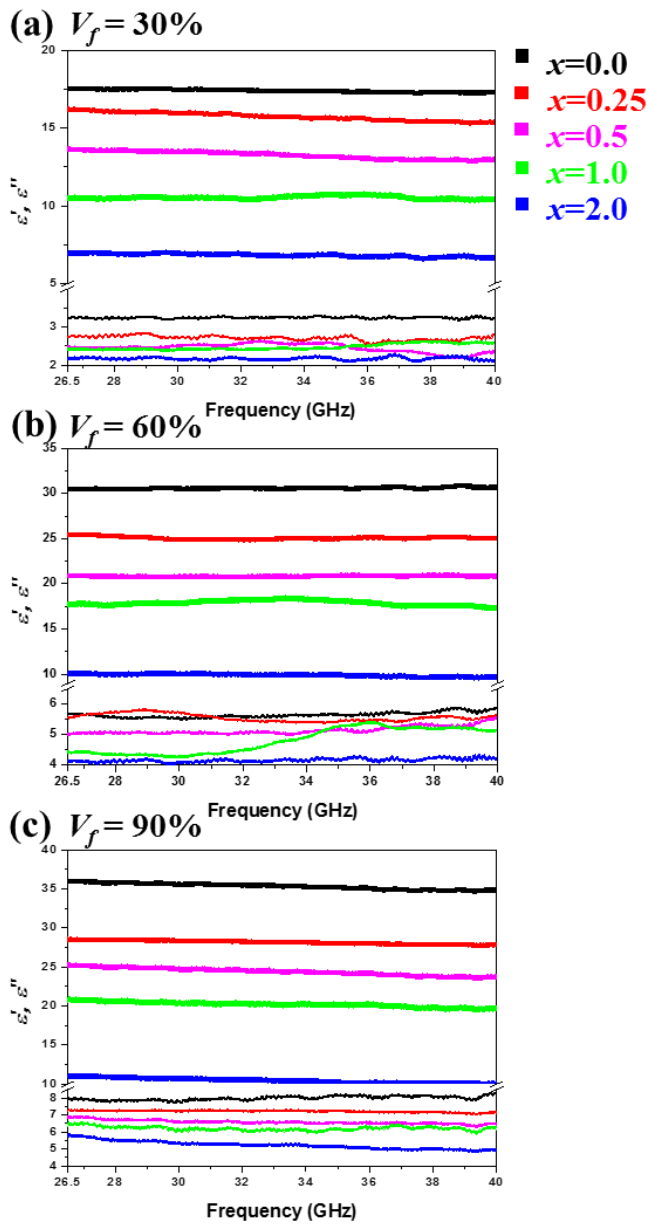


**Fig. 4.1.** The real and imaginary parts of complex permittivity for $SrFe_{2-x}Zn_xW$ ($x$ = 0.0, 0.25, 0.5, 1.0, and 2.0) composites with $V_f$ of (a) 30, (b) 60, and (c) 90%.

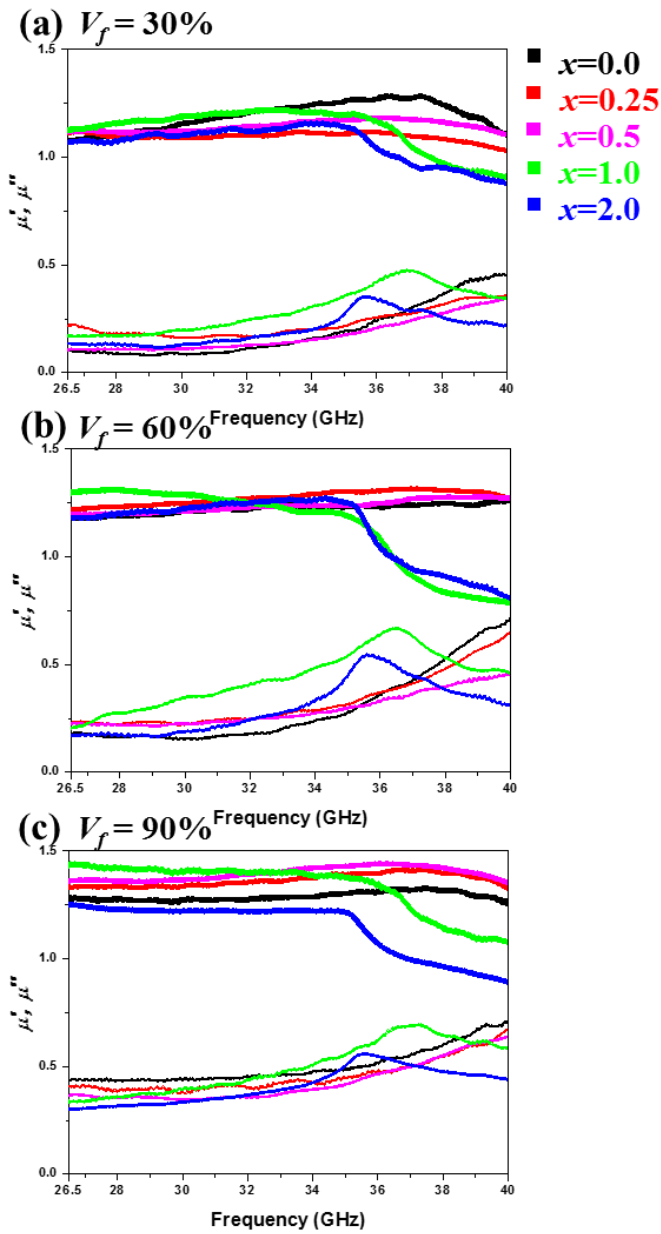


**Fig. 4.2.** The real and imaginary parts of complex permeability for $SrFe_{2-x}Zn_xW$ ($x$ = 0.0, 0.25, 0.5, 1.0, and 2.0) composites with $V_f$ of (a) 30, (b) 60, and (c) 90%.

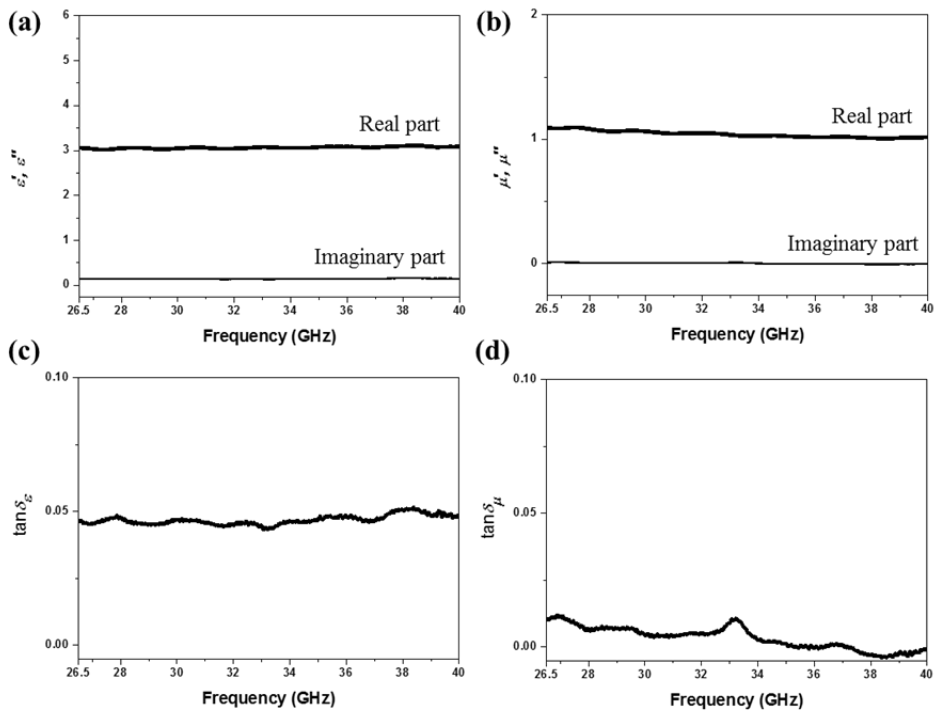


**Fig. 4.3.** Complex permittivity (a), permeability (b), dielectric loss tangent (c), and magnetic loss tangent (d) of pure epoxy resin.

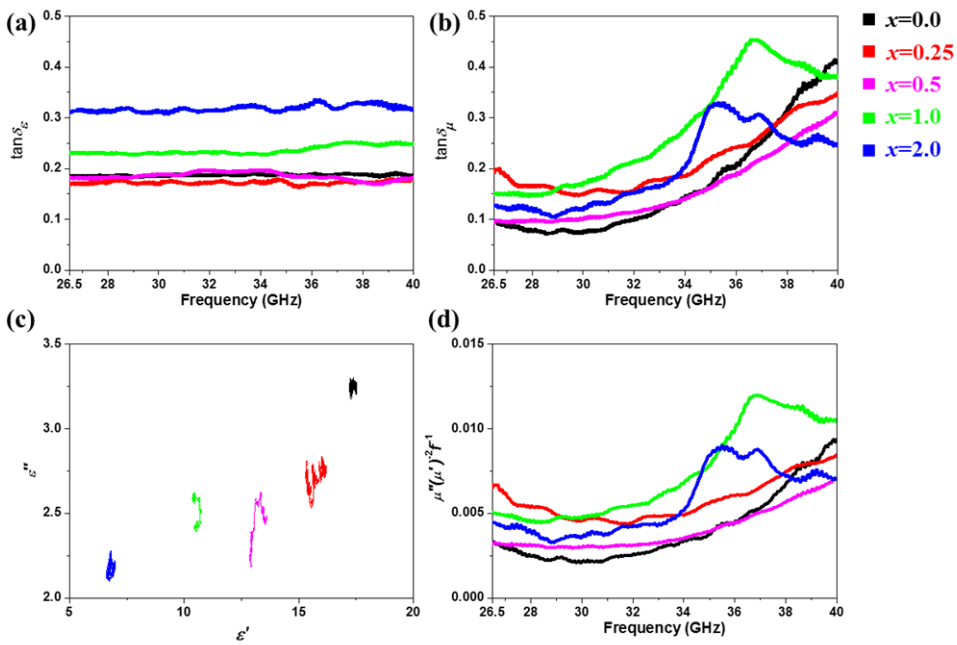


**Fig. 4.4.** (a) Dielectric loss tangent, (b) magnetic loss tangent, (c) Cole-Cole plot, and (d) $\mu''(\mu')^{-2}(f)^{-1}$ plot for $SrFe_{2-x}Zn_xW$ ($x$ = 0.0, 0.25, 0.5, 1.0, and 2.0) composites with $V_f$ of 30%.

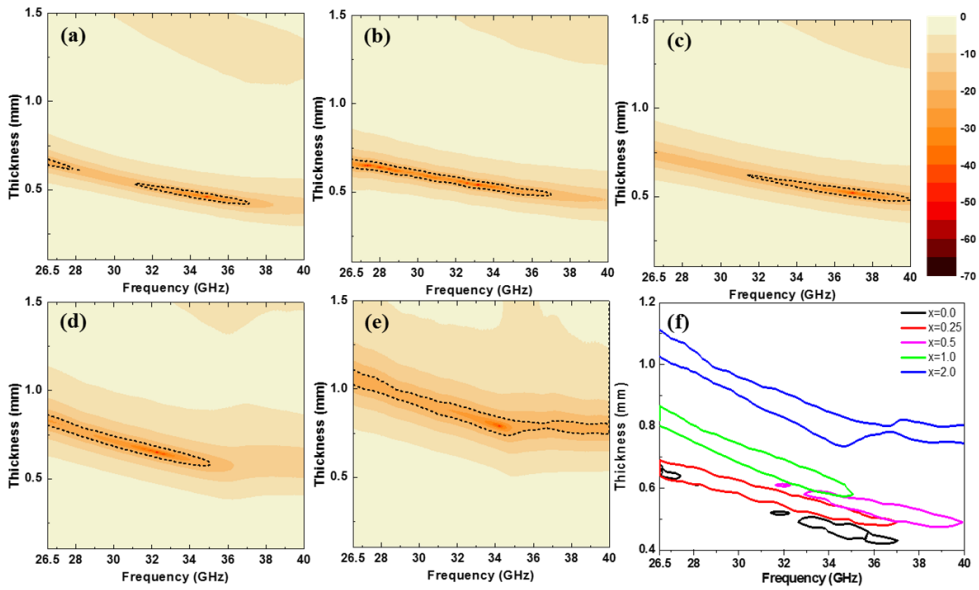


**Fig. 4.5.** *RL* maps for $SrFe_{2-x}Zn_xW$ composites of (a) $x = 0.0$, (b) $x = 0.25$, (c) $x = 0.5$, (d) $x = 1.0$, and (e) $x = 2.0$ with a $V_f$ of 30%. The regions of $RL \leq -20$ dB are represented together in for a comparison (f).

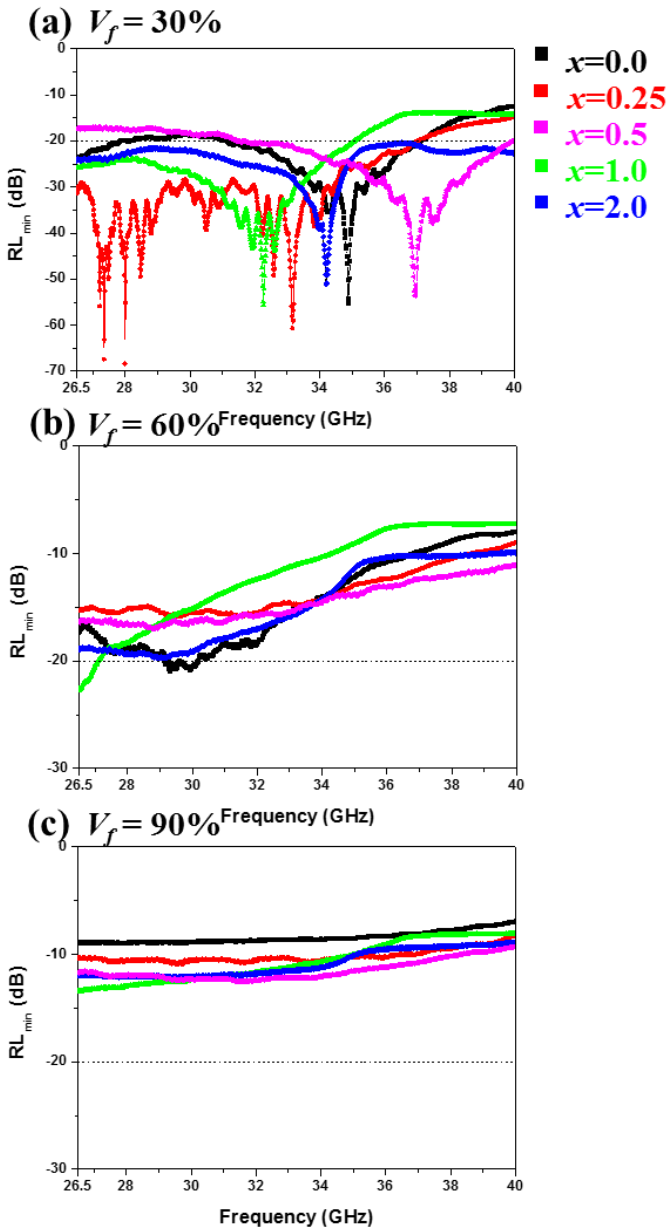


**Fig. 4.6.** Plots of $RL_{min}$ as a function of frequency for $SrFe_{2-x}Zn_xW$ composites with the $V_f$ values of (a) 30, (b) 60, and (c) 90%.

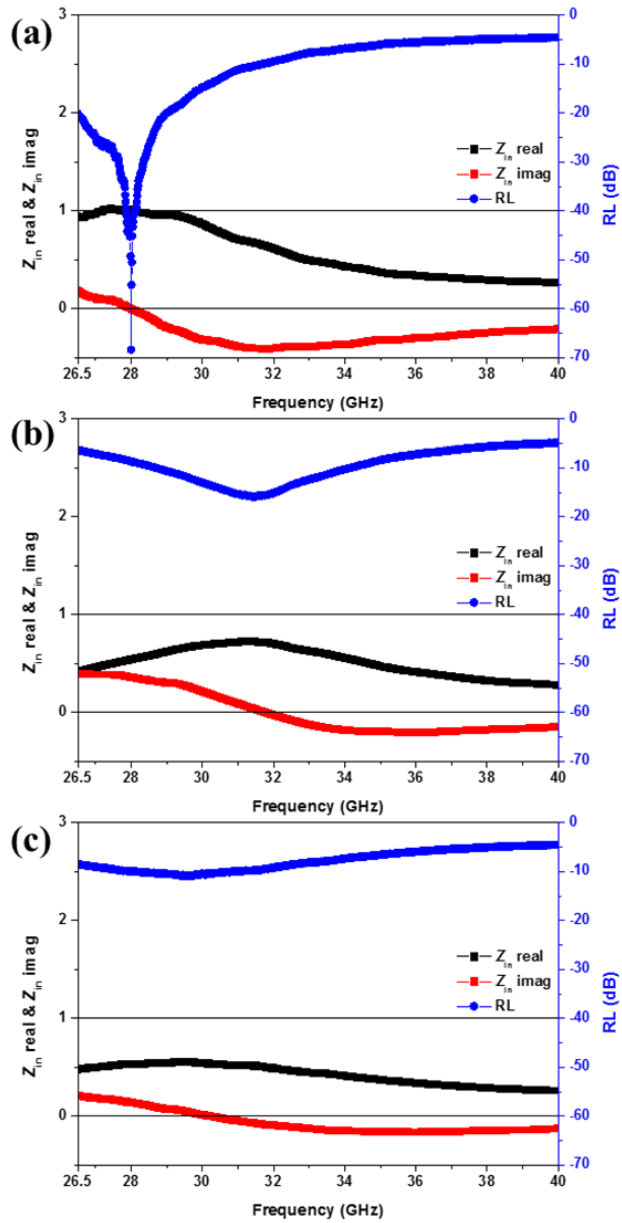


**Fig. 4.7.** Plots of the real and imaginary parts of the normalized input impedance $Z_{in}$ and the *RL* values as a function of frequency for the $SrFe_{1.75}Zn_{0.25}W$ composites with the $V_f$ values of (a) 30, (b) 60, and (c) 90%.

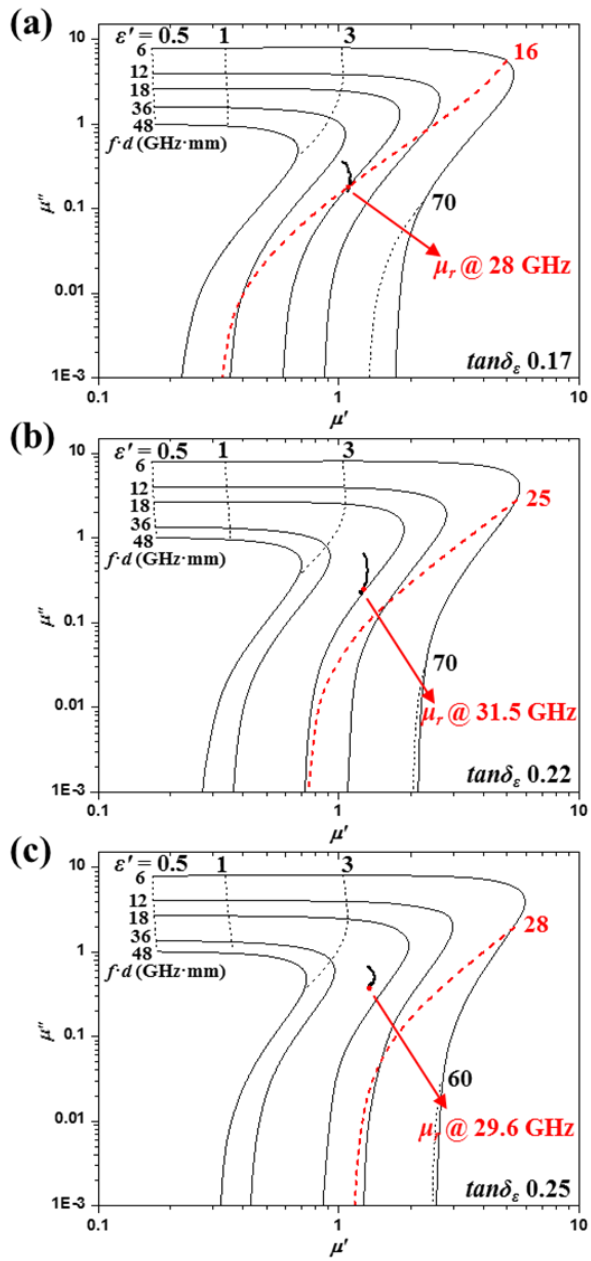


**Fig. 4.8.** The impedance matching solution maps for $SrFe_{1.75}Zn_{0.25}W$ composites with the $V_f$ values of (a) 30, (b) 60, and (c) 90% *complex permittivity ($\varepsilon_r$) and dielectric tangent loss ($tan\delta_e = \varepsilon''/\varepsilon'$) are calculated at the matching frequency.

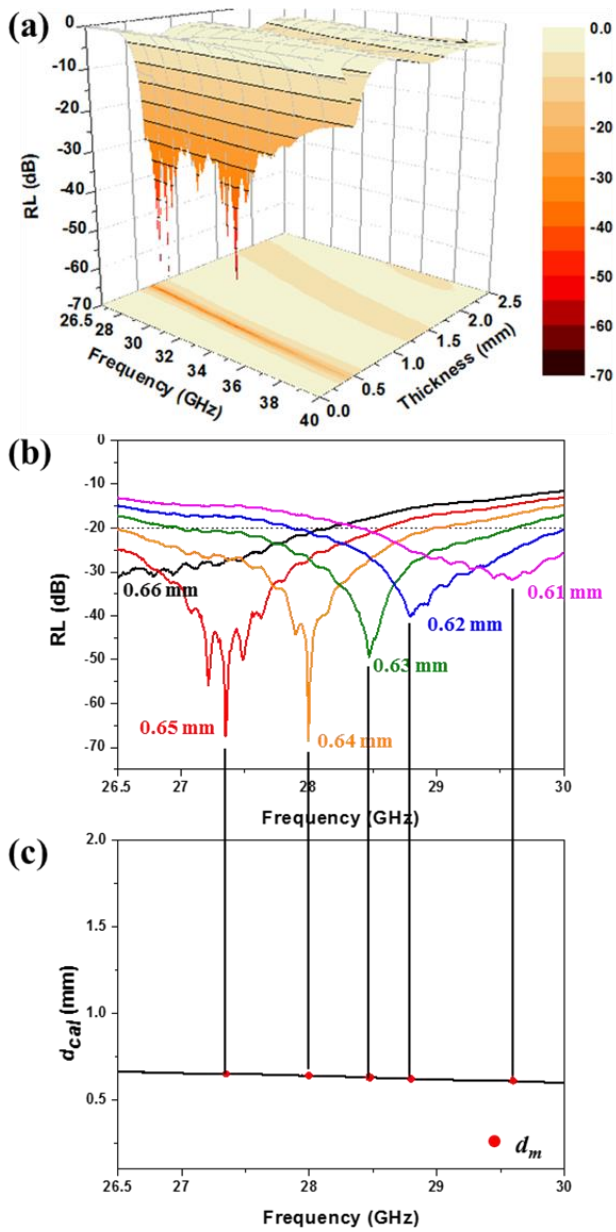


**Fig. 4.9.** (a) Three-dimensional plot of *RL* maps, (b) $RL_{min}$ as a function of frequency with $d$ = 0.61-0.66 mm, (c) $d_{cal}$ and $d_m$ as a function of frequency for the $SrFe_{1.75}Zn_{0.25}W$ composite. The vertical lines represent that the $d_m$ values of 0.65, 0.64, 0.63, 0.62, and 0.61 mm, exhibiting the largest *RL* humps at the given $f_m$ values in (b), are the same with the $d_{cal}$ values in (c).

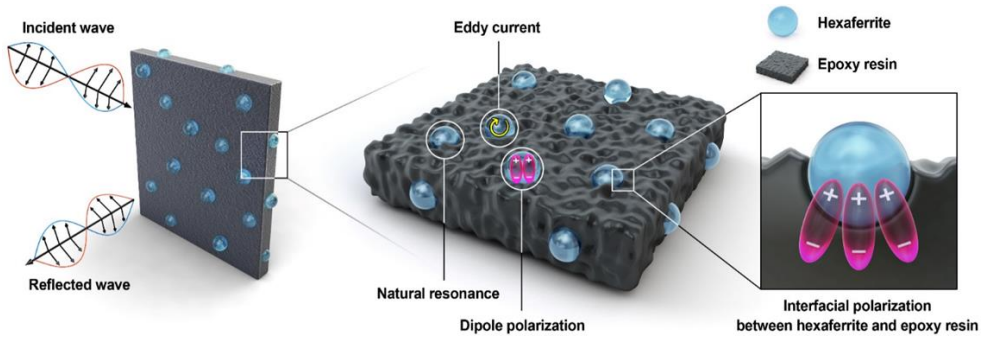


**Fig. 4.10.** Schematic of microwave absorption mechanisms for our composite samples.

# References

[1] G. Shao, J.F. Liang, W.Y. Zhao, B. Zhao, W. Liu, H.L. Wang, B.B. Fan, H.L. Xu, H.X. Lu, Y.G. Wang, R. Zhang, Co decorated polymer-derived SiCN ceramic aerogel composites with ultrabroad microwave absorption performance, Journal of Alloys and Compounds, 813 (2020) 152007.

[2] Y. Huang, J.D. Ji, Y. Chen, X. Li, J. He, X.W. Cheng, S.L. He, Y. Liu, J.P. Liu, Broadband microwave absorption of $Fe_3O_4$-$BaTiO_3$ composites enhanced by interfacial polarization and impedance matching, Composites Part B-Engineering, 163 (2019) 598-605.

[3] S. Vinayasree, M.A. Soloman, V. Sunny, P. Mohanan, P. Kurian, M.R. Anantharaman, A microwave absorber based on strontium ferrite-carbon black-nitrile rubber for S and X-band applications, Composites Science and Technology, 82 (2013) 69-75.

[4] Y.P. Sun, X.G. Liu, C. Feng, J.C. Fan, Y.H. Lv, Y.R. Wang, C.T. Li, A facile synthesis of $FeNi_3$@C nanowires for electromagnetic wave absorber, Journal of Alloys and Compounds, 586 (2014) 688-692.

[5] X.L. Guo, Z.J. Yao, H.Y. Lin, J.T. Zhou, Y.X. Zuo, X.Y. Xu, B. Wei, W.J. Chen, K. Qian, Epoxy resin addition on the microstructure, thermal stability and microwave absorption properties of core-shell carbonyl iron@epoxy composites, Journal of Magnetism and Magnetic Materials, 485 (2019) 244-250.

[6] B.C. Wang, J.Q. Wei, Y. Yang, T. Wang, F.S. Li, Investigation on peak frequency of the microwave absorption for carbonyl iron/epoxy resin composite, Journal of Magnetism and Magnetic Materials, 323 (2011) 1101-1103.

[7] S.C. Dang, Y. Lin, X.Z. Wei, H. Ye, Design and preparation of an ultrawideband gradient triple-layered planar microwave absorber using flaky carbonyl iron as absorbent, Journal of Materials Science-Materials in Electronics, 29 (2018) 17651-17660.

[8] Q.C. Liu, Z.F. Zi, M. Zhang, A.B. Pang, J.M. Dai, Y.P. Sun, Enhanced microwave absorption properties of carbonyl iron/$Fe_3O_4$ composites synthesized by a simple hydrothermal method, Journal of Alloys and Compounds, 561 (2013) 65-70.

[9] Z. Ma, Y. Zhang, C.T. Cao, J. Yuan, Q.F. Liu, J.B. Wang, Attractive microwave absorption and the impedance match effect in zinc oxide and carbonyl iron composite, Physica B-Condensed Matter, 406 (2011) 4620-4624.

[10] C. Stergiou, Magnetic, dielectric and microwave absorption properties of rare earth doped Ni-Co and Ni-Co-Zn spinel ferrites, Journal of Magnetism and Magnetic Materials, 426 (2017) 629-635.

[11] Y. Liu, X. Liu, X. Wang, Synthesis and microwave absorption properties of Ni-Zn-Mn spinel ferrites, Advances in Applied Ceramics, 114 (2015) 82-86.

[12] A. Ghasemi, G.R. Gordani, E. Ghasemi, $Co_2W$ hexaferrite nanoparticles-carbon nanotube microwave absorbing nanocomposite, Journal of Magnetism and Magnetic Materials, 469 (2019) 391-397.

[13] H. Nikmanesh, M. Moradi, G.H. Bordbar, R.S. Alam, Effect of multi dopant barium hexaferrite nanoparticles on the structural, magnetic, and X-Ku bands microwave absorption properties, Journal of Alloys and Compounds, 708 (2017) 99-107.

[14] A. Baniasadi, A. Ghasemi, A. Nemati, M.A. Ghadikolaei, E. Paimozd, Effect of Ti-Zn substitution on structural, magnetic and microwave absorption characteristics of strontium hexaferrite, Journal of Alloys and Compounds, 583 (2014) 325-328.

[15] V.K. Chakradhary, M.J. Akhtar, Highly coercive strontium hexaferrite nanodisks for microwave absorption and other industrial applications, Composites Part B-Engineering, 183 (2020).

[16] Z.D. Zhang, Z.C. Shi, R.H. Fan, M. Gao, J.Y. Guo, X.G. Qi, K.N. Sun, Microwave absorption properties of $Fe@Al_2O_3$ nanoembedments prepared by mechanosynthesis, Materials Chemistry and Physics, 130 (2011) 615-618.

[17] X.D. Chen, G.Q. Wang, Y.P. Duan, S.H. Liu, Microwave absorption properties of barium titanate/epoxide resin composites, Journal of Physics D-Applied Physics, 40 (2007) 1827-1830.

[18] I.S. Unver, Z. Durmus, Magnetic and Microwave Absorption Properties of Magnetite ($Fe_3O_4$)@ Conducting Polymer (PANI, PPY, PT) Composites, Ieee Transactions on Magnetics, 53 (2017) 2001708.

[19] D.C. Tiwari, P. Dipak, S.K. Dwivedi, T.C. Shami, P. Dwivedi, $PPy/TiO_2$(np)/CNT polymer nanocomposite material for microwave absorption, Journal of Materials Science-Materials in Electronics, 29 (2018) 1643-1650.

[20] Y.H. Chen, Z.H. Huang, M.M. Lu, W.Q. Cao, J. Yuan, D.Q. Zhang, M.S. Cao, 3D $Fe_3O_4$ nanocrystals decorating carbon nanotubes to tune electromagnetic properties and enhance microwave absorption capacity, Journal of Materials Chemistry A, 3 (2015) 12621-12625.

[21] H. Wang, F. Meng, J. Li, T. Li, Z. Chen, H. Luo, Z. Zhou, Carbonized Design of Hierarchical Porous Carbon/$Fe_3O_4$@Fe Derived from Loofah Sponge to Achieve Tunable High-Performance Microwave Absorption, Acs Sustainable Chemistry & Engineering, 6 (2018) 11801-11810.

[22] K.Q. He, L.M. Yu, L.M. Sheng, K. An, Y. Ando, X.L. Zhao, Doping Effect of Single-Wall Carbon Nanotubes on the Microwave Absorption Properties of Nanocrystalline Barium Ferrite, Japanese Journal of Applied Physics, 49 (2010) 125101.

[23] S. Kumar, G. Datt, A.S. Kumar, A.C. Abhyankar, Enhanced absorption of microwave radiations through flexible polyvinyl alcohol-carbon black/barium hexaferrite composite films, Journal of Applied Physics, 120 (2016) 164901.

[24] J. Qiu, T.T. Qiu, Fabrication and microwave absorption properties of magnetite nanoparticle-carbon nanotube-hollow carbon fiber composites, Carbon, 81 (2015) 20-28.

[25] S. Kumar, R. Chatterjee, Complex permittivity, permeability, magnetic and microwave absorbing properties of $Bi^{3+}$ substituted U-type hexaferrite, Journal of Magnetism and Magnetic Materials, 448 (2018) 88-93.

[26] G. Ramezanzaeh, A. Ghasemi, R. Mozaffarinia, A. Alizadeh, Electromagnetic wave reflection loss and magnetic properties of M-type $SrFe_{12-x}(Mn_{0.5}Sn_{0.5})_xO_{19}$ hexagonal ferrite nanoparticles in the Ku microwave band, Ceram. Int., 43 (2017) 10231-10238.

[27] R.C. Pullar, Hexagonal ferrites: A review of the synthesis, properties and applications of hexaferrite ceramics, Progress in Materials Science, 57 (2012) 1191-1334.

[28] A. Sharbati, J.M.V. Khani, Effect of $Ho^{3+}$ substitution on magnetic and microwave absorption properties of $Sr(ZnZr)_{0.5}Fe_{12}O_{19}$ hexagonal ferrite nanoparticles, Journal of Materials Science-Materials in Electronics, 24 (2013) 3629-3633.

[29] A. Arora, S.B. Narang, Investigation of electrical, dielectric and microwave properties of double substituted M-type $Ba_{(1-2x)}La_xNa_xFe_{10}Co_{0.5}TiMn_{0.5}O_{19}$ hexaferrite, Journal of Materials Science-Materials in Electronics, 29 (2018) 12718-12728.

[30] E. Kiani, A.S.H. Rozatian, M.H. Yousefi, Structural, magnetic and microwave absorption properties of $SrFe_{12-2x}(Mn_{0.5}Cd_{0.5}Zr)_xO_{19}$ ferrite, Journal of Magnetism and Magnetic Materials, 361 (2014) 25-29.

[31] P. Azizi, S.M. Masoudpanah, S. Alamolhoda, Magnetic and microwave absorption properties of $SrZnCoFe_{16}O_{27}$ powders synthesized by solution combustion method, Journal of Alloys and Compounds, 739 (2018) 211-217.

[32] L. Deng, L. Ding, K. Zhou, S. Huang, Z. Hu, B. Yang, Electromagnetic properties and microwave absorption of W-type hexagonal ferrites doped with $La^{3+}$, Journal of Magnetism and Magnetic Materials, 323 (2011) 1895-1898.

[33] M. Sun, J. Zheng, L. Liang, K. Sun, Y. Song, S. Zhao, Effect of Zn substitution on the electromagnetic and microwave absorbing properties of $BaCo_2$ hexaferrite, Journal of Materials Science-Materials in Electronics, 26 (2015) 9970-9976.

[34] W. Jing, Z. Hong, S.X. Bai, C. Ke, C.R. Zhang, Microwave absorbing properties of rare-earth elements substituted W-type barium ferrite, Journal of Magnetism and Magnetic Materials, 312 (2007) 310-313.

[35] R.A. Khan, S. Mizukami, A.M. Khan, B. Ismail, A.R. Khan, T. Miyazaki, Static and dynamic magnetic characteristics of Mg substituted Ba-$Co_2$ W-type hexaferrites, Journal of Alloys and Compounds, 637 (2015) 197-202.

[36] Y.J. Kim, S.S. Kim, Microwave absorbing properties of Co-substituted $Ni_2W$ hexaferrites in Ka-band frequencies (26.5-40 GHz), Ieee Transactions on Magnetics, 38 (2002) 3108-3110.

[37] J.H. You, S.I. Yoo, Improved magnetic properties of Zn-substituted strontium W-type hexaferrites, Journal of Alloys and Compounds, 763 (2018) 459-465.

[38] J.H. You, S. Choi, S.Y. Park, S.I. Yoo, Enhanced microwave absorption properties of Zn-substituted Y-type hexaferrites, Journal of Magnetism and Magnetic Materials, 491 (2019) 165640.

[39] H.L. Liu, T. Siriburanon, K. Nakata, W. Deng, J.H. Son, D.Y. Lee, K. Okada, A. Matsuzawa, A 28-GHz Fractional-N Frequency Synthesizer with Reference and Frequency Doublers for 5G Mobile Communications in 65nm CMOS, Ieice Transactions on Electronics, E101C (2018) 187-196.

[40] G.S. Karthikeya, M.P. Abegaonkar, S.K. Koul, Polycarbonate Based Overlapped Architecture for Landscape and Portrait Modes of mmWave 5G Smartphone, Progress in Electromagnetics Research M, 86 (2019) 135-144.

[41] K. Sakaguchi, T. Haustein, S. Barbarossa, E.C. Strinati, A. Clemente, G. Destino, A. Parssinen, I. Kim, H. Chung, J. Kim, W. Keusgen, R.J. Weiler, K. Takinami, E. Ceci, A. Sadri, L. Xian, A. Maltsev, G.K. Tran, H. Ogawa, K. Mahler, R.W. Heath, Where, When, and How mmWave is Used in 5G and Beyond, Ieice Transactions on Electronics, E100C (2017) 790-808.

[42] L. Wang, Z.Y. Li, J. Jiang, T.Y. An, H.W. Qin, J.F. Hu, Sample-size resonance, ferromagnetic resonance and magneto-permittivity resonance in multiferroic nano-$BiFeO_3$/paraffin composites at room temperature, Journal of Magnetism and Magnetic Materials, 421 (2017) 71-75.

[43] E. Ni, An uncertainty analysis for the measurement of intrinsic properties of materials by the combined transmission-reflection method, Ieee Transactions on Instrumentation and Measurement, 41 (1992) 495-499.

[44] Y. Naito, K. Suetake, Application of ferrite to electromagnetic wave absorber and its characeristics, Ieee Transactions on Microwave Theory and Techniques, MT19 (1971) 65-72.

[45] C.A. Stergiou, I. Manolakis, T.V. Yioultsis, G. Litsardakis, Dielectric and magnetic properties of new rare-earth substituted Ba-hexaferrites in the 2-18 GHz frequency range, Journal of Magnetism and Magnetic Materials, 322 (2010) 1532-1535.

[46] S. Choi, J.H. You, C.Y. Bon, S.Y. Park, S.I. Yoo, Enhanced microwave absorption properties of Zn-substituted SrW-type hexaferrite composites in the Ku-band, Ceram. Int., 47 (2021) 7571-7581.

[47] A. Strauchs, A. Mashkin, A. Schnettler, Effects of $SiO_2$ Nanofiller on the Properties of Epoxy Resin Based Syntactic Foam, Ieee Transactions on Dielectrics and Electrical Insulation, 19 (2012) 400-407.

[48] I. Araz, Microwave Charecterization of Co-Doped Barium Hexaferrite Absorber Metarial, Journal of Superconductivity and Novel Magnetism, 29 (2016) 1545-1550.

[49] A.M.A. El Ata, M.K. El Nimr, D. El Kony, A.H. Al-Hammadi, Dielectric and magnetic permeability behavior of $BaCo_{2-x}Ni_xFe_{16}O_{27}$W-type hexaferrites, Journal of Magnetism and Magnetic Materials, 204 (1999) 36-44.

[50] W. Xing, X.L. Liu, H. Wang, J. Chen, Q. Fan, Q. Lei, G. Xu, Tunable Microwave Absorption Properties in Ni-Zn-Substituted $BaCoTiFe_{10}O_{19}$, Journal of Superconductivity and Novel Magnetism, 31 (2018) 1411-1419.

[51] X. Sun, J.P. He, G.X. Li, J. Tang, T. Wang, Y.X. Guo, H.R. Xue, Laminated magnetic graphene with enhanced electromagnetic wave absorption properties, Journal of Materials Chemistry C, 1 (2013) 765-777.

[52] Y. Zhang, Y.a. Huang, X. Liang, Y. Yang, R. Zhang, R. Huang, Preparation and Microwave Absorption of Nitrogen-Doped Carbon Nanotubes With Iron Particles, Ieee Transactions on Magnetics, 54 (2018) 2300606.

[53] Y. Wei, H. Liu, S. Liu, M. Zhang, Y. Shi, J. Zhang, L. Zhang, C. Gong, Waste cotton-derived magnetic porous carbon for high-efficiency microwave absorption, Composites Communications, 9 (2018) 70-75.

[54] W.H. Gu, J.B. Chen, Y. Zhao, G.H. Wang, F. Wang, T.Z. Zhang, B.S. Zhang, Extending effective microwave absorbing bandwidth of CoNi bimetallic alloy derived from binary hydroxides, Scientific Reports, 10 (2020) .

[55] X.Y. Wang, T. Zhu, S.C. Chang, Y.K. Lu, W.B. Mi, W. Wang, 3D Nest-Like Architecture of Core-Shell $CoFe_2O_4$@1T/2H-$MoS_2$ Composites with Tunable Microwave Absorption Performance, Acs Applied Materials & Interfaces, 12 (2020) 11252-11264.

[56] W. Xing, J. Chen, H. Wang, Q. Fan, Q. Lei, G. Xu, Introduction of $Zn^{2+}$ in $BaCoTiFe_{10}O_{19}$ to tune electromagnetic parameters and improve microwave absorption properties, Journal of Alloys and Compounds, 731 (2018) 279-287.

[57] H. Kaur, C. Singh, A. Marwaha, S.B. Narang, R. Jotania, S.R. Mishra, Y. Bai, K.C.J. Raju, D. Singh, M. Ghimire, P. Dhruv, A.S.B. Sombra, Elucidation of microwave absorption mechanisms in Co-Ga substituted Ba-Sr hexaferrites in X-band, Journal of Materials Science-Materials in Electronics, 29 (2018) 14995-15005.

[58] J.G. Jia, C.Y. Liu, N. Ma, G.R. Han, W.J. Weng, P.Y. Du, Exchange coupling controlled ferrite with dual magnetic resonance and broad frequency bandwidth in microwave absorption, Science and Technology of Advanced Materials, 14 (2013).

[59] M.G. Han, D.F. Liang, L.J. Deng, Analyses on the dispersion spectra of permeability and permittivity for NiZn spinel ferrites doped with $SiO_2$, Applied Physics Letters, 90 (2007) 192507.

[60] F.S. Wen, F. Zhang, Z.Y. Liu, Investigation on Microwave Absorption Properties for Multiwalled Carbon Nanotubes/Fe/Co/Ni Nanopowders as Lightweight Absorbers, Journal of Physical Chemistry C, 115 (2011) 14025-14030.

[61] H.M. Musal, H.T. Hahn, Thin-layer electromagnetic absorber design, Ieee Transactions on Magnetics, 25 (1989) 3851-3853.

[62] P. Kaur, S.B. Narang, S. Bahel, Modulation of microwave properties of La-Sr hexagonal ferrite with doping of Co-Zr and change in thickness, Journal of Materials Science-Materials in Electronics, 28 (2017) 16077-16085.

[63] S.B. Narang, K. Pubby, C. Singh, Thickness and Composition Tailoring of K- and Ka-Band Microwave Absorption of $BaCo_xTi_xFe_{(12-2x)}O_{19}$ Ferrites, Journal of Electronic Materials, 46 (2017) 718-728.

[64] Y.J. Kim, S.S. Kim, Magnetic and microwave absorbing properties of Ti and Co substituted M-hexaferrites in Ka-band frequencies (26.5 similar to 40 GHz), Journal of Electroceramics, 24 (2010) 314-318.

[65] C. Liu, Q. Xu, Y. Tang, Z. Wang, R. Ma, N. Ma, P. Du, $Zr^{4+}$ doping-controlled permittivity and permeability of $BaFe_{12-x}Zr_xO_{19}$ and the extraordinary EM absorption power in the millimeter wavelength frequency range, Journal of Materials Chemistry C, 4 (2016) 9532-9543.

[66] A. Arora, S.B. Narang, K. Pubby, Enhanced Microwave Absorption Properties of Doped M-Type Barium Hexagonal Ferrites in Ka-band Frequencies, Journal of Superconductivity and Novel Magnetism, 32 (2019) 2705-2709.

[67] P. Kaur, S. Bahel, S.B. Narang, Broad-band microwave absorption of $Sr_{0.85}La_{0.15}(MnZr)_xFe_{12-2x}O_{19}$ hexagonal ferrite in 18-40 GHz frequency range, Journal of Magnetism and Magnetic Materials, 460 (2018) 489-494.

[68] C.L. Yuan, Y.S. Tuo, Microwave adsorption of $Sr(MnTi)_xFe_{12-2x}O_{19}$ particles, Journal of Magnetism and Magnetic Materials, 342 (2013) 47-53.

[69] K. Pubby, S.B. Narang, Ka band absorption properties of substituted nickel spinel ferrites: Comparison of open-circuit approach and short-circuit approach, Ceram. Int., 45 (2019) 23673-23680.

[70] A. Arora, S.B. Narang, Tuning of microwave absorptive behavior of double substituted barium hexaferrites with change in thickness in 26.5-40.0

GHz band, Applied Physics a-Materials Science & Processing, 123 (2017) 520.

[71] P. Kaur, S. Bahel, S.B. Narang, Electromagnetic Wave Absorption Properties of La-Doped Strontium M-Type Hexagonal Ferrite in a 18-40 GHz Frequency Range, Journal of Electronic Materials, 49 (2020) 1654-1659.

# Chapter 5

# Microwave absorption properties of $Al_2O_3$-coated carbonyl iron in the Ku-band (0.5-18 GHz)

## 5.1 Introduction

With the evolution of the fifth-generation (5G) technology, microwave electronic systems have been applied such as wireless communication and military applications in the Ku-band [1-3]. However, the electromagnetic pollution has become increasingly severe, leading to the electronic devices' malfunction and human physical health [4]. In order to solve the electromagnetic pollution problem, many researchers have focused on the development of efficient microwave absorbing materials (MAM) with lightweight, low loading of filler, wide bandwidth, and strong absorption property [5, 6].

In general, magnetics loss materials have been considered as a promising MAM. Especially, M and W-type hexaferrites have high $M_s$, excellent stability, and low cost [7-9]. Nevertheless, they are not suitable in Ku-band because their FMR frequencies are observed beyond the Ku-band. On the other hand, carbonyl iron is also a promising candidate for high-performance MAM because it exhibits the $M_s$ and $\mu_r$ in the microwave region [10]. However, the reason carbonyl iron has excellent electromagnetic properties but still is difficult to use in Ku-band for 5G applications is that the magnetic property is rapidly decreased with increasing frequency due to eddy current loss. The eddy current loss causes not only the degradation of property

but also the occurrence of Joule heating [11-14]. An effective method for reducing the eddy current loss is the formation of an insulation coating layer on the surface of Fe metal particles [15] since the inter-particle current path, which can lead to a macroscopic eddy current loss, can be effectively suppressed.

Insulation coating layers are normally either organic or inorganic materials [16]. An organic coating layer generally shows a good adhesivity, high flexibility, and non-toxicity. However, it suffers from poor thermal stability which may lead to a decomposition of the organic coating layer [13, 17-20]. On the other hand, an inorganic coating layer possesses good thermal stability. Thus, typical oxide insulators such as MgO, $TiO_2$, $SiO_2$, and $Al_2O_3$ have been employed as the coating layers of magnetic powders to reduce the resistivity. Among these materials, MgO and $TiO_2$ are reported to have a shortcoming that their electrical resistivity and adhesivity are relatively low [21-23]. Currently, $SiO_2$ is the most commonly reported insulation coating material due to its high electrical resistivity, chemical stability, and non-toxicity [10, 13, 15, 24-27]. In the case of alumina, $Al_2O_3$, although it must be a promising candidate for MAMs since it also possesses high electrical resistivity and good thermal stability, reports on its use as the insulation coating layer of magnetic powder are very limited so far [28, 29].

However, the insulation coating layer acts as a kind of air-gap which may deteriorate magnetic properties, especially the real part of $\mu_r$. Thus, it is important to control the thickness of the insulation layer on the surfaces of carbonyl iron in order to reduce the eddy current loss without significant degradation of real part of $\mu_r$.

In this part, the effect of the alumina coating time on the surface of carbonyl iron on microwave absorption property was investigated. Furthermore, in order to

improve the microwave absorption property, the effect of carbonyl iron mixed with dielectric powders has also been studied in the range of Ku-band.

## 5.2 Experimental

In this study, carbonyl iron FM powder (Fe 99.5%, BASF) with the average particle size of 2.5 ± 0.9 μm was used. FM powder was coated with alumina using the sol-gel method. D.I. water, absolute ethanol, and aluminum isopropoxide (98%, Sigma-Aldrich) were used to make a solution of 100 ml, acetylacetone (99%, Sigma-Aldrich) was added to the solution as a stabilizer, and this solution was homogenized at 60 ℃ for 30 min using a magnetic stirrer. To promote hydrolysis, the pH value was adjusted to 4 using nitric acid. FM powder was put into the solution, and mechanically stirred for 1 h at room temperature. Then, FM powder coated with alumina was washed three times using ethanol and then dried at 50 ℃ for 12 h in an oven.

The surface morphology of each type of alumina-coated powder was observed by field-emission scanning electron microscopy (FE-SEM, MERLIN Compact; Zeiss). In addition, In order to evaluate the microwave absorption properties of all composite samples, the specimens were prepared as follows. Carbonyl iron was mixed with epoxy resin powder to have the wt.% values of 30, 50, 70, and 90. Each powder mixture was pressed into a toroidal shape with an outer diameter of 7 mm and an inner diameter of 3.04 mm, and subsequently hardened at 175 ˚C for 1 h in air. The measurement of microwave $\varepsilon_r$ and $\mu_r$ was conducted for our toroidal samples by using a vector network analyzer (VNA) (Agilent PNA N5525A) with a coaxial

airline. Both $\varepsilon_r$ and $\mu_r$ were simultaneously measured in the Ku-band frequency region of 0.5–18 GHz by using a transmission and reflection method based on the algorithm developed by Nicolson and Ross [30].

### 5.3 Results and discussion

Here, the real and imaginary parts of both $\varepsilon_r$ and $\mu_r$ were presented as a function of frequency in the region of 0.5-18 GHz for our samples composed of carbonyl iron-epoxy resin composites with the wt.% values of 30, 50, 70, and 90. Next, their *RL* calculated by transmission line theory are presented as the function of frequency and sample thickness. Third, the effect of alumina coating on the surface of carbonyl iron and carbonyl iron mixed with dielectric materials, such as α-alumina and amorphous alumina on the microwave absorption properties were discussed in the Ku-band. Finally, high-performance MAMs were obtained for 5G applications at the 3.5 GHz.

Fig. 5.1 shows the real and imaginary parts of $\varepsilon_r$ and $\mu_r$ as the function of frequency for our composite samples. It is noteworthy that the real and imaginary parts of $\varepsilon_r$ and $\mu_r$ values are continuously decreased with decreasing carbonyl iron filler wt.% (or with increasing the epoxy-resin matrix fraction) as shown in Fig. 5.1. The reason is that the real and imaginary parts of $\varepsilon_r$ and $\mu_r$ are independent of frequency, and their values are $\varepsilon' \approx 3$, $\varepsilon'' \approx 0.1$, $\mu' \approx 1$, and $\mu'' \approx 0$. Thus, this decreasing tendency is ascribable to a continuous increase in the amount of epoxy resin since it has much lower real and imaginary parts of $\varepsilon_r$ and $\mu_r$ compared with carbonyl iron.

According to the transmission line theory, the normalized input impedance $Z_{in}$ of a single layer microwave absorber backed by a perfect conductor is given by

$$Z_{\text{in}} = Z_0\sqrt{\frac{\mu_r}{\varepsilon_r}}\tanh\left[\, j(2\pi fd/c)\sqrt{\mu_r\varepsilon_r}\,\right] \tag{5.1}$$

where $Z_0 = \sqrt{\mu_0/\varepsilon_0}$ is the characteristic impedance of free space. *c* is the speed of light, *f* is the frequency of the microwave, and *d* is the thickness of the absorber. The *RL* value (i.e., the microwave absorption ability of an incident microwave by a single-layer absorber) can be calculated by inserting the $Z_{in}/Z_o$ ratio in the following equation,

$$\text{Reflection loss (dB)} = 20\log\left|\frac{Z_{\text{in}} - Z_0}{Z_{\text{in}} + Z_0}\right| \tag{5.2}$$

One can see from Eq. (5.2) that the *RL* value becomes negatively infinite when the input impedance and impedance of free space are equal, which corresponds to a perfect absorption of the incident microwave.

The *RL* values were calculated by inserting $\varepsilon_r$ and $\mu_r$ spectra values of samples shown in Fig. 5.1 into Eqs. (5.1) and (5.2), and represented as the *RL* maps in Fig. 5.2 up to the thicknesses of 5 mm. In the *RL* maps, the regions with $RL \leq -20$ dB (99% absorption of incident microwave) are enclosed with black dots. Evaluated *RL* values for the carbonyl iron-epoxy composites with wt.% of 30, 50, 70, and 90 are displayed on the *RL* maps in Fig. 5.2. In these *RL* maps, the $RL_{min}$ of carbonyl iron composite with wt.% of 50% showed lower than −60 dB at 14.5 GHz as shown in Fig. 5.2(b). However, among all samples, it is impossible to obtain bandwidth for covering the region of 3.5 GHz. The reason for this poor microwave absorption properties is mainly from to high imaginary part of $\mu_r$ value. Thus, the eddy current loss should

be reduced. From this point of view, i tried to reduce the eddy current loss by adding dielectric materials and alumina insulating coating on the surface of carbonyl iron powder using the sol-gel method for 1h, 2h, and 4h.

The SEM micrographs of uncoated and alumina-coated carbonyl iron are shown in Fig. 5.3. This figure shows that the surface morphologies of uncoated particles are relatively smooth. While the surfaces of alumina-coated carbonyl iron obviously become rougher. To further analyze the alumina insulation coating, the compositional analysis with SEM-EDS was performed as shown in Fig. 5.4. The EDS spectra show that alumina-coated carbonyl iron has higher Al and O intensities than uncoated powder. From these results, it is obvious that alumina insulation layers are successfully coated on the surface of carbonyl iron via the sol-gel process. These results coincide very well with the SEM micrographs in Fig. 5.3. Thus, $\varepsilon_r$ and $\mu_r$ spectra of $Al_2O_3$-coated carbonyl iron for 1 h, 2h, and 4 h, carbonyl iron with α-alumina, and amorphous alumina 1wt.%, having wt.% of 70 are plotted in Fig. 5.5 as a function of frequency in the region of 0.5–18 GHz. As expected, the imaginary parts of $\mu_r$ values are decreased with increasing the coating time. As listed in Table 5.1, it was confirmed that the absorption properties were increased at 3.5 GHz, but the thickness were increased. Based on quarter wavelength principle, the reason why thickness is increased is that the real and imaginary parts of $\varepsilon_r$ and $\mu_r$ are decreased.

Unfortunately, since there are limitations in improving absorption properties through an increase in coating time. In order to improve microwave absorption properties, carbonyl iron was coated for 1 h and mixed with amorphous alumina or α-alumina. Their $\varepsilon_r$ and $\mu_r$ spectra are plotted in Fig. 5.6. As can be seen in Fig. 5.7 and Table 5.2, the $Al_2O_3$-coated carbonyl iron composite with amorphous alumina of 5wt.% have excellent microwave absorption properties with $RL \leq -20$ dB near 3.5

GHz. In addition, as the amount of dielectric materials increases, the areas with *RL* ≤ −20 dB are shifted to higher thickness region as listed in Table 5.2. This is due to the quarter wavelength principle which can be expressed as follows,

$$d = \frac{\lambda}{4} = \frac{c}{4f\sqrt{\mu_r \varepsilon_r}} \tag{5.3}$$

where $d$ is the thickness of the absorber, $\lambda$ is the wavelength of the microwave, $f$ is the frequency of the microwave, and $c$ is the speed of light. According to Eq. (5.3), one can see that the smaller refractive index, results in higher matching thickness, $d_m$. The imaginary part of $\mu_r$ are continuously decreased with increasing amorphous alumina due to a reduced eddy current loss as previously mentioned.

An impedance matching is very important factor for the achievement of strong microwave absorption ability. Thus, in order to confirm the degree of impedance matching for the $Al_2O_3$-coated carbonyl iron composites, the normalized real and imaginary parts of the input impedance $Z_{in}$, calculated by Eq. (5.1), together with the *RL* values calculated by Eq. (5.2) as a function of frequency are represented in Fig. 5.8. Theoretically, from Eq. (5.1), perfect impedance matching can be obtained when the normalized real part of the input impedance is 1 and the normalized imaginary part of the input impedance is 0. For the $Al_2O_3$-coated carbonyl iron composite with amorphous alumina of 5wt.%, impedance matching occurs at a $f_m$ of 3.5 GHz with a $d_m$ value of 4.36 mm, at which the minimum *RL* value of −28.9 dB was obtained as listed in Table 5.2. However, the only $Al_2O_3$-coated carbonyl iron for 1 h composite exhibits poor microwave absorption with *RL* > −20 dB overall measured frequency region due to a severe impedance mismatch. Consequently, it is clear that microwave

absorption properties are enhanced with $Al_2O_3$ insulation coating on the surface of carbonyl iron.

## 5.4 Summary

The real and imaginary parts of $\varepsilon_r$ and $\mu_r$ of uncoated and $Al_2O_3$-coated carbonyl iron-epoxy resin composite samples were measured in the frequency range of 0.5–18 GHz in order to evaluate their microwave absorption properties. Compared with uncoated carbonyl iron-epoxy resin composite, the $Al_2O_3$-coated carbonyl iron composites are very effective for the enhancement of microwave absorption properties due to a reduced $\mu''$. In addition, the effect of added amorphous alumina or alpha-alumina was very effective for enhancing microwave absorption properties and a wider absorber. Among all samples, a 4.36 mm-thick $Al_2O_3$-coated carbonyl iron composite with amorphous alumina of 5wt.% exhibited the most appropriate for real application, having the *RL* of −28.9 dB at 3.5 GHz with the bandwidth of 0.51 GHz (3.25-3.76 GHz) below −20 dB. In conclusion, the $Al_2O_3$-coated carbonyl iron-epoxy resin composites are favorable materials having lower *RL* value and broad bandwidth as a microwave absorber appropriate for 5G application near 3.5 GHz.

**Table 5.1.** The list of *RL*, *d*, and bandwidth (below ≤ −20 dB) of $Al_2O_3$-coated carbonyl iron for 1h, 2h, 4h and carbonyl iron with α-alumina and amorphous alumina 1wt.%, having wt.% of 70 at 3.5 GHz.

| Sample | *RL* (dB) | *d* (mm) | Bandwidth ≤ −20 dB (GHz) |
|---|---|---|---|
| $Al_2O_3$ for 1h | −18.7 | 3.94 | |
| $Al_2O_3$ for 2h | −20.4 | 4.02 | 0.16 (3.4-3.56 GHz) |
| $Al_2O_3$ for 4h | −21.1 | 4.26 | 0.25 (3.36-3.61 GHz) |
| α-alumina 1wt.% | -10.7 | 3.00 | |
| Amorphous alumina 1wt.% | -10.6 | 3.38 | |

**Table 5.2.** The list of *RL*, *d*, and bandwidth (below ≤ −20 dB) of $Al_2O_3$-coated carbonyl iron and $Al_2O_3$-coated carbonyl iron with dielectric materials composites having wt.% of 70 at 3.5 GHz.

| Sample | *RL* (dB) | *d* (mm) | Bandwidth ≤ −20 dB (GHz) |
|---|---|---|---|
| $Al_2O_3$ 1h | −18.7 | 3.94 | |
| $Al_2O_3$ 1h with Amorphous 1wt.% | −23.1 | 4.06 | 0.36 (3.31-3.67 GHz) |
| $Al_2O_3$ 1h with Amorphous 3wt.% | −25.1 | 4.36 | 0.43 (3.29-3.72 GHz) |
| $Al_2O_3$ 1h with Amorphous 5wt.% | −28.9 | 4.60 | 0.51 (3.25-3.76 GHz) |
| $Al_2O_3$ 1h with α-alumina 1wt.% | −21.0 | 4.14 | 0.25 (3.36-3.61 GHz) |

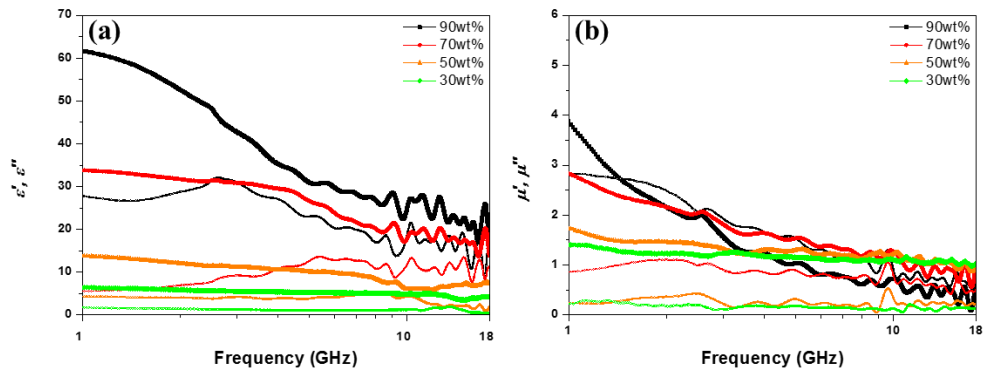


**Fig. 5.1.** The real and imaginary parts of complex (a) permittivity and (b) permeability for carbonyl iron composites with the wt.% of 30, 50, 70, and 90.

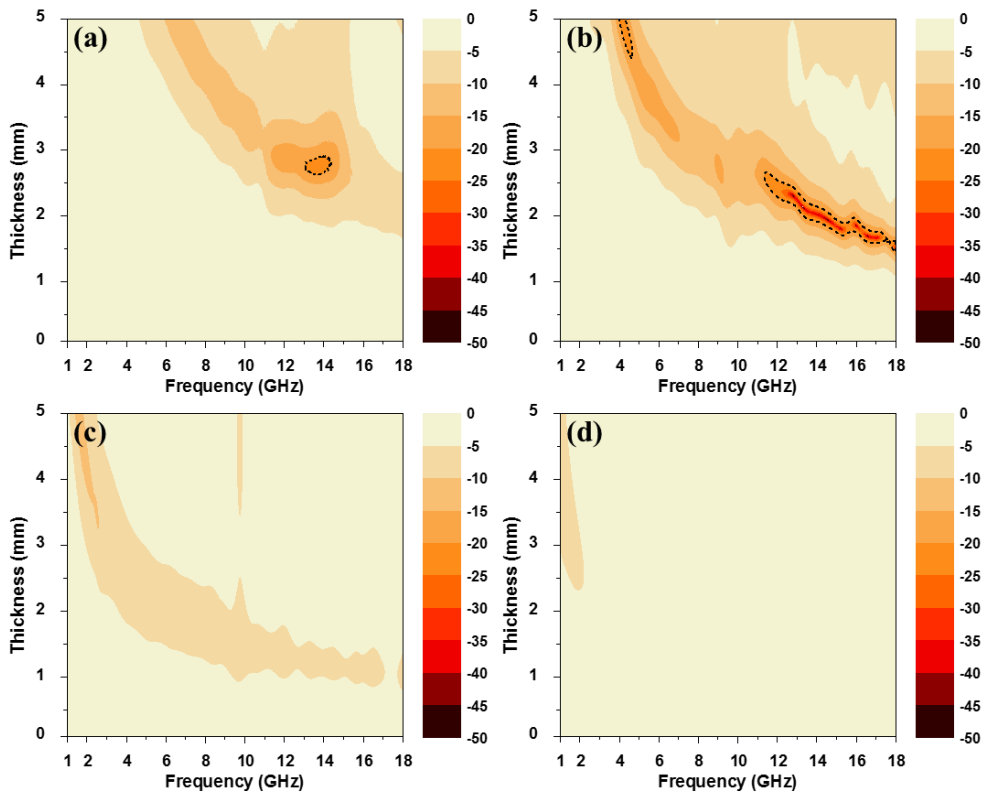


**Fig. 5.2.** *RL* maps for the carbonyl iron composites with the wt.% of (a) 30, (b) 50, (c) 70, and (d) 90.

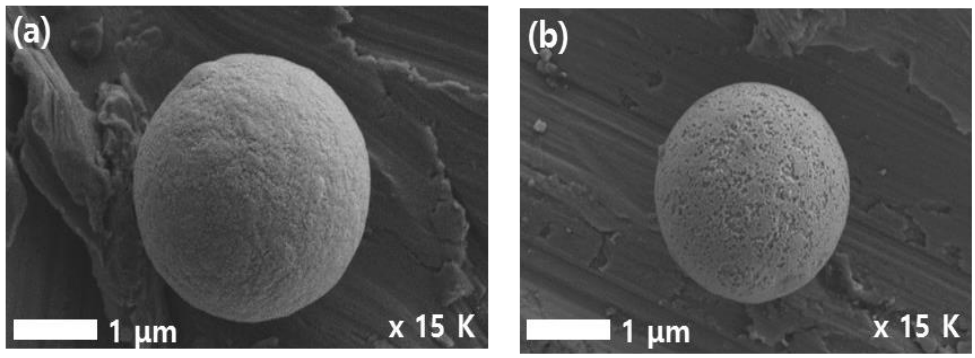


**Fig. 5.3.** SEM micrographs of carbonyl powder (a) uncoated and (b) alumina-coated for 1 h.

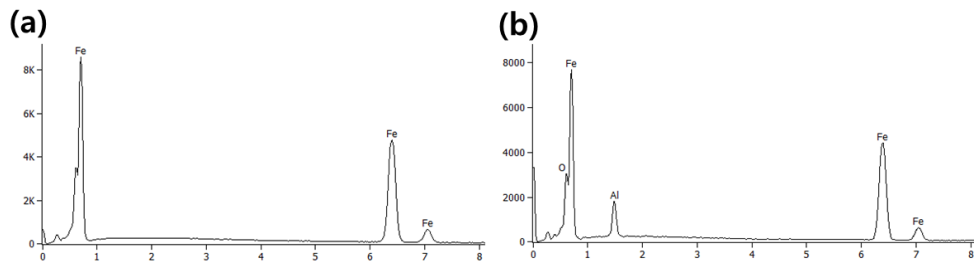


**Fig. 5.4.** EDS spectra of carbonyl powder (a) uncoated and (b) alumina-coated for 1 h.

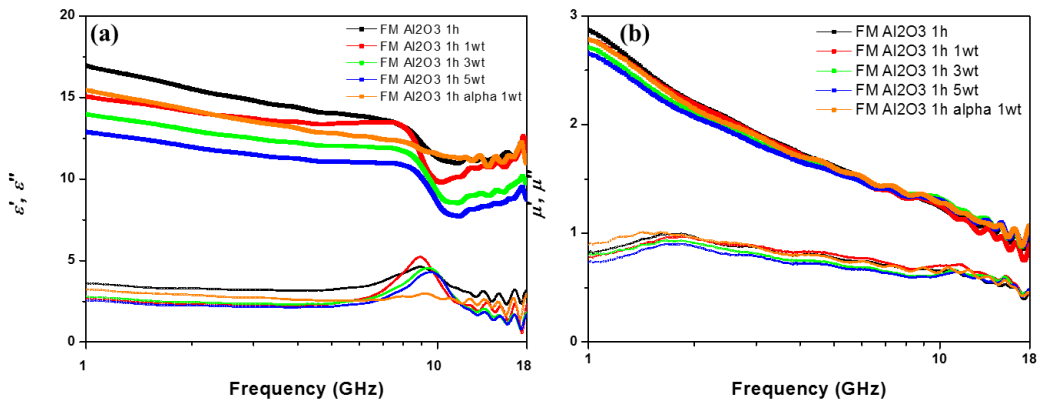


**Fig. 5.5.** The real and imaginary parts of complex (a) permittivity and (b) permeability of $Al_2O_3$-coated carbonyl iron for 1 h, 2h, 4 h, carbonyl iron with α-alumina 1wt.%, and amorphous alumina 1wt.%.

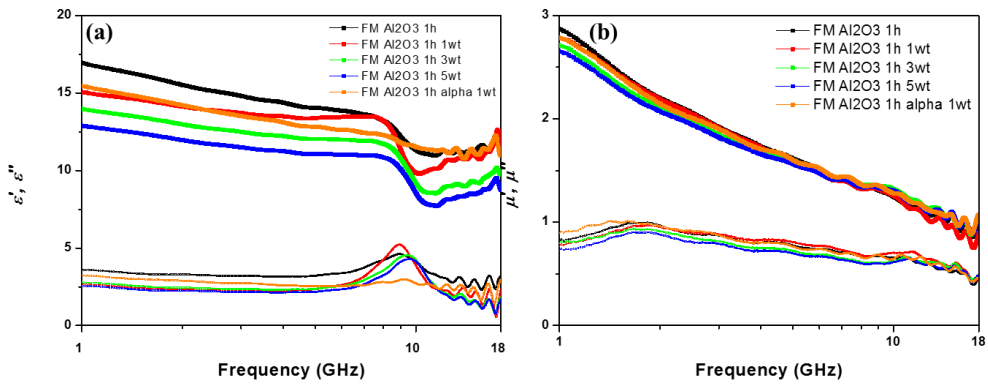


**Fig. 5.6.** The real and imaginary parts of complex (a) permittivity and (b) permeability for $Al_2O_3$-coated carbonyl iron and $Al_2O_3$-coated carbonyl iron with dielectric materials composites with the wt.% of 70.

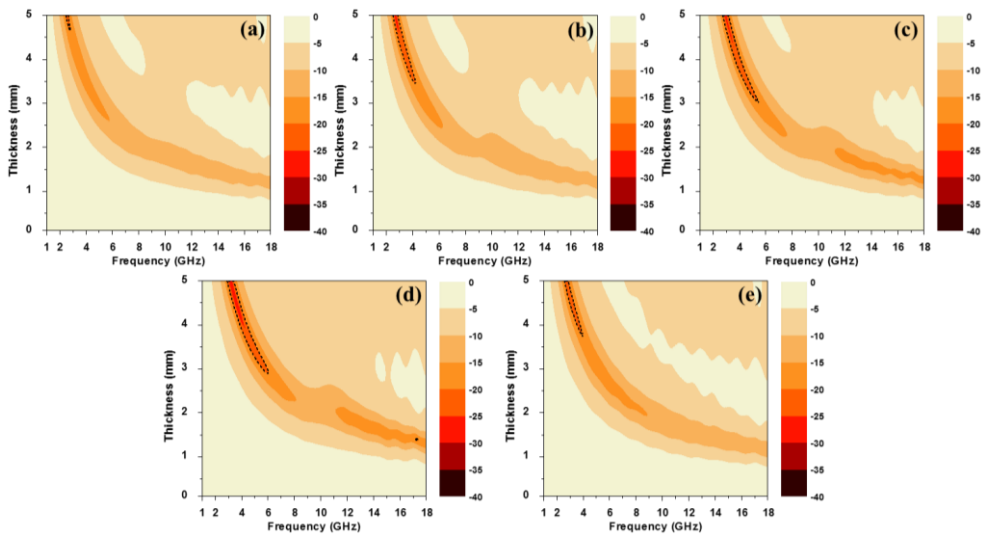


**Fig. 5.7.** *RL* maps for $Al_2O_3$-coated carbonyl iron (a), $Al_2O_3$-coated carbonyl iron with amorphous alumina 1wt.% (b), 3wt.% (c), 5wt.% (d), and $Al_2O_3$-coated carbonyl iron composites with α-alumina 1wt.% (e).

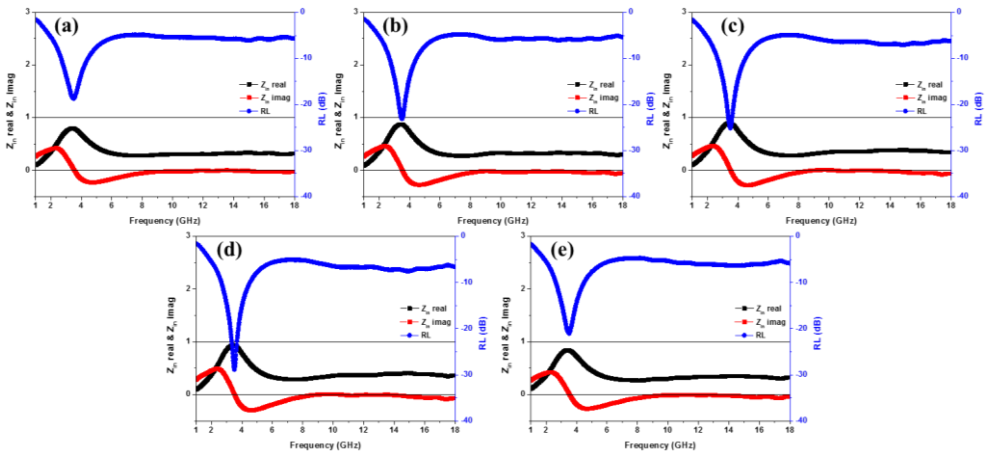


**Fig. 5.8.** Plots of the real and imaginary parts of the normalized $Z_{in}$ and *RL* as a function of frequency for $Al_2O_3$-coated carbonyl iron (a), $Al_2O_3$-coated carbonyl iron with amorphous alumina 1wt.% (b), 3wt.% (c), 5wt.% (d), and $Al_2O_3$-coated carbonyl iron composites with α-alumina 1wt.% (e).

# References

[1] P. Sanchez-Olivares, P. Sanchez-Dancausa, J.L. Masa-Campos, M. Iglesias-Menendez-de-la-Vega, E. Garcia-Marin, Circular Conformal Array Antenna With Omnidirectional and Beamsteering Capabilities for 5G Communications in the 3.5-GHz Range, Ieee Antennas and Propagation Magazine, 61 (2019) 97-108.

[2] I.P. Belikaidis, A. Georgakopoulos, E. Kosmatos, V. Frascolla, P. Demestichas, Management of 3.5-Ghz Spectrum in 5G Dense Networks A Hierarchical Radio Resource Management Scheme, Ieee Vehicular Technology Magazine, 13 (2018) 57-64.

[3] W. Debaenst, A. Feys, I. Cuinas, M.G. Sanchez, J. Verhaevert, RMS Delay Spread vs. Coherence Bandwidth from 5G Indoor Radio Channel Measurements at 3.5 GHz Band, Sensors, 20 (2020) 750.

[4] W. Xu, Y.F. Pan, W. Wei, G.S. Wang, Nanocomposites of Oriented Nickel Chains with Tunable Magnetic Properties for High-Performance Broadband Microwave Absorption, Acs Applied Nano Materials, 1 (2018) 1116-1123.

[5] C. Zhou, S. Geng, X. Xu, T. Wang, L. Zhang, X. Tian, F. Yang, H. Yang, Y. Li, Lightweight hollow carbon nanospheres with tunable sizes towards enhancement in microwave absorption, Carbon, 108 (2016) 234-241.

[6] C.H. Tian, Y.C. Du, C.S. Cui, Z.L. Deng, J.L. Xue, P. Xu, R. Qiang, Y. Wang, X.J. Han, Synthesis and microwave absorption enhancement of yolk-shell $Fe_3O_4$@C microspheres, Journal of Materials Science, 52 (2017) 6349-6361.

[7] A. Arora, S.B. Narang, Investigation of electrical, dielectric and microwave properties of double substituted M-type $Ba_{(1-2x)}La_xNa_xFe_{10}Co_{0.5}TiMn_{0.5}O_{19}$ hexaferrite, Journal of Materials Science-Materials in Electronics, 29 (2018) 12718-12728.

[8] A. Sharbati, J.M.V. Khani, Effect of $Ho^{3+}$ substitution on magnetic and microwave absorption properties of $Sr(ZnZr)_{0.5}Fe_{12}O_{19}$ hexagonal ferrite nanoparticles, Journal of Materials Science-Materials in Electronics, 24 (2013) 3629-3633.

[9] J. Singh, C. Singh, D. Kaur, S.B. Narang, R. Joshi, S.R. Mishra, R. Jotania, M. Ghimire, C.C. Chauhan, Tunable microwave absorption in Co-Al substituted M-type Ba-Sr hexagonal ferrite, Materials & Design, 110 (2016) 749-761.

[10] C.Q. Ge, L.Y. Wang, G. Liu, T. Wang, Enhanced electromagnetic properties of carbon nanotubes and $SiO_2$-coated carbonyl iron microwave absorber, Journal of Alloys and Compounds, 767 (2018) 173-180.

[11] J. Topfer, A. Angermann, Complex additive systems for Mn-Zn ferrites with low power loss, Journal of Applied Physics, 117 (2015) 17A504.

[12] A.H. Taghvaei, H. Shokrollahi, K. Janghorban, H. Abiri, Eddy current and total power loss separation in the iron–phosphate–polyepoxy soft magnetic composites, Materials & Design, 30 (2009) 3989-3995.

[13] X. Fan, J. Wang, Z.Y. Wu, G.Q. Li, Core-shell structured $FeSiAl/SiO_2$ particles and $Fe_3Si/Al_2O_3$ soft magnetic composite cores with tunable insulating layer thicknesses, Materials Science and Engineering B-Advanced Functional Solid-State Materials, 201 (2015) 79-86.

[14] Y. Zhao, X. Zhang, J. Q. Xiao, Submicrometer Laminated $FeSiO_2$ Soft Magnetic Composites—An Effective Route to Materials for High-Frequency Applications, Advanced Materials, 17 (2005) 915-918

[15] W.C. Li, C. Le, J.J. Lv, W. Huang, L. Qiao, J.W. Zheng, Y. Ying, J. Yu, S.L. Che, Electromagnetic and oxidation resistance properties of core-shell structure flaked carbonyl iron powder@$SiO_2$ nanocomposite, Physica Status Solidi a-Applications and Materials Science, 214 (2017) 1600747.

[16] J.N. Calata, G.-Q. Lu, N. Khai, Soft Magnetic Alloy-Polymer Composite for High-Frequency Power Electronics Application, Journal of Electronic Materials, 43 (2014) 126-131.

[17] D. Liu, C. Wu, M. Yan, Investigation on sol–gel $Al_2O_3$ and hybrid phosphate-alumina insulation coatings for FeSiAl soft magnetic composites, Journal of Materials Science, 50 (2015) 6559-6566.

[18] Y.D. Peng, J.W. Nie, W.J. Zhang, J. Ma, C.X. Bao, Y. Cao, Effect of the addition of $Al_2O_3$ nanoparticles on the magnetic properties of Fe soft magnetic composites, Journal of Magnetism and Magnetic Materials, 399 (2016) 88-93.

[19] D. Luo, C. Wu, M. Yan, Incorporation of the $Fe_3O_4$ and $SiO_2$ nanoparticles in epoxy-modified silicone resin as the coating for soft magnetic composites with enhanced performance, Journal of Magnetism and Magnetic Materials, 452 (2018) 5-9.

[20] H. Shokrollahi, K. Janghorban, Soft magnetic composite materials (SMCs), Journal of Materials Processing Technology, 189 (2007) 1-12.

[21] A. Hossein Taghvaei, A. Ebrahimi, K. Gheisari, K. Janghorban, Analysis of the magnetic losses in iron-based soft magnetic composites with MgO insulation produced by sol–gel method, Journal of Magnetism and Magnetic Materials, 322 (2010) 3748-3754.

[22] B. Zhou, Y.Q. Dong, L. Liu, Q. Chi, Y.Q. Zhang, L. Chang, F.Q. Bi, X.M. Wang, The core-shell structured Fe-based amorphous magnetic powder cores with excellent magnetic properties, Advanced Powder Technology, 30 (2019) 1504-1512.

[23] B. Zhou, Y.Q. Dong, L. Liu, L. Chang, F.Q. Bi, X.M. Wang, Enhanced soft magnetic properties of the Fe-based amorphous powder cores with novel $TiO_2$ insulation coating layer, Journal of Magnetism and Magnetic Materials, 474 (2019) 1-8.

[24] N.J. Tang, W. Zhong, H.Y. Jiang, Z.D. Han, W.Q. Zou, Y.W. Du, Complex permeability of $FeNi_3/SiO_2$ core-shell nanoparticles, Solid State Communications, 132 (2004) 71-74.

[25] D. Wang, G.P. Bierwagen, Sol–gel coatings on metals for corrosion protection, Progress in Organic Coatings, 64 (2009) 327-338.

[26] A. Guerrero-Martinez, J. Perez-Juste, L.M. Liz-Marzan, Recent progress on silica coating of nanoparticles and related nanomaterials, Advanced materials, 22 (2010) 1182-1195.

[27] M. Wu, Y.D. Zhang, S. Hui, T.D. Xiao, S. Ge, W.A. Hines, J.I. Budnick, M.J. Yacaman, Magnetic properties of $SiO_2$-coated Fe nanoparticles, Journal of Applied Physics, 92 (2002) 6809-6812.

[28] M. Yaghtin, A.H. Taghvaei, B. Hashemi, K. Janghorban, Effect of heat treatment on magnetic properties of iron-based soft magnetic composites with $Al_2O_3$ insulation coating produced by sol–gel method, Journal of Alloys and Compounds, 581 (2013) 293-297.

[29] Y. Guo, X. Jian, L. Zhang, C.H. Mu, L.J. Yin, J.L. Xie, N. Mahmood, S.X. Dou, R.C. Che, L.J. Deng, Plasma-induced FeSiAl@$Al_2O_3$@$SiO_2$ core-shell structure for exceptional microwave absorption and anti-oxidation at high temperature, Chemical Engineering Journal, 384 (2020).

[30] E. Ni, An uncertainty analysis for the measurement of intrinsic properties of materials by the combined transmission-reflection method, Ieee Transactions on Instrumentation and Measurement, 41 (1992) 495-499.

# Chapter 6

## Overall conclusion

Among various MAMs, while both spinel ferrites and M-type hexaferrites have been most widely used for real applications, W-type hexaferrites and carbonyl iron have been rarely reported. In particular, 3.5 and 28 GHz are regarded as the frequencies for 5G communication. Thus, in this study, the microwave absorption properties of the partially Zn-substituted W-type hexaferrites ($SrFe_{2-x}Zn_xFe_{16}O_{27}$; $SrFe_{2-x}Zn_xW$, $0.0 \leq x \leq 2.0$) were carefully investigated to develop thin broadband microwave absorbers at two different frequencies of 3.5 and 28 GHz. In addition, the $Al_2O_3$-coated carbonyl irons prepared by the sol-gel method were investigated to develop high performance microwave absorbers at 3.5 GHz. The reason for the selection of partial Zn substitution is as follows. First, according to our previous study on Zn-substituted SrW-type hexaferrites, with increasing $x$ up to 1.0 in $SrFe_{2-x}Zn_xW$, the saturation magnetization ($M_s$) is almost linearly increased while the magnetic anisotropy field ($H_a$) is abruptly decreased. With further increase of $x$ up to 2.0, the $M_s$ value is largely decreased while the $H_a$ value is slightly decreased. Therefore, the real parts of $\mu_r$ are expected to continuously increase up to $x$ =1.0 since they are proportional to the ratio of $M_s/H_a$. Second, higher real and imaginary parts of the $\varepsilon_r$ value is expected due to an increased electric conductivity through electron hopping between $Fe^{2+}$ and $Fe^{3+}$ ions. Therefore, the partial substitution of $Zn^{2+}$ for the $Fe^{2+}$ site of SrW-type hexaferrite is expected to increase the real and imaginary parts of both $\varepsilon_r$ and $\mu_r$ values, leading to an improvement in the microwave absorption

properties. On the other hand, since the carbonyl iron has very high $M_s$ with very low $H_a$, it is possible to obtain high real parts of $\mu_r$. However, an excessive eddy current loss hindered to achieve high performance microwave absorber. To overcome this problem, we synthesized a core-shell of carbonyl iron-amorphous alumina by the sol-gel method since the inter-particular current path can be effectively reduced. As the alumina insulation coating layer acts as a non-magnetic material which deteriorates their magnetic properties, especially the real part of $\mu_r$, its thickness was carefully controlled. Also, the dielectric materials such as amorphous alumina and α-alumina were mixed additionally to control the complex permittivity.

The microwave absorption properties of $SrFe_{2-x}Zn_xW$ ($0.0 \leq x \leq 2.0$) hexaferrite-epoxy resin composites were investigated in both Ku (0.5–18 GHz) and Ka (26.5-40 GHz) bands. For $Al_2O_3$-coated carbonyl iron-epoxy resin composites, their microwave absorption properties were studied only in the Ku band. As expected, owing to the increased real and imaginary parts $\varepsilon_r$ and $\mu_r$, the partially Zn-substituted SrW-type hexaferrite composites exhibited lower *RL* values with wider bandwidth. Especially, a 2.8 mm-thick $SrFe_{1.5}Zn_{0.5}W$ ($x$ = 0.5) composite with $V_f$ of 90% exhibited the most appropriate for 5G application at 3.5 GHz in the Ku band, having the *RL* value of −46 dB at 3.6 GHz with the bandwidth of 0.43 GHz (3.38-3.81 GHz) below −10 dB. In the Ka-band, a 0.64 mm-thick $SrFe_{1.75}Zn_{0.25}W$ ($x$ = 0.25) composite with the $V_f$ of 30% exhibited the most appropriate for 5G application at 28 GHz, having the *RL* value of −68.4 dB at 28 GHz with the bandwidths of 5.16 GHz (26.50-31.66 GHz) and 2.48 GHz (26.50-28.98 GHz) below −10 and −20 dB, respectively. Meanwhile, $Al_2O_3$-coated carbonyl iron composite with amorphous alumina of 5wt.% exhibited the highest performance having the *RL* value of −28.9 dB at 3.5 GHz with

a thickness of 4.36 mm and the bandwidth of 0.51 GHz (3.25-3.76 GHz) below −20 dB.

In conclusion, partially Zn-substituted SrW-type hexaferrites are appropriate as the filler of MAM for 5G application near 3.5 and 28 GHz since thin broadband microwave absorbers can be fabricated with epoxy resin. Nano-coating of amorphous alumina on the surface of carbonyl iron is essential for the improvement of microwave absorption properties of carbonyl iron by greatly reducing the eddy current loss, leading to higher performance broadband microwave absorbers at 3.5 GHz. Further improvement of microwave absorption properties is expected by the following approaches. One is to fully optimize the processing parameters of partially Zn-substituted SrW-type hexaferrite composites, including the amount of Zn substituent $x$, its $V_f$, the kind and amount of polymer matrix, and the fabrication processing of specimen. Another may be to make other SrW-type hexaferrite fillers by the partial substitution of other stable divalent ions such as $Co^{2+}$, $Ni^{2+}$, $Mn^{2+}$, $Mg^{2+}$, and etc. for the $Fe^{2+}$ sites.

# 국문 초록

## 5 세대 통신을 위한 Zn 치환된 W-타입 헥사페라이트와 카보닐 철의 마이크로파 흡수 특성

최 성 준

서울대학교 공과대학 재료공학부

5 세대 (5G) 기술의 발달로 무선 통신을 위한 마이크로파 전자 기기들이 사용되어 오고 있다. 이와 동시에 인간과 동물에 심각한 문제를 일으키고, 뿐만 아니라 전자 기기에도 오작동을 일으킬 수 있는 전자기파 간섭(EMI)이 큰 문제로 떠오르고 있다. 따라서 이러한 EMI 문제를 해결하기 위해서 많은 그룹에서 무게가 가볍고, 낮은 부피 분율, 넓은 대역폭, 우수한 마이크로파 흡수 특성을 가지는 고특성 마이크로파 흡수 재료(MAM)의 개발을 위해 노력하고 있다.

한편 마이크로파 흡수 특성은 주로 복소 유전율 ($\varepsilon_r = \varepsilon' - j\varepsilon''$)과 복소 투자율 ($\mu_r = \mu' - j\mu''$)에 의해 결정되며, 흡수체의 두께는 굴절률 ($n = \mathrm{Re}\sqrt{\mu_r \varepsilon_r}$ )에 반비례하기 때문에 연구자들은 실제 응용을 위해 유전율과 투자율의 값을 개선시키는 데 중점을 두고 있다.

다양한 마이크로파 흡수 재료 중에서 스피넬 페라이트와 M-타입 헥사페라이트는 가장 널리 사용되는 재료이며, W-타입 헥사페라이트와 카보닐 철은 거의 보고되어 있지 않은 실정이다. 특히 5 세대 통신에서 3.5 GHz 와 28 GHz 는 가장 보편적인 주파수로 알려져 있다. 따라서 본

연구에서는 3.5 GHz 와 28 GHz 주파수 영역에서 얇고 넓은 대역폭의 전자파 흡수체를 위해 Zn 가 치환된 SrW-타입 헥사페라이트 ($SrFe_{2-x}Zn_xFe_{16}O_{27}$; $SrFe_{2-x}Zn_xW$, $0.0 \leq x \leq 2.0$)의 마이크로파 흡수 특성을 살펴보고자 했다. 또한 3.5 GHz 에서 우수한 특성의 전자파 흡수체를 위해 sol-gel 법으로 합성한 알루미나 코팅된 카보닐 철의 마이크로파 흡수 특성을 살펴보고자 했다. Zn 이온을 부분적으로 치환한 이유는 다음과 같다. 첫 번째, 포화 자화값 ($M_s$)은 $x$ = 1.0 까지 증가함에 따라 거의 선형적으로 증가하는 반면 자기 이방성 ($H_a$)은 감소한다. 그 이후부터 $x$ = 2.0 까지는 포화 자화값은 아주 크게 감소하는 반면에 자기 이방성 값은 약간 감소한다. 복소 투자율은 $M_s/H_a$ 에 비례 관계에 있기 때문에 복소 투자율의 값은 $x$ = 1.0 까지는 증가할 것이라 예상했다. 두 번째, $Fe^{2+}$와 $Fe^{3+}$ 이온 사이의 전자 도약에 따른 분극의 증가로 복소 유전율 또한 향상될 것이라 예상했다. 따라서, 부분적으로 Zn 가 치환된 SrW-타입 헥사페라이트의 복소 유전율과 복소 투자율의 값을 동시에 증가시킴으로써 마이크로파 흡수 특성도 향상될 것이라 판단했다.

반면에 카보닐 철은 높은 포화 자화값과 낮은 자기 이방성 값 때문에 높은 실수부 투자율 값을 가진다고 알려져 있다. 그러나 높은 와전류 손실 때문에 우수한 특성의 전자파 흡수체를 얻는 데 어려움을 겪고 있다. 이러한 문제점을 해결하기 위해서 sol-gel 법을 통한 카보닐 철과 비정질 알루미나의 core-shell 구조를 만들어 줌으로써 입자 간 와전류 손실을 효과적으로 억제하고자 하였다. 알루미나 절연 코팅 층은 비자성 물질로서 자기적 특성을 감소시키며 특히 투자율의 허수부를 감소시키는 역할을 하기 때문에 알루미나 코팅 두께를 섬세하게 조절하였다. 또한

복소 유전율을 조절하기 위해서 비정질 알루미나 또는 α-알루미나와 같은 유전 물질을 추가적으로 섞어주었다.

복합체 샘플의 전자파 흡수 특성 측정을 위해서 시편은 다음과 같은 과정을 통해 준비하였다. 각 헥사페라이트 또는 카보닐 철 분말은 에폭시 레진과 함께 섞어주었고, 직사각형 또는 toroidal 형태로 일축 성형한 다음 175 ℃ 에서 1 시간 동안 경화하였다. 복소 유전율과 복소 투자율 측정을 위해서 VNA (Agilent PNA N5525A) 사용하였다. 복소 유전율과 복소 투자율은 Nicolson and Ross 알고리즘에 의해 계산된 S-변수들을 통해 계산되었다.

$SrFe_{2-x}Zn_xW$ ($0.0 \leq x \leq 2.0$) 헥사페라이트의 마이크로파 흡수 특성을 Ku (0.5-18 GHz)와 Ka (26.5-40 GHz)의 영역에서 살펴보았다. 반면 알루미나 코팅된 카보닐 철의 마이크로파 흡수 특성은 Ku-band 에서만 살펴보았다. 예상한 것과 같이 증가한 복소 유전율 그리고 복소 투자율 덕분에 Zn 치환된 SrW-타입 헥사페라이트는 넓은 대역폭을 가지며 우수한 마이크로파 흡수 특성을 보였다. 특히 90% 부피 분율에서 2.8 mm 두께의 $SrFe_{1.5}Zn_{0.5}W$ ($x = 0.5$) 복합체는 -10 dB 이하에서 0.43 GHz (3.38-3.81 GHz)의 대역폭과 3.6 GHz 에서 -46 dB 의 마이크로파 흡수 특성을 나타냄으로써 3.5 GHz 에서 5 세대 통신 활용을 위한 적절한 흡수체임을 알 수 있었다. Ka-band 에서는 30% 부피 분율에서 0.64 mm 두께의 $SrFe_{1.75}Zn_{0.25}W$ ($x = 0.25$) 복합체는 -10 dB 이하에서 5.16 GHz (26.50-31.66 GHz)의 대역폭, -20 dB 이하에서는 2.48 GHz (26.50-28.98 GHz) 대역폭과 28 GHz 에서 -68.4 dB 의 마이크로파 흡수 특성을 나타냄으로써 28 GHz 에서 5 세대 통신 활용을 위한 우수한 흡수체임을 확인하였다. 한편 알루미나가 코팅된

카보닐 철과 5wt.%의 비정질 알루미나 분말을 섞은 복합체는 4.36 mm 의 두께를 가질 때 −20 dB 이하에서 0.51 GHz (3.25−3.76 GHz)의 대역폭과 −28.9 dB 마이크로파 흡수 특성을 보임으로써 3.5 GHz 에서 5 세대 통신 활용을 위한 적절한 흡수체임을 확인하였다.

결론적으로, Zn 부분 치환된 SrW−타입 헥사페라이트는 두께가 얇고 넓은 대역폭을 가짐으로써 3.5 GHz 와 28 GHz 주파수 영역에서 5 세대 통신 응용에 적합한 마이크로파 흡수 재료임을 확인하였다. 또한 3.5 GHz 에서 카보닐 철이 우수한 전자파 흡수 특성과 넓은 대역폭을 가지기 위해선 카보닐 철 분말의 표면에 비정질 알루미나의 나노 코팅을 하여 와전류를 억제해야 하는 것이 필수적임을 확인하였다. 또한 마이크로파 흡수 특성의 개선을 위해서는 다음과 같은 새로운 방법이 요구될 것으로 생각된다. 하나, Zn 부분 치환된 SrW−타입 헥사페라이트 복합체의 최적화를 위해서는 Zn 치환의 양과 필러의 부피 분율, 폴리머 매트릭스의 종류와 양 그리고 시편 제조 방법을 바꿔볼 수 있다. 다른 하나는 $Fe^{2+}$ 자리에 $Co^{2+}$, $Ni^{2+}$, $Mn^{2+}$, $Mg^{2+}$ 등과 같은 다른 안정한 2 가 이온을 부분적으로 치환함으로써 다른 형태의 W−타입 헥사페라이트를 합성해볼 수 있을 것이다.

**키워드:** SrW−타입 헥사페라이트, Zn 치환, 카보닐 철, 알루미나 코팅, 복소 유전율, 복소 투자율, 반사 손실, 마이크로파 흡수 특성, 5G 활용

**학번:** 2014−21446